AFGL-TR-78-0286 SIO Ref. 79-5

AIRBORNE MEASUREMENTS OF OPTICAL ATMOSPHERIC PROPERTIES, SUMMARY AND REVIEW III

Seibert Q. Duntley, Richard W. Johnson, and Jacqueline I. Gordon

Visibility Laboratory
University of California, San Diego
Scripps Institution of Oceanography
La Jolla, California 92093

Approved:

James L. Harris, Sr., Director
Visibility Laboratory

Approved:

William A. Nierenberg, Director
Scripps Institution of Oceanography

CONTRACT NO. F19628-76-C-0004
Project No. 7621
Task No. 7621-11
Work Unit No. 7621-11-01

Final Report
1 August 1975 - 30 September 1978

Contract Monitor
Major Ted S. Cress, Atmospheric Optics Branch, Optical Physics Division

Prepared for
AIR FORCE GEOPHYSICS LABORATORY
AIR FORCE SYSTEMS COMMAND
UNITED STATES AIR FORCE
HANSCOM AFB, MASSACHUSETTS 01731

UNCLASSIFIED

SECURITY CLASSIFICATION OF THIS PAGE *(When Data Entered)*

REPORT DOCUMENTATION PAGE

READ INSTRUCTIONS BEFORE COMPLETING FORM

1. REPORT NUMBER AFGL-TR-78-0286	2. GOVT ACCESSION NO.
3. RECIPIENT'S CATALOG NUMBER	
4. TITLE *(and Subtitle)* AIRBORNE MEASUREMENTS OF OPTICAL ATMOSPHERIC PROPERTIES, SUMMARY AND REVIEW III	5. TYPE OF REPORT & PERIOD COVERED Final Report 1 August 1975 - 30 September 1978
	6. PERFORMING ORG. REPORT NUMBER SIO Ref. 79-5
7. AUTHOR(s) Seibert Q. Duntley Richard W. Johnson Jacqueline I. Gordon	8. CONTRACT OR GRANT NUMBER(s) F19628-76-C-0004
9. PERFORMING ORGANIZATION NAME AND ADDRESS University of California, San Diego Visibility Laboratory La Jolla, California 92093	10. PROGRAM ELEMENT, PROJECT, TASK AREA & WORK UNIT NUMBERS Project, Task, Work Unit No. 7621-11-01
11. CONTROLLING OFFICE NAME AND ADDRESS Air Force Geophysics Laboratory Hanscom AFB, Massachusetts 01731 Contract Monitor: Major Ted S. Cress/OPA	12. REPORT DATE December 1978
	13. NUMBER OF PAGES 117
14. MONITORING AGENCY NAME & ADDRESS*(if different from Controlling Office)*	15. SECURITY CLASS. *(of this report)* UNCLASSIFIED
	15a. DECLASSIFICATION/DOWNGRADING SCHEDULE

16. DISTRIBUTION STATEMENT *(of this Report)*

Approved for public release; distribution unlimited.

17. DISTRIBUTION STATEMENT *(of the abstract entered in Block 20, if different from Report)*

18. SUPPLEMENTARY NOTES

19. KEY WORDS *(Continue on reverse side if necessary and identify by block number)*

Albedos
Atmospheric Optical Properties
Atmospheric Scattering Coefficient
Atmospheric Beam Transmittance
Natural Daytime Irradiance
Temperature Profile
Relative Humidity Profile

20. ABSTRACT *(Continue on reverse side if necessary and identify by block number)*

This report summarizes a three year period devoted primarily to collection and evaluation of optical atmospheric data describing the western European environment. Five field expeditions were made between April 1976 and September 1978. They were conducted as a cooperative, but independent effort associated with the NATO Research Study Group 8 of Panel IV,

DD FORM 1 JAN 73 1473 EDITION OF 1 NOV 65 IS OBSOLETE
S/N 0102-014-6601

UNCLASSIFIED

SECURITY CLASSIFICATION OF THIS PAGE *(When Data Entered)*

AC243 and their Program OPAQUE. Measurements were made in six representative geographical areas during each of the four seasons, Summer, Fall, Winter and Spring. Optical measurements were made in four regions within the visual spectrum as follows: two moderately narrow bands having mean wavelengths of 478 and 664 nanometers, one slightly wider band at 765 nanometers and one relatively broad band representing the photopic response having a mean wavelength of 557 nanometers.

The daytime optical measurements included total volume scattering coefficient, sky and terrain radiances, and both upwelling and downwelling irradiances. Simultaneous meteorological measurements included temperature, dewpoint temperature and atmospheric pressure.

The optical atmospheric properties derived from these data and presented in reports typified by AFGL-TR-76-0188 and AFGL-TR-78-0168 are reviewed as are their methods of derivation and validation. The methods of data collection and processing are summarized and reviewed as is the overall resulting data bank. Examples related to the use of the data are included as well as recommendations for further data study and interpretation.

SUMMARY

This is the Final Report prepared in compliance with AFGL Contract F19628-76-C-0004. The principal task under this contract was to conduct a series of experimental field trips to collect atmospheric optical data in a variety of European locations, and to analyze and report these data upon completion of the deployment. The daytime optical measurements collected during these deployments are appropriate for use in determining optical atmospheric properties for any upward or downward path of sight. The derivable properties include the natural irradiance upon horizontal plane surfaces, scalar irradiances, total volume scattering coefficients, atmospheric beam transmittances, path radiances, directional path reflectances, and directional sky and terrain reflectances.

Five field trips were conducted during this contract interval. They were conducted as a cooperative but independent effort associated with the NATO Research Study Group 8 of Panel IV, AC243 and their Program OPAQUE. A comprehensive overview of Program OPAQUE is presented in AFGL-TR-78-0011, Fenn (1978). The five field trips documented European optical atmospheric characteristics during each of the four seasons, Summer, Fall, Winter and Spring in a broad variety of geographical areas.

The status of the total data bank resulting from this three year period plus the backlog developed in preceding years is reviewed in this report, as are the procedures involved in collecting and processing the data.

TABLE OF CONTENTS

LIST OF ILLUSTRATIONS

Figure | Page

RELATED CONTRACTS AND PUBLICATIONS

Related Contracts: None

Publications:

Duntley, S. Q., R. W. Johnson, and J. I. Gordon, "Airborne Measurements of Optical Atmospheric Properties in Southern Germany," AFCRL-72-0255, SIO Ref. 72-64 (July 1972).

Duntley, S. Q., R. W. Johnson, and J. I. Gordon, "Airborne and Ground-Based Measurements of Optical Atmospheric Properties in Central New Mexico," AFCRL-72-0461, SIO Ref. 72-71 (September 1972).

Duntley, S. Q., R. W. Johnson, and J. I. Gordon, "Airborne Measurements of Optical Atmospheric Properties, Summary and Review," AFCRL-72-0593, SIO Ref. 72-82 (November 1972).

Duntley, S. Q., R. W. Johnson, and J. I. Gordon, "Airborne Measurements of Optical Atmospheric Properties in Southern Illinois," AFCRL-TR-73-0422, SIO Ref. 73-24 (July 1973).

Duntley, S. Q., R. W. Johnson, and J. I. Gordon, "Airborne and Ground-Based Measurements of Optical Atmospheric Properties in Southern Illinois," AFCRL-TR-74-0298, SIO Ref. 74-25 (June 1974).

Duntley, S. Q., R. W. Johnson, and J. I. Gordon, "Airborne Measurements of Optical Atmospheric Properties in Western Washington," AFCRL-TR-75-0414, SIO Ref. 75-24 (September 1975).

Duntley, S. Q., R. W. Johnson, and J. I. Gordon, Airborne Measurements of Optical Atmospheric Properties, Summary and Review II," AFCRL-TR-75-0457, SIO Ref. 75-26 (September 1975).

Duntley, S. Q., R. W. Johnson, and J. I. Gordon, "Airborne Measurements of Optical Atmospheric Properties in Northern Germany," AFGL-TR-76-0188, SIO Ref. 76-17 (September 1976).

Duntley, S. Q., R. W. Johnson, and J. I. Gordon, "Airborne Measurements of Atmospheric Volume Scattering Coefficients in Northern Europe, Spring 1976," AFGL-TR-77-0078, SIO Ref. 77-8 (March 1977).

Duntley, S. Q., R. W. Johnson, and J. I. Gordon, "Airborne Measurements of Atmospheric Volume Scattering Coefficients in Northern Europe, Fall 1976," AFGL-TR-77-0239, SIO Ref. 78-3 (January 1978).

Duntley, S. Q., R. W. Johnson, and J. I. Gordon, "Airborne Measurements of Atmospheric Volume Scattering Coefficients in Northern Europe, Summer 1977," AFGL-TR-78-0168, SIO Ref. 78-28 (December 1978).

Gordon, J. I., J. L. Harris, Sr., and S. Q. Duntley, "Measuring Earth-to-Space Contrast Transmittance from Ground Stations," Appl. Opt. 12, 1317-1324 (1973).

Gordon, J. I., C. F. Edgerton, and S. Q. Duntley, "Signal-Light Nomogram," J. Opt. Soc. Am. 65, 111-118 (1975).

1. INTRODUCTION

This Final Report has been prepared under Contract F19628-76-C-0004. It discusses activities, accomplishments and recommendations related to an atmospheric optical properties measurement program conducted during the interval 1 August 1975 through 30 September 1978. The program has been conducted by the Visibility Laboratory of the University of California, San Diego under the sponsorship of, and in cooperation with the Air Force Geophysics Laboratory, Hanscom AFB, Massachusetts.

The experimental data collection flights made during this contract interval are a continuation of this joint on-going program of environmental documentation, and are listed in Table 1.1. Selected sets of the data measured during these preceding flights have been presented in four preceding reports: AFGL-TR-76-0188, "Airborne Measurements of Optical Atmospheric Properties in Northern Germany", Duntley, *et al.* (1976); AFGL-TR-77-0078, "Airborne Measurements of Atmospheric Volume Scattering Coefficients in Northern Europe, Spring 1976", Duntley, *et al.* (1977); AFGL-TR-77-0239, "Airborne Measurements of Atmospheric Volume Scattering Coefficients in Northern Europe, Fall 1976", Duntley, *et al.* (1978a); AFGL-TR-78-0168, "Airborne Measurements of Atmospheric Volume Scattering Coefficients in Northern Europe, Summer 1977", Duntley, *et al.* (1978b). These measurements and the computations related to their use are examples of a continuous effort to determine and apply quantitative as well as qualitative values to the atmospheric optical properties most effecting the performance of visual and/or electro-optical tasks within the troposphere.

The flight program during the three year interval covered by this report has been organized as a cooperative but independent effort associated with the NATO Research Study Group 8 of Panel IV, AC 243. As illustrated in Table 1.1, five separate European deployments were accomplished during this contract interval. European optical atmospheric characteristics were documented during each of the four seasons, summer, fall, winter, and spring, in a broad variety of geographical areas. A comprehensive overview of the background rationale and the theoretical basis for the OPAQUE plan is presented in AFGL-TR-78-0011, Fenn (1978).

A summary of the general theory and computational methods used to derive the optical atmospheric properties reported during this contract interval is presented in Section 2. This summary reviews determinations of the properties useful in computing contrast transmittance along upward and/or downward inclined paths of sight as in AFGL-TR-76-0188, Duntley, *et al.* (1976). This section also includes a review of the pertinent modifications to these methods which were completed or initiated during this contract period, some of which are still under evaluation and development.

Table 1.1. Summary of Airborne Data Collection Flights

Flight Nos.	Inclusive Dates	Project Title	Flight Track Areas in Chronological Order
C-370 - C-382	7 APR 76 - 26 MAY 76	OPAQUE I	Northern Germany Southern England Centeral Netherlands Southern Denmark
C-390 - C-402	25 OCT 76 - 6 DEC 76	OPAQUE II	Southern Denmark Northern Germany Northern France
C-410 - C-422	4 JUL 77 - 11 AUG 77	OPAQUE III	Northern France Northern Germany Southern Denmark
C-430 - C-456	31 JAN 78 - 31 MAR 78	OPAQUE IV	Western Sicily Southern Germany Southern England Central Netherlands Northern Germany Southern Denmark
C-460 - C-479	2 AUG - 26 SEP 78	OPAQUE V	Western Sicily Northern Germany Central Netherlands Southern Germany Southern England Southern Denmark

The optical instrumentation utilized during this report interval was developed at the Visibility Laboratory, and has been reported in detail in AFCRL-70-0137, Duntley, *et al.* (1970), AFCRL-72-0593, Duntley, *et al.* (1972c), and AFCRL-TR-73-0422, Duntley, *et al.* (1973). During the five OPAQUE deployments, these airborne equipments plus several ground based instrument systems were employed in the total data collection effort. The primary instruments, as in previous deployments, were airborne and ground based integrating nephelometers for determining the total and directional proportional volume scattering coefficients, and two airborne scanning radiometers for the measurement of sky and terrain radiances. Several of the revisions to the hardware which have occurred during the life of this contract are summarized and discussed in Section 3.

Data collection methods throughout this report interval have remained similar to those described

in AFCRL-TR-73-0422, Duntley, *et al.* (1973). A short review of the technique is discussed in Section 4.

The computer techniques used during this report interval are also well-documented in the previously identified references. A summary of the most significant alterations introduced during this contract is presented in Section 5.

Section 6 presents a review of the five OPAQUE related deployments conducted during the three year period covered by this report. Locations, dates and general terrain characteristics related to each deployment and the particular sites utilized are summarized. Site location maps are included for each area to illustrate the geographical relationships between the flight tracks and the associated ground based OPAQUE data station. A summary of the data flights accomplished during these deployments and the status of the resultant data bank is also included in this section.

Sample data illustrating the types of data available from the flight program are presented in Section 7. Examples illustrating the use of these data in typical applications are also included.

A discussion of projected procedural updates and recommendations for future program activities is included in Section 8.

2. COMPUTATIONAL PROCEDURES

The underlying theoretical considerations upon which the data presentations made during this report interval are based, have been specified for the most part in two early publications, "Image Transmission by the Troposphere I" Duntley, *et al.* (1957) and "Model for a Clear Atmosphere", Gordon (1969). A discussion of the directional path reflectance format used in those reports which preceded the program OPAQUE series, can be found in "Directional Reflectance of Atmospheric Paths of Sight," Duntley (1969).

For the convenience of those unfamiliar with the notation and definitions utilized throughout the report series documenting this contract effort, a complete glossary and discussion of each measured and derived quantity is provided in Appendix A and Appendix B.

2.1. PROCEDURAL OVERVIEW

The basic task in all of the field deployments referenced in this report, whether OPAQUE related or those preceding, has been to collect a set of measured data from which one could determine the optical atmospheric properties in existence at the time of measurement. The optical properties of primary concern were those appropriate for the determination of universal contrast transmittance along upward and downward inclined paths of sight. In the interests of broad applicability it was desired to determine a set of fundamental properties associated with the atmosphere alone. i.e., not related to any particular scene or artifact within that scene, not irretrievably combined with specific background characteristics. Thus, the development of the measurement program was directed toward acquiring the input data necessary for the determination of path radiances, $N_r^*(z,\theta,\phi)$, beam transmittances, $T_r(z,\theta)$, and downwelling irradiances, $H(z,d)$. These properties being the basic measureables required for determinations of directional path reflectance $R_r^*(z,\theta,\phi)$ as shown in the following defining equation:

$$R_r^*(z,\theta,\phi) = \pi N_r^*(z,\theta,\phi) / [H(z_{t,d})\ T_r(z,\theta)] \ , \tag{2.1}$$

whence the subsequent determination for slant path contrast transmittance ${}_b\tau_r(z,\theta,\phi)$, as shown by

$${}_b\tau_r(z,\theta,\phi) = [\ 1 + R_r^*(z,\theta,\phi)/{}_bR_o(z_t,\theta,\phi)\ ]^{-1} \ . \tag{2.2}$$

The experimental interrelationships which exist among the various pieces of project hardware, the radiometric measurements made by them, and the computational chains associated with each of the measured values is illustrated in Fig. 2-1. In this figure, abstracted from AFGL-TR-76-0188, Duntley, *et al.* (1976), the instrument providing each basic measurement is indicated at the top of the figure, and the development of the computational procedure progresses down the figure to the desired values indicated by the entries at the bottom of the figure.

During the three year period covered by this report, the computational procedure outlined in Fig. 2-1 was modified and augmented in several ways. Some modifications were designed to extend the applicability to a broader range of search angles, and some were intended to improve the quality of a derived quantity, or to provide additional interpretive insights. Several of the more significant of these procedural improvements are summarized in the following sections.

2.2. PROCEDURAL IMPROVEMENTS

The following three basic improvements were made to the computational and interpretive method during this contract interval.

1. Adding computations for upward looking paths of sight,
2. Computing beam transmittances from sky radiance ratios, and
3. The use of non-Rayleigh Atmosphere models as diagnostics.

A few comments related to the applicability and pertinent details of each of these procedural items are included in the following paragraphs.

PROPERTIES OF UPWARD LOOKING PATHS OF SIGHT

For general applicability, the specification of optical atmospheric properties should be complete enough for application to contrast transmittance determinations along any specified path of sight. The implication of Eqs. (2.1) and (2.2) and the computational procedures outlined in Fig. 2-1 support this generality. However, due to several computer programming simplifications, the computational routines outlined in Fig. 5-1 originally were restricted to the computation of properties related to only downward looking paths of sight. This shortcoming was rectified prior to the issuance of AFGL-TR-76-0188, Duntley, *et al.* (1976). The programming improvement involved a major redefinition of terms and procedures in the computer program AVIZC130 which computes the point function equilibrium radiance, and subsequently path radiances and directional path reflectances for all paths of sight. Discussion covering the linking relationships between these optical properties is furnished in Appendix B. With the modification of program AVIZC130 completed, the same basic data array could be used to compute highly directional optical properties for both upward and downward looking paths of sight as are reported in Duntley, *et al.* (1976).

COMPUTATIONS FROM BASIC AIRBORNE DATA

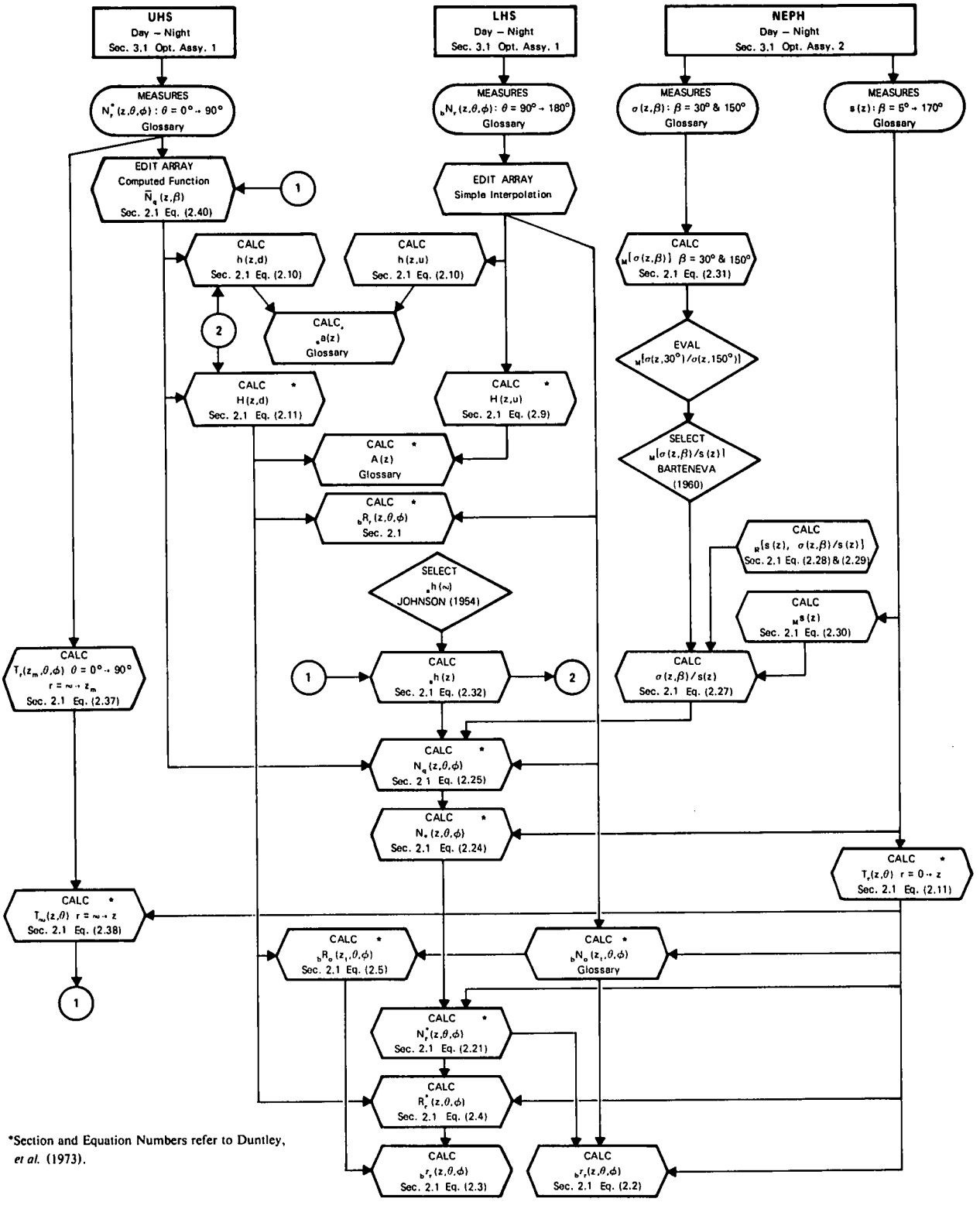

*Section and Equation Numbers refer to Duntley, *et al.* (1973).

Fig. 2-1. Computations from Basic Airborne Data.

DETERMINATION OF BEAM TRANSMITTANCE FROM SKY RADIANCE RATIOS

For the computational scheme in Fig. 2-1 to be effective, it is essential that the upper hemisphere radiance arrays possess reliable values at each flight altitude, and that the apparent solar irradiances at each altitude be properly determined for use with these arrays. As discussed in Appendix B, this requires a reliable value for space-to-altitude beam transmittance. Several techniques for determining space-to-altitude beam transmittances were discussed in AFCRL-72-0593, Duntley, *et al.* (1972c). The sky radiance ratio method of Kushpil' and Petrova (1971) was one proposed for utilization, which was later implemented into the general procedure. See Appendix B, Eq. (A.31).

Since the transmittance term derived from this technique is an important term, it was desired to test the procedure as thoroughly as possible. An extensive body of data collected during an earlier program at the Visibility Laboratory was available and used for this validation study which is discussed in the following paragraphs.

Ground-based data from a solar transmissometer, sky scanner, and irradiometer mounted on a rooftop of the Visibility Laboratory during 1964 include many cases when the sky was completely free of clouds. These data have been used to further validate and develop the method of obtaining space-to-sensor beam transmittance from sky radiance ratios.

As noted in Kushpil' and Petrova (1971), atmospheric absorption acts to reduce the incoming sun irradiance but has no effect on the sky radiance relative distribution. Thus the transmittance based upon the sky radiance ratios is due to scattering only whereas the solar transmissometer measured the attenuation of the atmosphere which is the combined effect of scattering and absorption.

The Telluric spectrum [Goldberg (1954)] indicates that the spectral region 365 to 540 nm is essentially free of absorption. There is only one absorption band at 477.4 nm for O_4 which is very weak, i.e., detectable only for path lengths greater than one airmass. The 1964 Visibility Laboratory rooftop data included one narrow band optical filter, Filter 1 with mean wavelength 459 nanometers, for which the attenuation would be due to scattering only, and thus the transmittance from the sky radiance ratios would be equivalent to the transmittance from the solar transmissometer. A second filter, Filter 2 had a broadband sensitivity with a mean wavelength of 505 nanometers, and 71% of its response below 540 nm. Thus, the solar transmittance measured using Filter 2 is also relatively unaffected by absorption. A graph of the relative spectral response using the filters for the 1964 data is given in Fig. 2-2.

The sky radiances were measured for a set zenith angle and azimuth pattern and not at positions where each pair would be at equivalent angles β from the sun. Therefore radiance pairs for the ratio in Eq. A.31 were accepted if the absolute difference in angle from sun $|\Delta\beta|$ was less than or equal to 2.5°. The angles used for calculation were the theoretical angular positions since the angles were measured only periodically to see if the scanner needed adjustment or maintenance.

An error analysis of the transmittance obtained by Eq. A.31 indicates that the precision error difference of the two radiances is generally multiplied by a factor of between 1 and 2 for many zenith angle combinations. Thus, use of a series of measurements to obtain an average transmittance enhances the reliability of the resultant transmittance. The error analysis also indicated that errors in

the angles θ and θ' affected the transmittance least at large θ and small θ'. Transmittance was calculated using Eq. A.31 for each pair of radiances using a range of θ and θ' selected on the basis of the error analysis. The resultant average transmittance for each θ θ' combination was divided by the transmittance from the solar transmissometer. This table of transmittance ratios indicated that transmittances from Eq. A.31 from the largest θ with a fully unobstructed field of view of the horizon sky (81.6°) with θ' ranging from 2.8° to 64.7° yielded the transmittance ratios closest to 1. Thus, the sky ratio based transmittance for a given case (date, time, and filter) was computed by averaging all the transmittances obtained from θ=81.6° and θ'=2.8°→64.7° with $|\Delta\beta|$=2.5°.

Both sky radiance and solar transmissometer data were available for over 100 cases with clear skies for each of the two filters. The ratios of the transmittance from sky radiance ratios divided by the transmittance from the solar transmissometer were averaged for each filter; this average of the ratios is given in Table 2.1. The average ratios for both filters was 0.992 for 213 cases and the standard deviation was ±5%.

The analysis of these early data, and their application to the method of Kushpil' and Petrova thus revalidates the sky radiance ratio procedure as a reliable method for determining beam transmittances from outside the atmosphere down to any intermediate flight altitude, or to the ground. In this context the procedure is a valuable tool in adding to the internal consistency and self-contained character of the computations illustrated in Fig. 2-1.

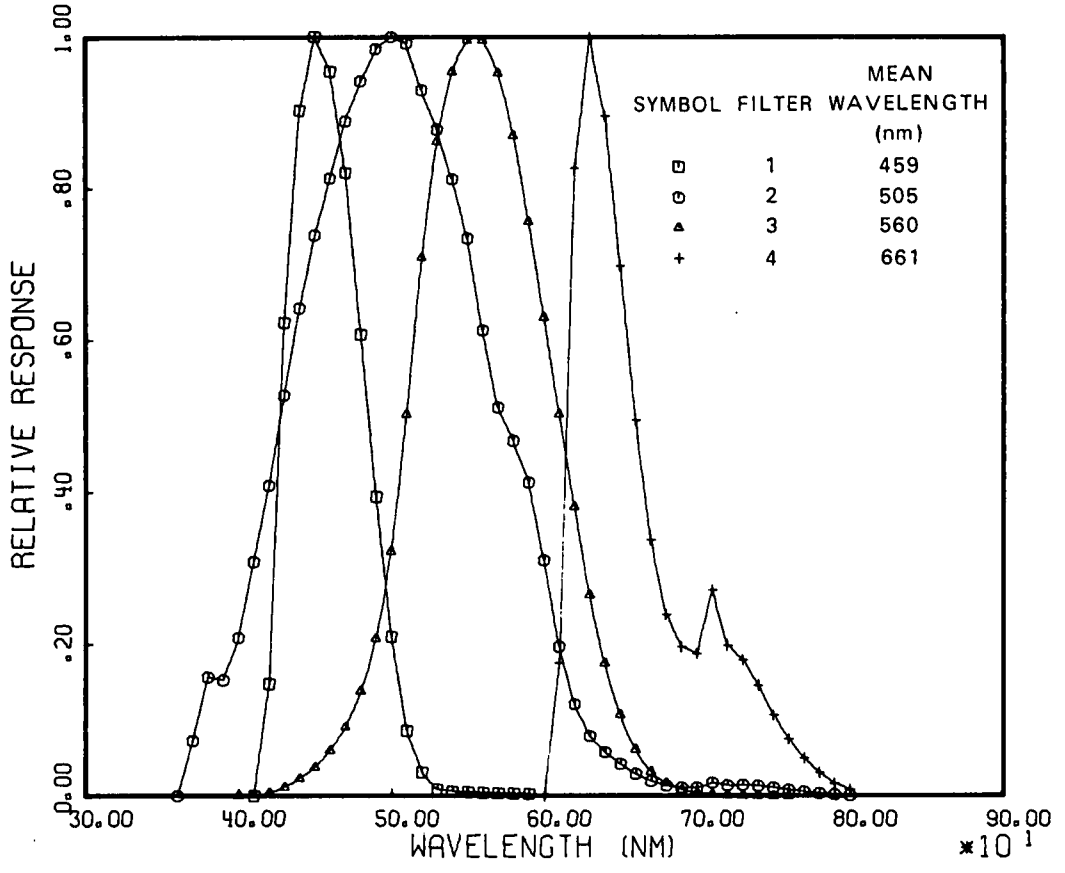

Fig. 2-2. Relative Spectral Response for the 1964 Data from the Visibility Laboratory Rooftop Station.

Table 2.1. Average Ratio of Transmittance from Sky Radiance Ratios Divided by the Transmittance from the Solar Transmissometer

Filter	Mean Wavelength nm	Average Transmittance Ratio	Standard Deviation	Average Transmittance	Number of Cases
1	459	.989	.051	.713	110
2	505	.997	.047	.750	103
TOTAL		.992			213

MODELING OPTICAL PROPERTIES OF NON-RAYLEIGH ATMOSPHERES

It continues to be desirable to develop diagnostic materials to aid in the evaluation of the measurements of the optical properties of the atmosphere. During a previous contract period a computer program was developed to compute atmospheric optical properties based on the clear atmosphere model in Gordon (1969). This program was used to produce a set of values for the photopic Rayleigh atmosphere as described in Duntley, *et al.* (1975b). This same program was used during the current contract interval to compute the optical properties of non-Rayleigh atmospheres. The development of a broad catalog of optical properties based upon the Gordon (1969) model and the Barteneva (1960) scattering coefficient data is a particularly attractive concept since both are used extensively in the development illustrated in Fig. 2-1. Thus there would be an immediate link between the characteristics of the modeled properties and those derived from the measurements made during the OPAQUE deployments. The development and some of the results of this modeling procedure are discussed in the following paragraphs.

The model atmosphere equations from Gordon (1969) may be utilized for computing optical atmospheric properties if a proportional volume scattering function and an appropriate vertical space-to-earth beam transmittance can be specified. Barteneva (1960) provides an extensive catalog of ground-level proportional volume scattering functions with an appropriate range of values of ground-level total volume scattering coefficient for each proportional scattering function for the photopic sensor. By making some limiting assumptions about the structure of the volume scattering coefficient with altitude, it was possible to establish a range of appropriate vertical space-to-earth beam transmittance values for each scattering function.

A lower limit space-to-earth vertical transmittance was computed by assuming the aerosol constant in composition but varying in density with altitude. An upper limit transmittance for each scattering coefficient was computed by assuming the ground-level volume scattering coefficient decreases with density up to 2 km altitude and then changes to a Rayleigh scattering coefficient.

Transmittances below 0.5 were not used since measured values of photopic space-to-earth vertical transmittance from two large bodies of solar transmissometer data do not go below 0.5. Fig. 2-3 contains the photopic* space-to-earth vertical transmittance values measured during 1964 on the rooftop of the Visibility Laboratory. A similar graph of photopic solar transmissometer data measured between 1962 and 1967 at various other locations was presented as Fig. 2-7 in Duntley, *et al.* (1975b). These

*The photopic filter is designated as Filter No. 3 in Fig. 2-2.

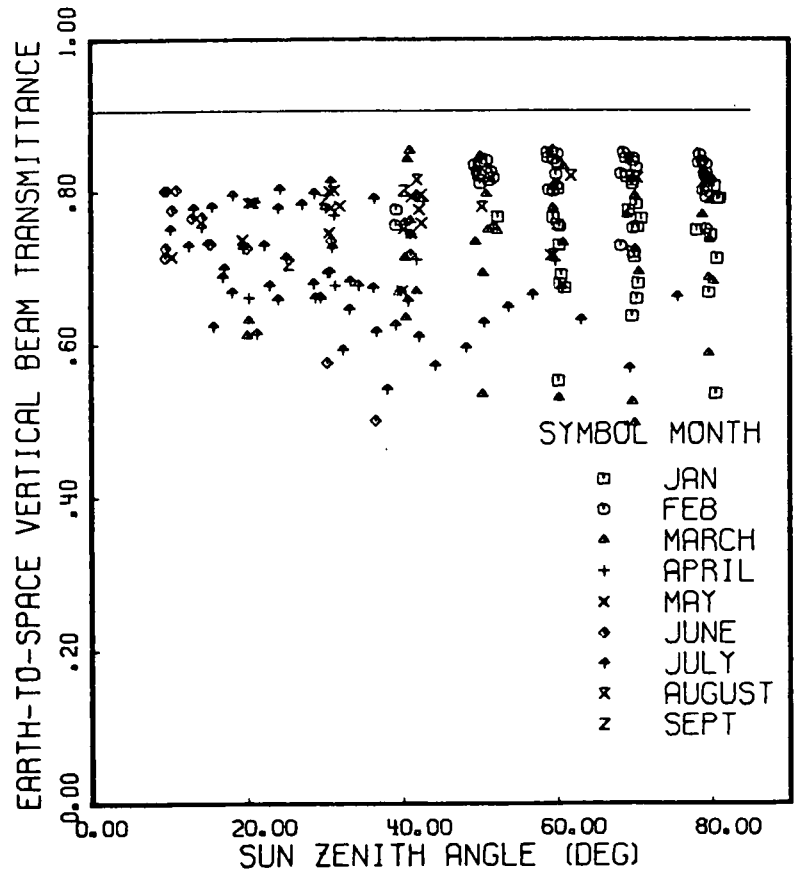

Fig. 2-3. Photopic Earth to Space Vertical Beam Transmittance as measured by the Solar Transmissometer at the Visibility Laboratory, San Diego in 1964.

two data sets total approximately 570 points, measured during all seasons at various locations. These two data sets indicate photopic space-to-earth transmittance lies in the 0.9 to 0.5 range when the sun is unobscured.

By evaluating transmittances from 0.9 to 0.5 at set intervals of 0.1, it was possible to explore the influence on given variables of a range of proportional scattering functions for a constant transmittance, or a range of transmittances for one proportional scattering function, as well as the overall range of reasonable values for that variable. The resultant 22 combinations of Barteneva scattering class functions and beam transmittances used for the model atmosphere computations are summarized in Table 2.2.

The model atmosphere equations were evaluated for seven sun zenith angles: 0°, 20°, 40°, 60°, 70°, 80° and 85°. Also a full range of scalar albedos were assumed: 0 as the lower limit case, 0.04 representing dark forest, 0.10 for fields, 0.20 for desert, 0.80 for fresh snow and 1.0 the upper limiting case. The ground-level atmospheric optical properties computed were: sky and total downwelling irradiance, earth-to-space vertical path radiance and reflectance, equilibrium radiance and reflectance as a function of angle from sun, sky radiance and path function.

Table 2.2. Transmittance and Scattering Function Specifications for Evaluation of Model Atmosphere Equations

Earth-to-Space Vertical Transmittance	Barteneva Scattering Function Class No.								Total No. of Cases
0.9	2	3							2
0.8	2	3	4	5					4
0.7		3	4	5	5′	6			5
0.6		3	4	5	5′	6			5
0.5			4	5	5′	6	6′	7	6
Total No. of Cases	2	4	4	4	3	3	1	1	22

The model atmosphere values for sky irradiance on a horizontal plane are directly affected by the scalar albedo. There is a factor of 2 or more to 1 between the sky irradiance for 1.0 and zero scalar albedos. The factor increases as solar zenith angle increases and increases as transmittance decreases, to a maximum factor of 5.5 for sun zenith angle 85° and a beam transmittance of 0.5.

The computed sky irradiance increases with scattering function class number, all else being equal. The average values of sky irradiance for each transmittance are graphed as a function sun zenith angle for the 0.10 scalar albedo case in the left graph of Fig. 2-4. The values for the Rayleigh case albedo 0.10 are given as a solid curve. The range of sky irradiance for albedo 0.10 due to changing scattering function class is within ± 0.17 of the average for each transmittance. Since scalar albedo 0.10 not only represents cultivated fields but is a reasonable average albedo for non-snow covered terrains, the sky irradiances in Fig. 2-4 may be considered to represent the average sky irradiance as a function of transmittance and sun zenith angle based upon the model equations and the Barteneva scattering functions.

Total irradiance is the sum of the sun irradiance, which is not affected by albedo, and the sky irradiance. Hence it is less affected by albedo than the sky irradiance.

The average values of total irradiance for scalar albedo 0.10 for each transmittance are graphed as a function of sun zenith angle in the right hand graph of Fig. 2-4. The total irradiance for the photopic Rayleigh atmosphere for 0.10 scalar albedo is given as a solid curve, as well as the total irradiance from Brown (1952) for the average clear day. The Brown curve is similar to the model average values for 0.70 transmittance for sun zenith angles 0 to 70° but is higher at sun zenith angles 80 and 85 degrees.

The range of total irradiance due to changing scattering function for albedo 0.10 is small, being within ± 0.045 of the average for each transmittance.

The interpretation of these modeled optical properties is continuing. The understanding of the boundary conditions and trends indicated by these data should contribute to the basic diagnostic evaluation of the OPAQUE in-flight measurements, and should also establish a framework against which the codification of real world optical atmospheric properties might be established.

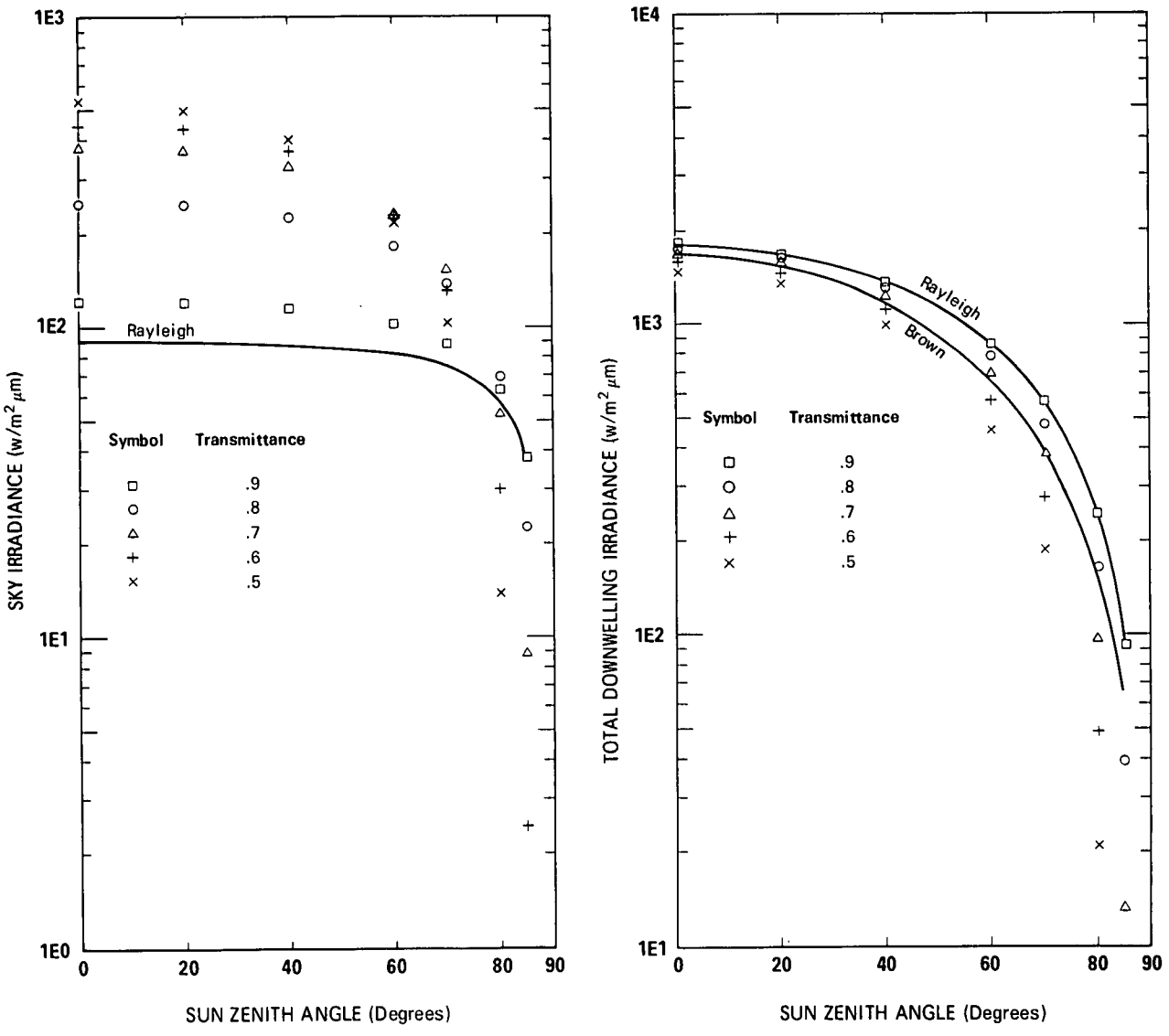

Fig. 2-4. Average Sky and Total Irradiance for a Model Atmosphere (For Transmittances 0.9 to 0.5 and Scalar Albedo 0.1 with Gordon (1969) Model and Barteneva (1960) Scattering Functions).

2.3. PROCEDURES FOR CLOUDY DAYS

As noted at the beginning of this section, the underlying basis for the computations employed during this contract interval were established under the concept of clear day conditions. In many applications, however, particularly those associated with the European weather regime as is program OPAQUE, clear days are in short supply and do not represent the conditions of critical interest. Consequently, during the progress of this contract, several concepts have been under development to improve the applicability of the computational and interpretive procedures to the cloudy day situation. Two of these concepts, equilibrium reflectance, $R_q(z,\theta,\phi)$ and the correlation between cloud cover and total irradiance are discussed in the following paragraphs.

EQUILIBRIUM RADIANCE AND REFLECTANCE

On clear days the equilibrium radiance has been found to be relatively invariant with altitude (Fig. 2, Gordon (1969)). It was this constancy with altitude which led to the use of Eq. A.24 and the interpolation of equilibrium radiance between the fixed altitudes of the straight and level flight elements to establish equilibrium radiance profiles. These interpolated equilibrium radiances were then used with the measured total volume scattering coefficients to obtain path function $N_*(z,\theta,\phi)$ using Eq. A.23.

The variable path function meter measures path function for one path of sight during the vertical profile flight elements. Usually the meter is directed so as to measure the path function for the vertically downward path of sight. This path of sight is often at scattering angles from the sun of between 90 and 120°, that is, near the angle of inflection for the volume scattering function. Hence, small changes in sun angle or path function meter position have little effect on the path function value.

The point function equilibrium radiance, $N_q(z,\theta,\phi)$, for non-clear days can be computed from measured path function, $N_*(z,\theta,\phi)$, and total volume scattering coefficient, $s(z)$, by rearranging Eq. (A.23) as follows:

$$N_q(z,\theta,\phi) = N_*(z,\theta,\phi)/s(z) \ . \tag{2.3}$$

Fig. 2-5 presents a sample graph of computed equilibrium radiance in the lower right-hand quadrant. The total volume scattering coefficient and path function measurements from which it was computed are in the upper half of the figure. In the lower left hand of the figure is a graph of the measured downwelling irradiance. The data are for Flight C-399 which was flown in northwestern France during the OPAQUE II deployment on 3 December 1976. It was a midday flight with scattered low clouds and high overcast. The volume scattering coefficient and irradiance data for this flight were reported in Duntley, *et al.* (1978a). The path function path of sight was vertically downward at 180° zenith angle. The sun zenith angle was 70° to 71° and the scattering angle from the sun for the path of sight was 109° to 110° for the three filters.

Note that most of the path function data for Filter 5 (52 out of 69 data points) were offscale low and thus graphed at the minimum calibratable value (MCV). Thus equilibrium radiance is not shown for Filter 5 since the few remaining data values for path function are unreliable when so nearly offscale low. Note also that the decrease in computed equilibrium radiance at the lower altitudes is similar to the decrease in irradiance at the same altitudes.

Equilibrium reflectance $R_q(z,\theta,\phi)$ is defined as a function of the equilibrium radiance and the downwelling irradiance $H(z,d)$

$$R_q(z,\theta,\phi) \equiv \pi N_q(z,\theta,\phi)/H(z,d) \ . \tag{2.4}$$

The equilibrium reflectance computed for the vertical downward path of sight for Flight C-399 is presented in Fig. 2-6. Whereas the equilibrium radiance tended to be less variant with altitude than the path function or the total volume scattering coefficient, the equilibrium reflectance is even more invariant with altitude than all its component parameters and the equilibrium radiance. This is illustrated in Table 2.3 which gives the fractional standard deviation of each of the measured parameters and the computed equilibrium radiance and reflectance.

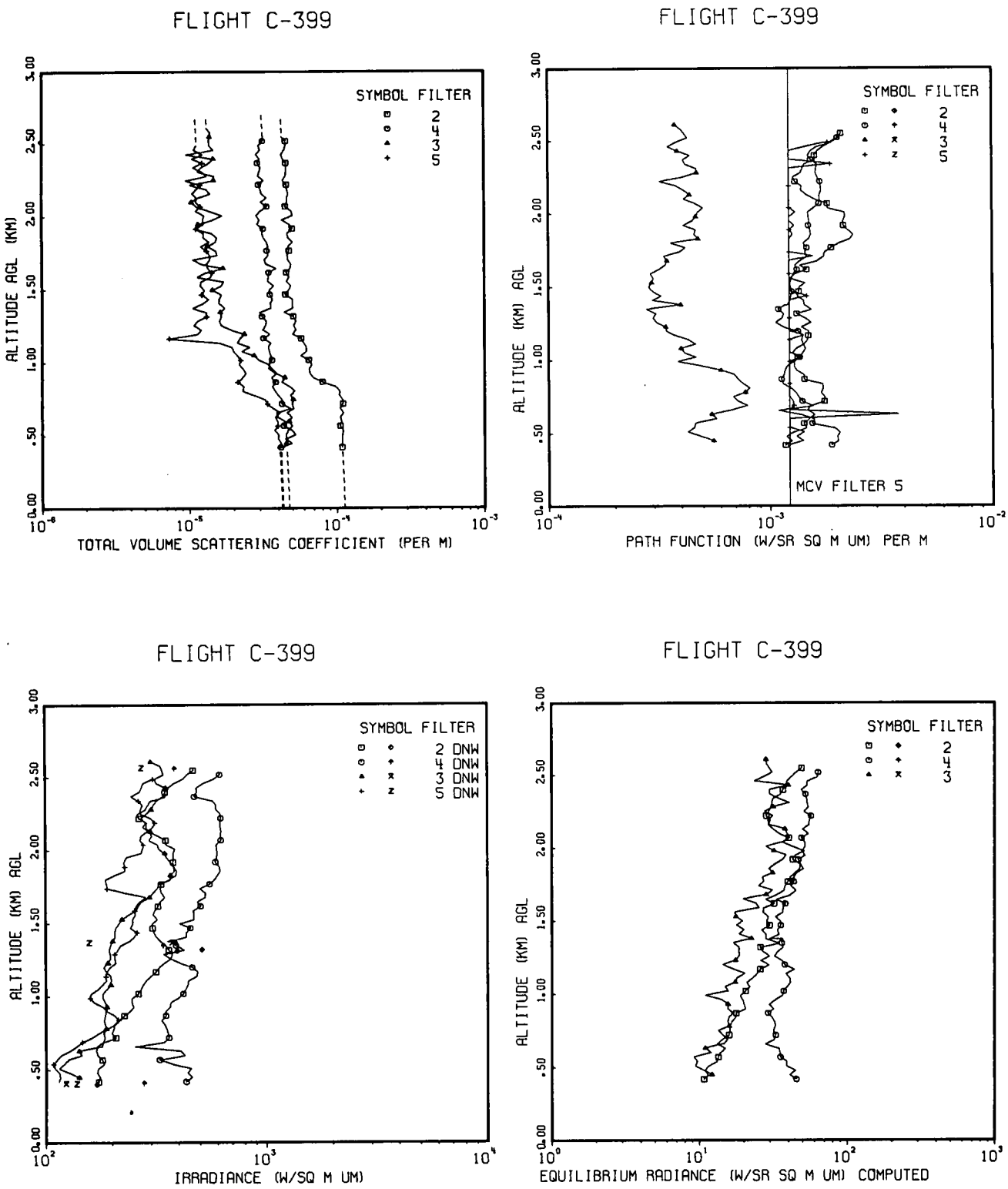

Fig. 2-5. Total Volume Scattering Coefficient, Path Function, Irradiance, and Computed Equilibrium Radiance for Flight C-399.

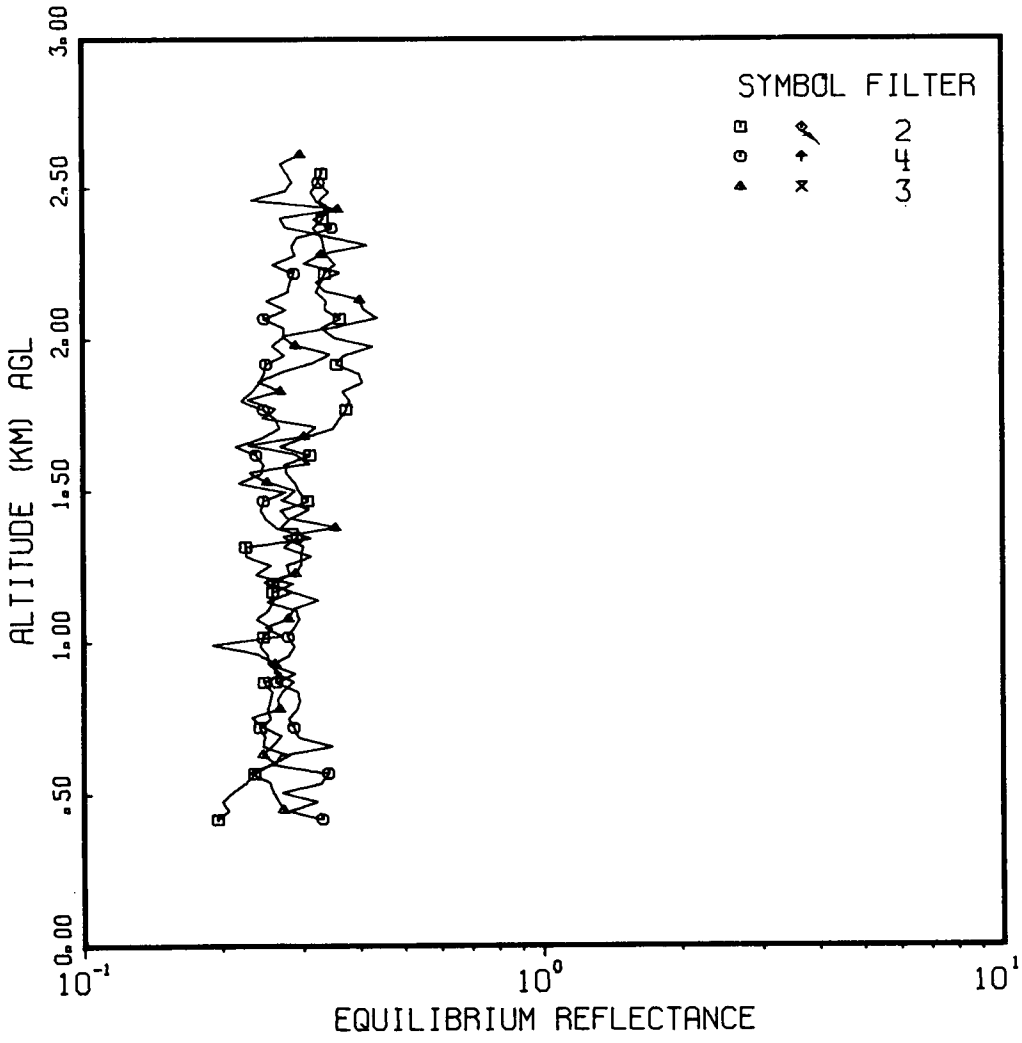

Fig. 2-6. Equilibrium Reflectance Computed for Flight C-399.

Table 2.3. Fractional Standard Deviation of Equilibrium Radiance and Reflectance for Flight C-399

Filter	Fractional Standard Deviation				
	Total Volume Scattering Coefficient	Path Function	Equilibrium Radiance	Downwelling Irradiance	Equilibrium Reflectance
2	.39	.19	.38	.25	.18
3	.15	.17	.22	.21	.11
4	.60	.30	.38	.30	.16

The flights for OPAQUE II were all under conditions of scattered to broken clouds or under overcast yet the computed equilibrium reflectances were relatively invariant with altitude for a large proportion of the profiles. In fact, large deviations in equilibrium reflectance could generally be traced to a few values in a single measured parameter which might be questionable.

The relative invariance of equilibrium reflectance with altitude for paths of sight near 90° can thus be used as a diagnostic to test the consistency of measured values of total volume scattering coefficient, downwelling irradiance, and path function.

A more important ramification is that through the use of the R_q concept, the computational technique for computing path reflectance can be modified so that it is equally as valid for cloudy day data as it is for clear day data. Hitherto, the equilibrium radiance was computed by means of Eq. A.24 and then interpolated by altitude before path function, path radiance and path reflectance were computed. By computing equilibrium reflectance (or the proportional equilibrium radiance function $N_q(z,\beta)/h(z)$ which is even better for theoretical reasons to be explained next) and interpolating this parameter with altitude, a parameter is used which is relatively invariant with altitude for both clear and cloudy days.

MODEL COMPARISONS

The model atmospheres described in Section 2.2 have been used in evaluating the R_q concept. The initial analysis of the values for equilibrium radiance and equilibrium reflectance indicates consistency with the findings in equilibrium radiance and reflectance computed from path function and total volume scattering coefficient measurements.

The range of values (from 22 combinations of transmittance and proportional scattering function) for equilibrium radiance and reflectance for scalar albedo 0.10 is summarized in Table 2.4. This table is the ratio of the maximum to the minimum value of equilibrium radiance and reflectance for a constant angle from sun β regardless of earth-to-space beam transmittance or scattering function. The table summarizes the value at scattering angle 0°, 180° and at the scattering function inflection angle which lies between 90° and 120°. The maximum to minimum ratio or range of values for equilibrium reflectance is smaller than for the equilibrium radiance except at small sun zenith angles. This difference in range is dramatic.

This is consistent with the findings of point function equilibrium radiance and reflectance computed from airborne data as described in the previous paragraphs. Those data were for scattering angles near the inflection of the scattering function (i.e., β=90–120°) and sun zenith angles greater than 60°. For those data the range of equilibrium reflectance as indicated by the fractional standard deviation, was less than the range of values for equilibrium radiance for the same vertical flight profile.

Equilibrium radiance does not have the same cosine weighting as the flat plate irradiance. Therefore dividing the equilibrium radiance by the total scalar irradiance $h(z)$ more clearly neutralizes the effect of changes in the ambient lighting than dividing by the flat plate irradiance $H(z,d)$. The ratio $N_q(\beta)/h$ is designated as the proportional equilibrium radiance function. The range of values for the proportional equilibrium radiance function is also summarized in Table 2.4. The range of this parameter essentially does not vary with sun zenith angle. In addition, its range is nearly equivalent to the smallest range for both the equilibrium radiance and reflectance.

Table 2.4. Summary of ratios of maximum to minimum value of equilibrium radiance and reflectance and proportional equilibrium radiance function $N_q(\beta)/h$ for albedo 0.10 from the photopic non-Rayleigh model atmosphere calculations

Optical Property	Scattering Angle β	MAX/MIN						
		Sun Zenith Angle = 0	20	40	60	70	80	85
Equilibrium Radiance $N_q(\beta)$	0°	2.46	2.43	2.41	2.85	4.40	16.9	276.
	90°-120°	1.39	1.36	1.43	1.97	3.69	18.8	325.
	180°	2.55	2.59	2.86	4.18	7.36	38.1	665.
Equilibrium Reflectance $R_q(\beta)$	0°	2.69	2.65	2.55	2.37	2.22	2.27	2.56
	90°-120°	1.51	1.50	1.43	1.32	1.34	1.62	2.14
	180°	2.43	2.39	2.33	2.38	2.53	3.34	4.40
All sun zenith angles								
$N_q(\beta)/h$ Proportional Equilibrium Radiance Function	0°	2.66						
	90°-120°	1.43						
	180°	2.44						

The proportional equilibrium radiance function is the parameter which will be computed from the airborne data after using Eq. A.24 to obtain equilibrium radiance, before interpolating by altitude and computing the path function, path radiance and path reflectance as described in Appendix B and illustrated in Fig. 2-1. Thus, the changes in ambient lighting so prevalent on days with scattered to broken clouds, should be adequately neutralized and the computational techniques made appropriate for both clear and cloudy days.

CLOUD COVER AND TOTAL IRRADIANCE

A continuing goal of the joint program conducted by the Geophysics and Visibility Laboratories has been the classification of the relationships between the optical properties of the atmosphere and the meteorological specifications of that atmosphere. One of the common meteorological parameters used to describe the state of the atmosphere is cloud cover. A preliminary effort to establish the correlation between the optical property of downwelling irradiance, and the meteorological property of cloud cover has begun and seems appropriate for application to the typically cloudy day OPAQUE data base.

The OPAQUE III report, Duntley, *et al.* (1978b) contains two tables which were used for this purpose. Table 7.2 in that report contained a summary of the cloud cover for each straight and level flight element based upon hemispherical pictures taken during the flight element and the in-flight

descriptions of the sky by the meteorologist on-board the aircraft. Table 8.6 in the same report contained the ratio of the total irradiance measured during straight and level flight element to the clear day photopic downwelling irradiance based on Brown (1952) for the same sun zenith angle. During the straight and level flight elements the irradiometer is kept horizontal within relatively close angular tolerances except in a few cases as noted in the table.

The irradiance ratios were averaged for each filter for each cloud cover category clear ○ , scattered ◔ , broken ◑ , and overcast ⊕ . If the cloud situation was variable over the flight track so that more than one cloud category was indicated in Table 7.2, the irradiance ratio was used for both cloud categories. The irradiance ratios for Flight C-414 were not used in the averages since the plane altitude was highly variable during this flight and the irradiance ratios were larger than all the other values for those cloud categories.

The averages of the total irradiance divided by the Brown irradiance for each cloud cover category are summarized in Table 2.5.

Table 2.5. Average Ratios of Total Irradiance Divided by Irradiance from Brown (1952) for same Sun Zenith Angle as a Function of Filter and Cloud Category for the Straight and Level Flight Elements during OPAQUE III

Cloud Category	Average Irradiance Ratio, Total/Brown			
	Filter 2 Mean Wavelength 478	Filter 4 Mean Wavelength 557	Filter 3 Mean Wavelength 664	Filter 5 Mean Wavelength 765
Clear	1.11	-	.77	-
Scattered	1.12	.96	.82	.56
Broken	1.03	.90	.80	.55
Overcast	.63	.51	.50	.30
Clear Rayleigh	1.06	1.01	.88	.71

Dividing by the irradiance based on the photopic Brown (1952) values essentially takes out the effect of sun zenith angle, thus allowing a direct comparison for the other factors of cloud cover and optical filter.

To obtain an idea of the expected effect by filter for a clear day, the sun irradiance for sun zenith angle 0° was computed for a Rayleigh atmosphere for each filter and this value divided by the Brown irradiance. These ratios are given in the bottom row of Table 2.5. This ratio shows a decrease of the irradiance ratio with mean wavelength of filter which is consistent with the general trend of the average irradiance ratios from the OPAQUE III data.

The correlation of the average irradiance ratios with cloud cover in Table 2.5 is consistent with Fig. 6 from Brown (1952) which is depicted herein as Fig. 2-7. The average cloud condition curve in Fig. 2-7 is comparable to an illuminance (or irradiance) ratio with the clear day curve of 0.5 and the extreme cloud curve is comparable to an illuminance or irradiance ratio of 0.1. Thus, Brown correlated the ratio of the measured illuminance to the clear day illuminance to cloud conditions but did not use the terminology of the meteorological observations on cloud cover.

Note that the average ratio in Table 2.5 for overcast for Filter 4 (the filter similar to the photopic filter used by Brown) is 0.51 which is directly comparable to Brown's ratio of 0.5 for average cloud conditions.

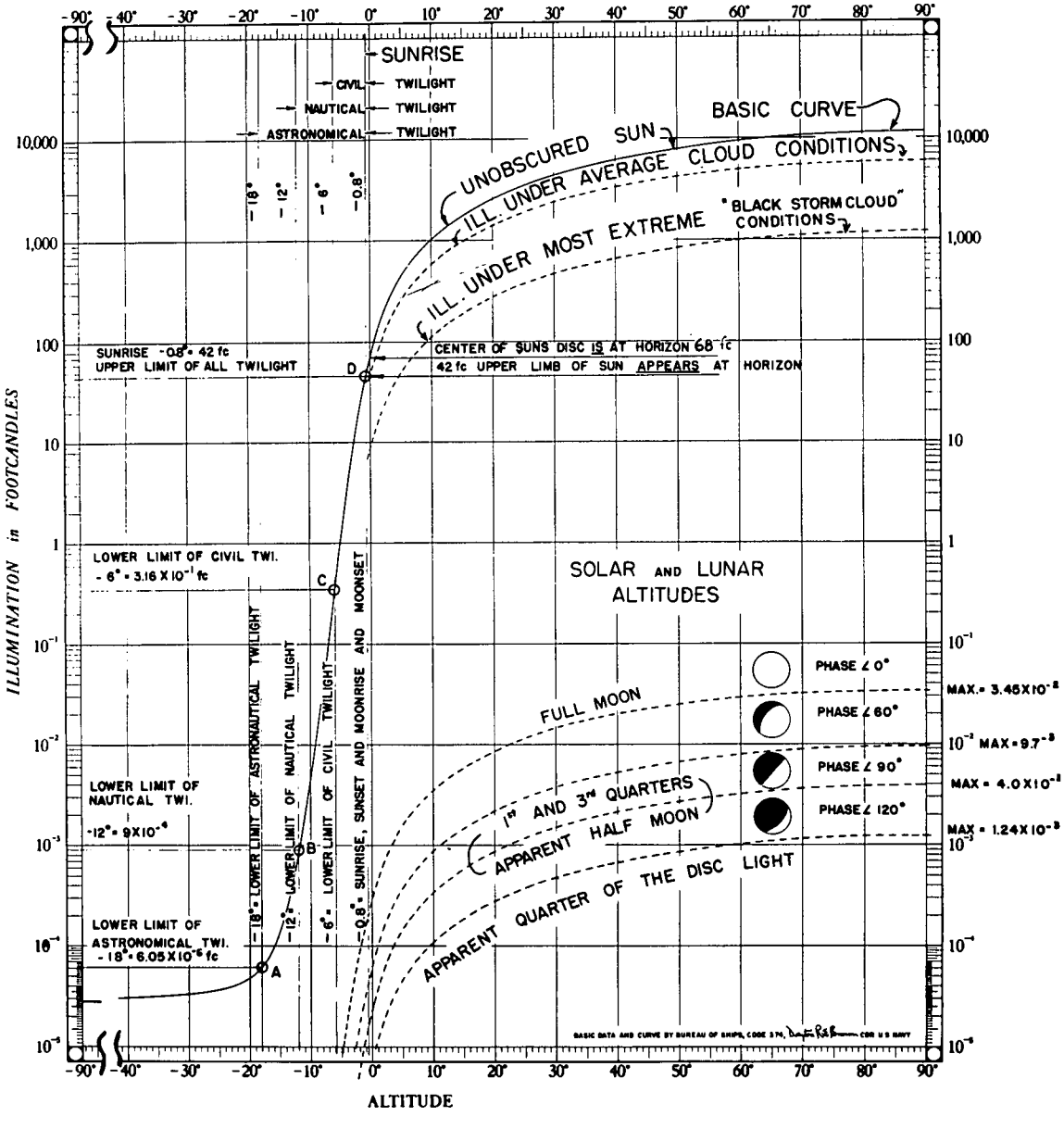

Fig. 2-7. Photopic Downwelling Illuminance as a Function of Sun Altitude from Brown (1952).

This is sufficiently encouraging that the analysis should be extended to other OPAQUE data, both the airborne data and the data from the OPAQUE ground stations. Validation studies could readily be accomplished on the extensive and well controlled data base presently on tape from the early 1964 experiments at the Visibility Laboratory's rooftop station. In any case, it is quite encouraging to have obtained such an initially good correlation from such a highly variable set of cloud cover conditions as were encountered during the flights on OPAQUE III.

3. INSTRUMENTATION

The scientific instrumentation utilized during the interval 1 August 1975 through 30 September 1978 was first described in AFCRL-70-0137, Duntley, *et al.* (1970). In that report, the descriptions of the radiometric systems reflected the nighttime, low flux configuration for which they were initially designed and fabricated. Subsequent to that report, several additional reports were issued which described in general the basic system modifications required to convert the radiometric devices from nighttime to daytime operating configurations, and to debug the electrical and optical characteristics of the resultant modified system. The first was AFCRL-72-0255, Duntley, *et al.* (1972a), a second was AFCRL-72-0461, Duntley, *et al.* (1972b), a third, AFCRL-72-0593, Duntley, *et al.* (1972c), and a fourth AFCRL-TR-0457, Duntley, *et al.* (1975b) which summarized all modifications up to August 1975.

The atmospheric visibility program discussed in this report has been planned and organized as a continuing activity under the sponsorship of the Air Force Geophysics Laboratory. Thus, a variety of instrumentation modifications have been implemented by the Visibility Laboratory not only to improve the systems reliability and quality, but also to maintain continuing applicability to the changing requirements as priorities shifted from night to daytime operations, and from clear day to cluttered, poor weather flight conditions. The following paragraphs summarize the most significant of these modifications which have been implemented subsequent to the period reported in AFCRL-TR-75-0457, Duntley, *et al.* (1975b).

All primary instrument systems and subassemblies utilized during this report interval are tabulated in Table 3.1 and illustrated in their deployment configurations in Fig. 3-1 and 3-2.

3.1. RADIOMETRIC SYSTEMS

MULTIPLIER PHOTOTUBE AND RADIOMETER MEASURING CIRCUIT ASSEMBLIES

The multiplier phototube assemblies and the related radiometer measuring circuit assemblies first described in AFCRL-70-0137, Duntley, *et al.* (1970), have been superceded by the integrated radiation detection assembly described in AFCRL-TR-75-0457, Duntley, *et al.* (1975b).

Table 3.1. Project Instrumentation

I. Radiometric

A. Multiplier Phototube Assembly
B. Temperature Control Housing Assembly
C. Optical Filter Assembly
D. Radiometer Measuring Circuit Assembly
E. Optical Collector Assembly

1. Automatic 2π Scanner Assembly
2. Integrating Nephelometer Mode Selector Head Subassembly
3. Dual Irradiometer Assembly
4. Variable Path Function Meter Assembly
5. Equilibrium Radiance Telephotometer
6. Contrast Reduction Meter

II. Meteorological

A. Royco Model 220 Particle Counter
B. Cambridge Model 137-C3 Aircraft Hygrometer System
C. AN/AMQ-17 Aerograph Set
D. Bourns Model 430/530 Absolute Pressure Transducer
E. Bourns Model 509 Differential Pressure Transducer
F. Bendix Model 566 Aspirated Hygrometer
G. Science Associates Windspeed and Direction Set
H. Taylor Model SMT-5-51 Aneroid Barometer

III. Control and Communication

A. Automatic 2π Scanner Control Console
B. Photometer Temperature Control Panel
C. Optical Filter Control Panel
D. Camera Control Panel
E. Flight Dynamics Display Panel
F. 42 Channel Data Logger

IV. Photographic

A. Automax G-1 Airborne Camera System
B. Ground-Based Soligor System
C. Ground-Based Northridge Camera System

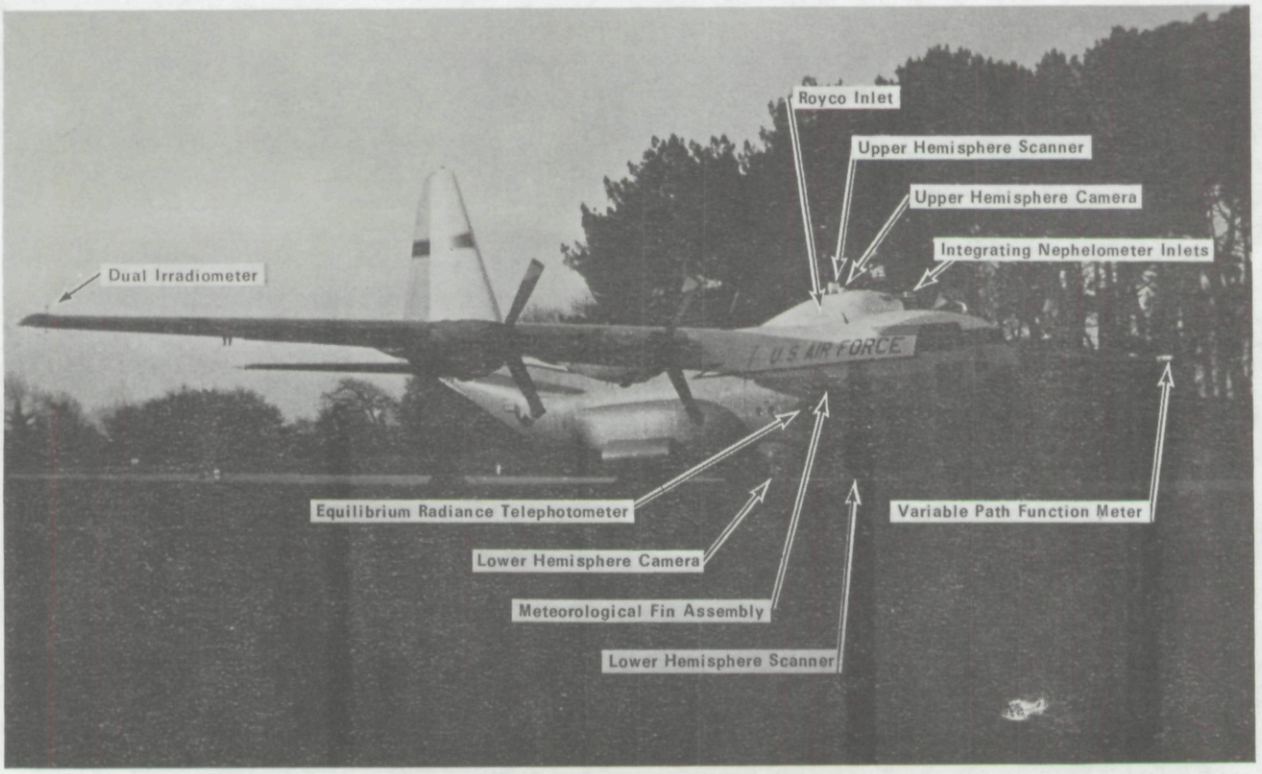

Fig. 3-1. C-130 Airborne Instrument System.

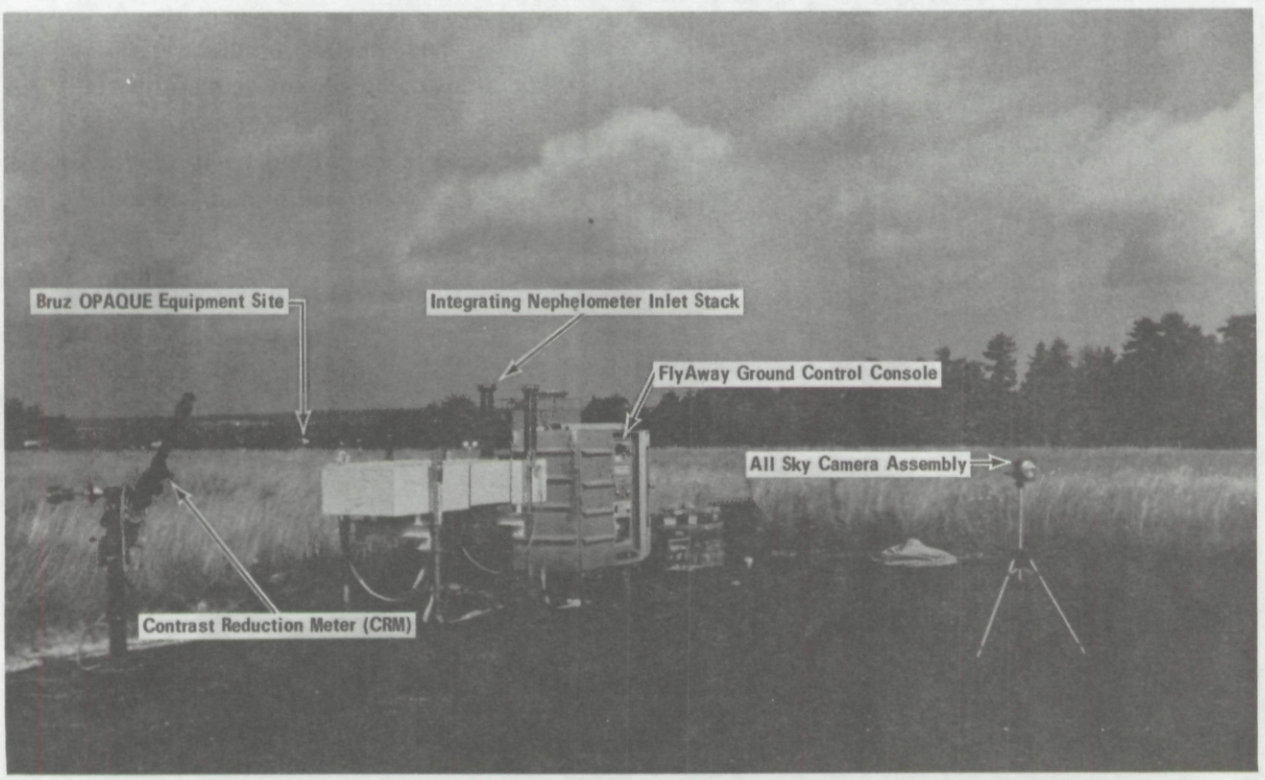

Fig. 3-2. Ground-Based Instrument System.

The prototype of this new system was successfully test flown during the SEEKVAL deployment of July 1974 which was reported in AFCRL-TR-75-0414, Duntley, *et al.* (1975a). As a result of this very satisfactorily completed field test, a retrofit of the new system was made to each project radiometer prior to the OPAQUE I deployment in April, 1976.

OPTICAL FILTER ASSEMBLY

As recommended in AFCRL-TR-75-0457, Duntley, *et al.* (1975b), the optical filter assembly used with each project radiometer system was modified to eliminate an undesirable biasing signal produced by stray MEMORY flux within the housing. This modification was accomplished by removing the swinging mirror feature originally described in AFCRL-70-0137, Duntley, *et al.* (1970) and replacing it with a fixed mirror and a rotating cutoff sleeve.

This modification, which was a direct retrofit into the original basic housing was first flown as a prototype during the OPAQUE III deployment in the summer of 1977. For this first field test, the modified filter assembly was used on the dual irradiometer system throughout the deployment. There were no system anomalies induced by the modification, which worked reliably throughout the twelve mission deployment. Pre and Post-Deployment calibration data were markedly improved by the surpression of the stray MEMORY flux. Consequently, all project radiometer filter assemblies were updated with this new MEMORY cutoff system prior to the OPAQUE IV deployment in January 1978.

The radiometer spectral responses were standardized during this contract interval, as illustrated in Fig. 3-3. They were discussed in detail in Section 3.6 of AFCRL-TR-73-0422, Duntley, *et al.* (1973). For the daytime flights conducted during the five OPAQUE deployments, only filter selections 2, 3, 4, and 5 were used for data collection. Filter number 4, the pseudo-photopic response is quite similar to the photopic response utilized for optical measurements at each of the participating NATO OPAQUE data stations. Filter number 6, the S-20 response is actually an "open hole" filter selection which was not used during the OPAQUE flight program.

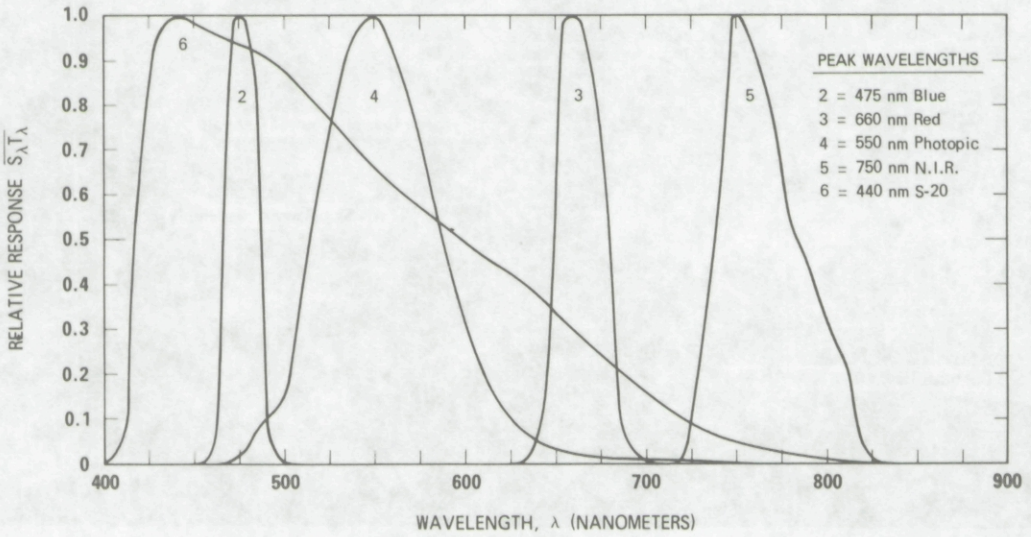

Fig. 3-3. Standard Spectral Responses.

OPTICAL COLLECTOR ASSEMBLIES

Of the seven optical collector assemblies listed in Table 3.1, only the integrating nephelometer system has had major modification during this contract interval.

The conversion of the airborne integrating nephelometer from its original straight through design as illustrated in AFCRL-70-0137, Duntley, *et al.* (1970), into a more compact, folded path configuration was initiated in late 1974. By April 1975 the revised folded path configuration was satisfactorily defined and the redesign and refabrication task was begun as discussed in AFCRL-TR-75-0457, Duntley, *et al.* (1975b). This refabrication was completed and the new system was reinstalled on the project aircraft prior to the OPAQUE I deployment in April, 1976. The revised folded path configuration is illustrated in Figs. 3-4 and 3-5.

In Fig. 3-4 the integrating nephelometer in its trapezoidal shroud is to the right, and the upper hemisphere scanner and camera assemblies are to the left. The entire structure fits within the modified radome assembly shown in Fig. 3-1.

In Fig. 3-5 the nephelometer shroud is shown in the open position illustrating the location of the projector assembly on the right, with the top of the mode selector head appearing immediately to the left of the projector lamp housing.

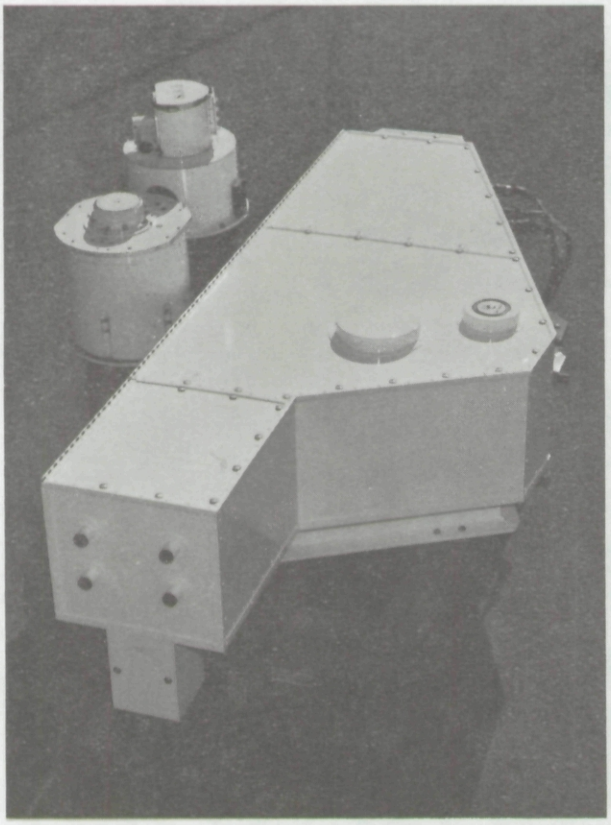

Fig. 3-4. Airborne Folded Path Integrating Nephelometer Assembly, Shroud Closed

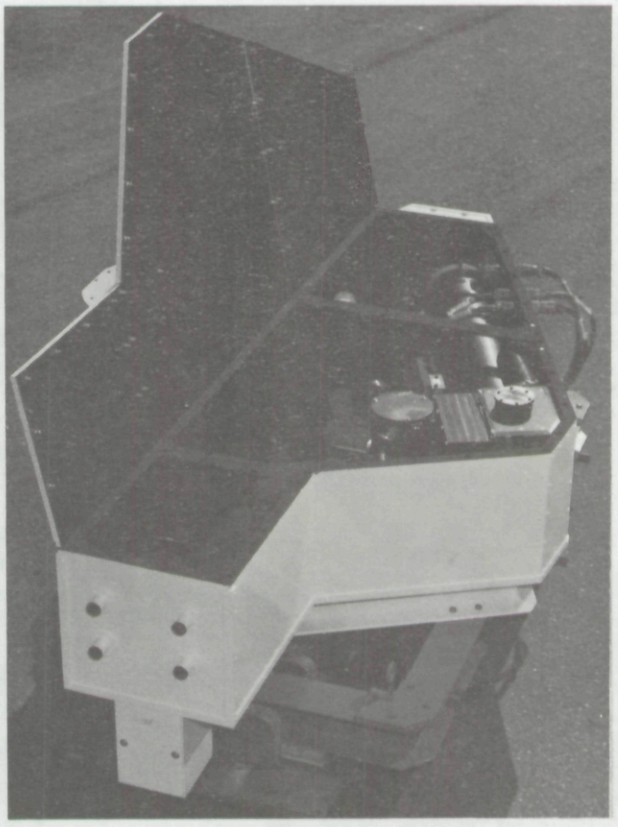

Fig. 3-5. Airborne Folded Path Integrating Nephelometer Assembly, Shroud Open

A summary of the systems optical and operating characteristics has been presented in AFGL-TR-77-0078, Duntley, *et al.* (1977).

Following the OPAQUE II deployment, AFGL-TR-77-0239, Duntley, *et al.* (1978a), it was decided to augment the air transportable ground station with the addition of an integrating nephelometer. This new ground based nephelometer was designed to be as identical to the airborne unit as was possible within the time and dollar constraints imposed upon its fabrication.

In order to complete the ground based nephelometer prior to the OPAQUE III departure in late June 1977, it was assembled using the component sub-assemblies previously used in the truck mounted version last utilized during Project SEEKVAL, AFCRL-TR-75-0414, Duntley, *et al.* (1975a). The new composite system thus used the same basic projector, mode selector head and detector assemblies, and folded frame that were used on the airborne system. Only the enclosing shroud and light trap were different. As an additional fabrication expediancy, the rectangular shroud from the original truck mounted system was modified to contain the new folded path configuration. Thus, the only basic difference between the airborne and ground based nephelometers is in the shroud. The rectangular configuration of the ground-based integrating nephelometer is illustrated in Fig. 3-2.

3.2. METEOROLOGICAL SYSTEMS

The airborne meteorological package during the OPAQUE deployments was basically unchanged from that reported in AFCRL-72-0593, Duntley, *et al.* (1972c). It included one Royco Model 220 particle counter, one Cambridge Model 137-C3 aircraft hygrometer system, one AMQ-17 aerograph set and two Bourns aneroid pressure transducers. Operating and maintenance instructions for these purchased items are covered in their manufacturer's brochures, e.g. "TP-133", USNAF, Indianapolis, Indiana for AMQ-17 data, "T.O. 12M3-4-2-1", EG&G Environmental Equip. Div., Waltham, Massachusetts for Cambridge 137-C3 data, and "Operating and Servicing Manual for Royco Aerosol Particle Monitor", Royco Instruments, Inc., Menlo Park, California for Royco data.

No modifications to the meteorological equipment were instituted during this contract interval, except to the Royco system. This multiple unit assembly was maintained and operated by personnel from the Geophysics Laboratory. This Air Force team made extensive "fine tune" adjustments to the system's internal and external plumbing to insure proper leak proof operation within the pressurized cabin of the C-130.

3.3. CONTROL AND COMMUNICATION SYSTEMS

The control panels, consoles, and other support facilities listed in Table 3.1 are described along with their most significant earlier modifications in AFCRL-70-0137 and AFCRL-72-0593, Duntley, *et al.* (1970 and 1972c). Only minor additional modifications have been made to these items during the contract interval covered by this report.

The Ten Slide Photometer Module which was listed in these earlier references was eliminated in early 1976 when the new integrated radiation detection circuits were implemented. At this time the

function of the Ten Slide Photometer Module and its related power supplies was replaced by a simple Photometer Power Distribution and Readout Panel. This panel, illustrated in Fig. 3-6 controls the application of +26.5 VDC regulated power to each project detector assembly, and permits manual selection of each detector output circuit for display on the built-in panel meter. With this system, the in-flight performance on any radiometer circuit can be monitored simultaneously and in parallel with the normal data logging sequence.

Fig. 3-6. Photometer Power Distribution and Readout Panel.

3.4. PHOTOGRAPHIC SYSTEMS

No modifications have been made to the airborne photographic system since the system was first reported and updated in AFCRL-72-0461, AFCRL-72-0593, and AFCRL-TR-75-0457, Duntley, *et al.* (1972b, 1972c, and 1975b).

The ground-based photographic system was however supplemented with an additional camera. Between the OPAQUE III and the OPAQUE IV deployments, a Northridge Cinetracker Model RZ15C, 35mm data camera was adapted for use using the Soligor 180° fisheye lens. This camera system using a 50 ft. film magazine and remote control circuits considerably simplified the task of ground-based sky and cloud cover documentation.

4. DATA COLLECTION METHODS

During this contract interval, several independent but OPAQUE related data collection activities were maintained in close association with one another. The basic network was of course established by the multi-nation collection of ground based data stations described in AFGL-TR-78-0011, Fenn (1978). Supplementing these fixed station operations with an extensive distribution of airborne measurements was the primary goal of the joint Geophysics Laboratory/Visibility Laboratory flight program which is summarized in this report.

The C-130 flight program was in actuality, a two part operation. That is, two independent data gathering activities were maintained simultaneously, an airborne unit, and a ground based unit. The basic concept of each experimental sequence was built around the joint operation of these two units in a highly coordinated, simultaneous measurement routine. The primary procedure followed during each of the five OPAQUE deployments was to establish a predetermined flight track in the immediate vicinity of each host nations OPAQUE data stations. (See Section 6, Figs. 6-1 thru 6-8.) The secondary feature of the procedure was to establish a preselected site for the operation of the air transportable ground unit. This site was preferably co-located with the official OPAQUE data station, but in any case was located as near the flight track as possible. Once these locations were established, the procedural routine was for each unit to run full data collection sequences at every opportunity on a daily schedule. If for any reason the joint sequences were aborted, both units were to automatically revert to independent operation. Partial data sets were thus often obtained even when the inevitable exigencies of joint field operations defeated the basic routine.

The general procedures followed by the airborne and ground based teams are well documented in Duntley, *et al.* (1970, 1975a, 1978a, etc.). Only a few comments regarding specific variations in the procedural priorities seem appropriate at this time, and they are contained in the following paragraphs.

4.1. AIRBORNE SYSTEM

The airborne data collection was accomplished through the use of an instrumented C-130A aircraft in a manner similar to that reported by Duntley, *et al.* (1970, 1975a, and 1978a). During each data collection flight, the aircraft flew a predetermined pattern within the specified test area. An illustration of a typical flight pattern is shown in Fig. 4-1. In this stylized pattern, two basic elements, the "straight and level" and the "vertical profile," are combined to yield the total mission flight plan. A more detailed description of all flight pattern elements is presented in the above referenced reports.

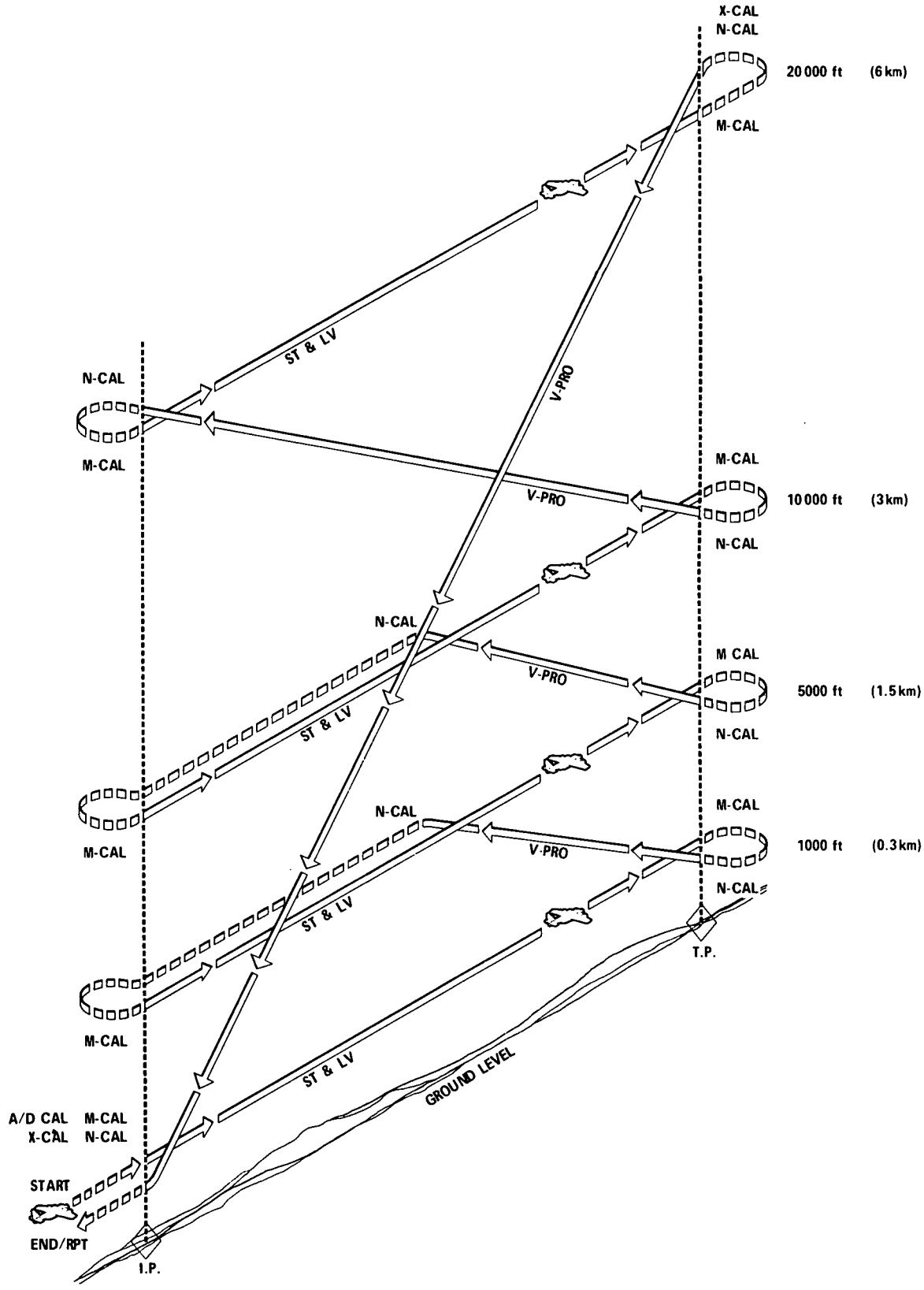

Fig. 4-1. Typical Visibility Laboratory Flight Profile.

In most previous deployments, the data collection sequence for the airborne system has been broken into five standardized elements: (1) preflight warmup, and calibration check, (2) straight and level sequences (ST&LV), (3) vertical profile sequences (V-PRO), (4) in-flight calibration checks (M-CAL and N-CAL), and (5) postflight calibration check. During any specific deployment, however, the flight profile may be customized by making minor variations in the sequence and number of these five elements.

The standardized D(2+4) flight profile, i.e. dual two plus four implying measurements made in two spectral bands at each of four altitudes with the total sequence repeated in a second pair of spectral bands, was the goal of each mission. However, due to the extreme short term variability encountered in typical European weather patterns, many variations in this basic flight pattern were utilized during the five OPAQUE deployments. Broad discretion was permitted in defining acceptable weather conditions and flight patterns in order to maximize the number of missions in the vicinity of each OPAQUE ground site.

The two most commonly substituted profiles were the "D(2+2)" and the "V-PRO ONLY" profiles.

The D(2+2) profile, in which measurements are made at only two straight and level altitudes, was normally used when there were particularly low ceilings along the track. In these instances the two altitudes chosen were 1000 ft. AGL and 500 ft. below the cloud bases.

The V-PRO ONLY profiles were flown when the cloud conditions along the track were so severe that it was impossible to maintain the ten minute straight and level runs for the automatic scanner systems. In these instances the scanner data was abandoned, and measurements of total volume scattering coefficient profiles were designated as adequate for justifying a completed mission.

A brief summary of the data flights made during this contract interval using the general procedures discussed in Section 4.1 is presented in Table 1.1. A more complete review of the data flights is presented in Section 6.

4.2. GROUND-BASED SYSTEM

The ground-based data collection sequence was designed to supplement the airborne data whenever the aircraft was operating in the immediate vicinity. However, it is also complete enough to stand alone when the aircraft mission is diverted or aborted. The general operating procedures have been described in the references noted in Section 4.1.

The ground-based instrument system has several operational responsibilities. First, it must supply a ground-level data base to allow interpolation of various measurements between ground altitude and the lowest attainable aircraft altitude. Second, it must supply long term temporal sampling of those meteorological and radiometric quantities which relate to the project task. Third, the ground system serves as a spare parts and repair facility for the entire air/ground operation. In the event of a catastrophic failure in a primary airborne instrument or assembly, the equivalent piece of instrumentation is reassigned to the aircraft from the ground-based system. The aircraft can then return to service with a minimum of "down-time," and repairs can be accomplished under the more convenient ground station conditions.

During the five OPAQUE deployments which occurred during this contract period, the ground-based system operated within one additional constraint. Due to the variety of locations visited during each deployment, it was essential that the ground-based equipment be completely transportable in the project C-130, and that it be readily deployable from the aircraft's staging bases to the data collection sites by ground vehicle.

As a result of this logistical requirement, the ground-based system was limited to only the highly portable Contrast Reduction Meter, AFGL-TR-76-0188 and AFGL-TR-77-0078, Duntley, *et al.* (1976 and 1977) during OPAQUE I and OPAQUE II. However, by the time the OPAQUE III deployment occurred, a ground-based integrating nephelometer had been devised, and it was added to the ground station inventory. During OPAQUE III, IV and V both the Contrast Reduction Meter and Ground-Based Integrating Nephelometer were in full operation. The availability of a C-130 class nephelometer at the ground site should contribute significantly to the eventual linking between the extensive OPAQUE ground level data base and the more limited Geophysics Laboratory/Visibility Laboratory airborne data, an ultimate and necessary goal in the determination of the near ground level optical-meteorological relationships.

5. DATA PROCESSING TECHNIQUE

The degree of data processing sophistication utilized during this contract interval is illustrated in Figs. 5-1 and 5-2. In these generalized flow charts, the basic functional steps utilized in the data processing of the raw field data are clearly specified. They do not illustrate, however, all of the miscellaneous routines used for data base management and special diagnostic purposes. A more complete description of each phase of the processing sequence is contained in AFCRL-72-0255, AFCRL-72-0593, AFCRL-TR-75-0457, and AFCRL-TR-76-0188, Duntley, *et al.* (1972a, 1972c, 1975b, and 1976).

During the contract interval covered by this report, the major software effort was in the development and efficient implementation of the procedures illustrated in Figs. 5-1 and 5-2. The specific emphasis on the data processing development has been twofold: directed first at isolating the automatic scanner data and streamlining the procedure of converting the measured field data directly into report format, and second, at developing an automatically documented data bank so that additional analysis using computer methods could readily be undertaken. The use of the technical documentation procedure described in AFCRL-72-0593, Duntley, *et al.* (1972c), has worked effectively in recording data quality. The implementation of the procedures outlined in AFCRL-TR-75-0457, Duntley, *et al.* (1975b) for the separate handling of the automatic 2π scanner data has been accomplished. The data presented in AFGL-TR-76-0188, Duntley, *et al.* (1976), was produced using these procedures with fully satisfactory results. Short summaries of the sub-routines utilized in the processing of these data, i.e., Programs FLTDOC, MIRESCAN, SCANTSUM, and a revised AVIZC130, are also contained in the above 1976 reference.

No substantive changes to the routines illustrated in Figs. 5-1 and 5-2 beyond those referenced above have been incorporated during this contract interval. However, a significant number of display and diagnostic options have been made available. Typical of these displays are the comparative plots of relative humidity and total volume scattering coefficient profiles illustrated in Fig. 8-11 of AFGL-TR-77-0239, Duntley, *et al.* (1978a), and Fig. 7-15 herein.

Another potentially useful display has been developed to simplify the presentation of sky and terrain radiance distributions. Program ASCANPLT operates on the data tables which list the sky and terrain radiances used for determining computed optical properties such as those reported in AFGL-TR-76-0188, Duntley, *et al.* (1976), i.e. path radiance, directional path reflectance, etc. The sky and terrain radiance tables generated for each data flight are relatively bulky, and therefore have not normally been among the items included in each technical report. However, it has been apparent for some time that many users could take advantage of this basic data base, if some convenient manner of presentation could be devised. Program ASCANPLT automatically generates iso-radiance maps as illustrated in Fig. 5-3 from each pair of sky and terrain radiance tables provided as input. In these graphical

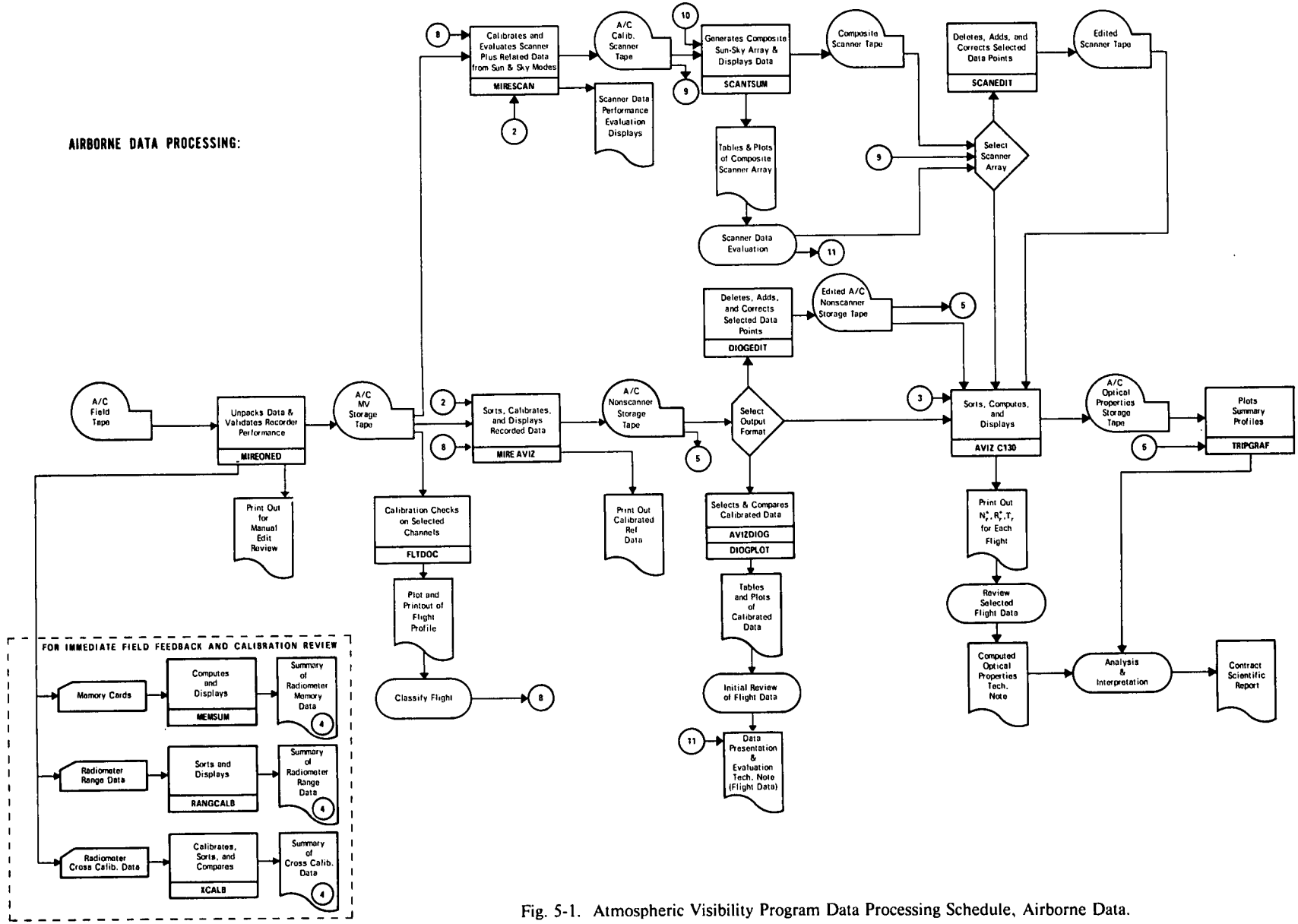

Fig. 5-1. Atmospheric Visibility Program Data Processing Schedule, Airborne Data.

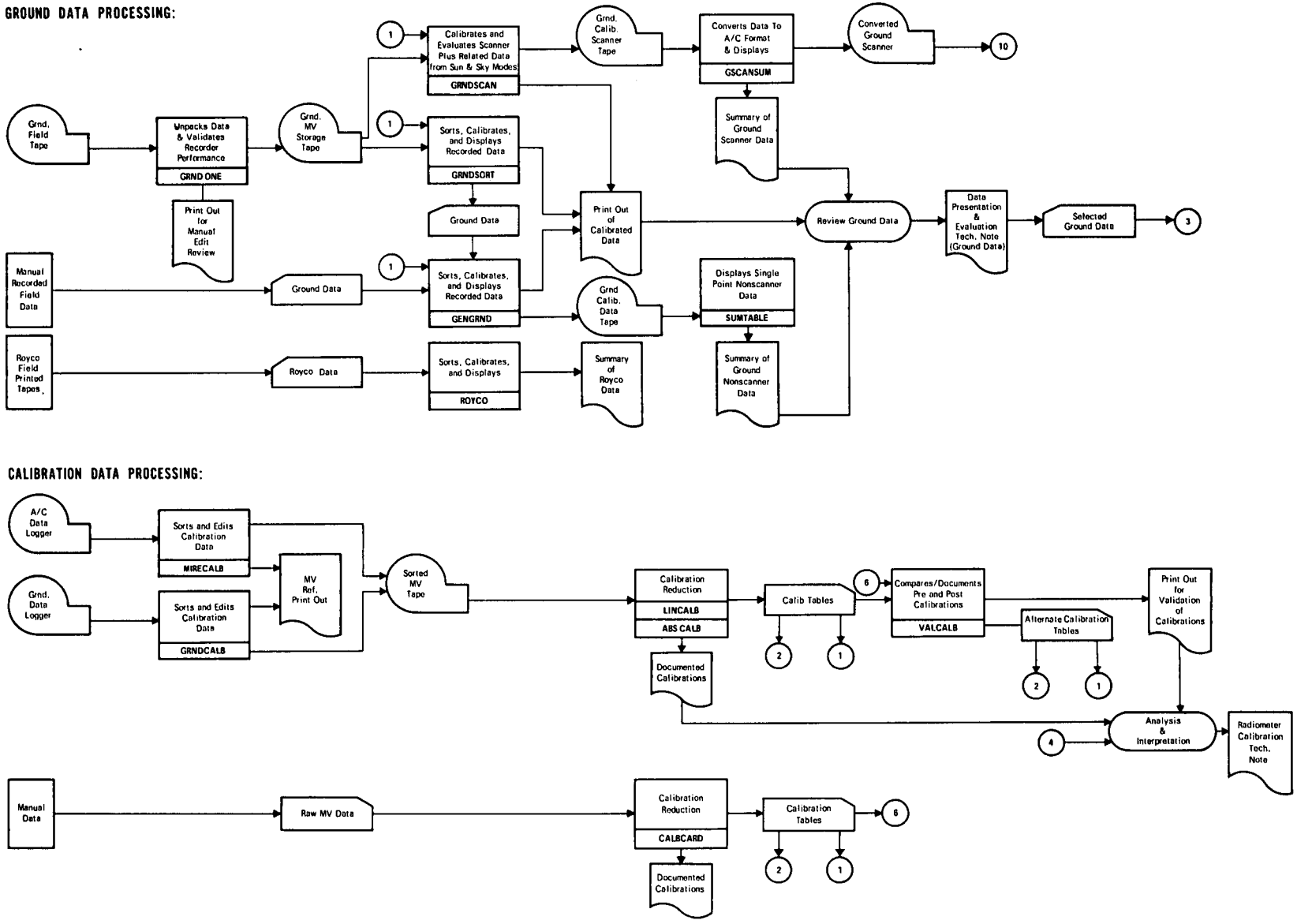

Fig. 5-2. Atmospheric Visibility Program Data Processing Schedule, Ground-Based and Calibration Data.

displays, the radiance pattern that was measured in each hemisphere is plotted in polar format. The azimuths in the display are in degrees from the sun. That is, the solar azimuth at the time of measurement has been made zero degrees azimuth in the plots. In the sky radiance plot, the center of the plot represents the zenith, and the outer periphery the horizon. In the terrain plot, the center is the nadir and the periphery the horizon.

These iso-radiance maps, in which lines of equal radiance value are connected as contours, are much more compact than tabular displays and permit rapid visual sorting of smooth or cluttered radiance patterns. A compendium of sky and terrain radiance maps of this type would be a valuable tool to many users. The development of a technique to sort and classify these representations using automatic pattern recognition routines would open the door to a broad variety of user studies and applications.

Several of the software changes implemented during the recent interval do not affect the flow chart sequencing illustrated in Figs. 5-1 and 5-2, but were among the most important ever instituted. These modifications were those instituted to permit terminal access to the basic data base and the program routines required for data base manipulation. With the capability of controlling the basic processing procedures completely by remote control via telephonic terminal access, the efficiency of the data processing was dramatically increased, and its cost substantially reduced. As both the airborne and ground level data bases from program OPAQUE become more readily available for analysis and application to the task of defining the low altitude electro-optical operating regime, quick, selective data access will become more and more important. With the imminent arrival of this next phase of the program currently upon us, the growing development of this terminal capability will soon be fully rewarded.

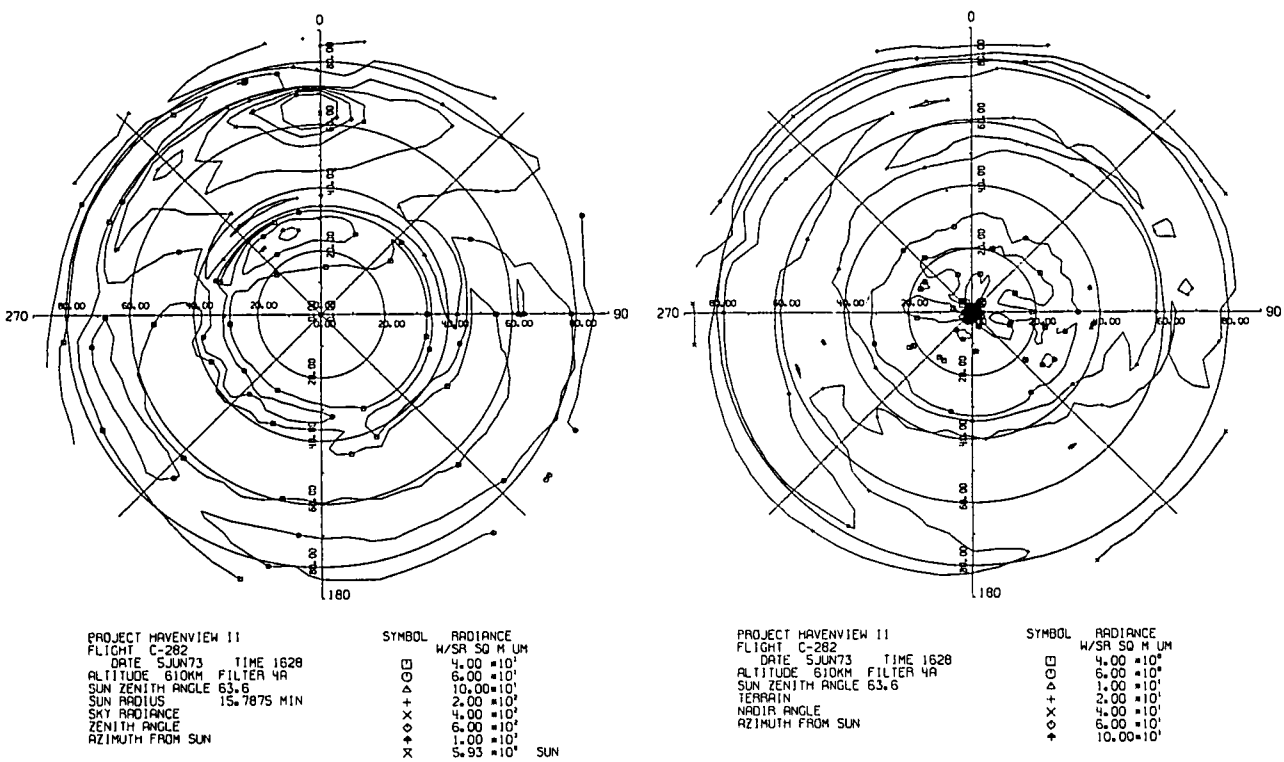

Fig. 5-3. Sky and Terrain Iso-Radiance Plots

6. DEPLOYMENT AND DATA SUMMARY

6.1. FIELD TRIP SUMMARY

During the three year contract interval described in this report, there were five major overseas deployments made in conjunction with the program OPAQUE effort. These deployments involved the airborne and ground based instrument systems described in Section 3, and were organized and coordinated through the efforts of the Air Force Geophysics Laboratory. Air Force flight crews and maintenance teams required for the operation and support of the C-130A aircraft were provided through the 4950th Test Wing at Wright-Patterson AFB. Technical flight and ground based personnel required for the operation and maintenance of the equipment described in Section 3 were provided through the Air Force Geophysics Laboratory and the Visibility Laboratory of the University of California, San Diego.

Each of the five trips was planned to provide daytime atmospheric measurements as a function of altitude in the immediate vicinity of several different OPAQUE data stations. Whereas the host nations OPAQUE stations were normally operating on a continuous basis, making hourly measurements on a 24 hour a day schedule, the C-130 would therefore be able to productively supplement these ground based measurements even though it could be over each site on only an occasional basis.

The five OPAQUE deployments were scheduled to insure a reasonably diverse geographical sampling of vertical profile data during each of the four seasons of the year, Spring, Summer, Fall, and Winter. The degree of success in achieving an optimum mix of flights was as usual determined primarily by the vagaries of the European weather pattern and the unscheduled maintenance requirements of the aircraft.

Table 6.1 lists the general location of each of the different flight tracks utilized during the OPAQUE deployments, and also the locations where the air transportable ground unit was established. As a tabulating convenience, the entries in both Table 6.1 and 6.2 are listed in order of increasing degrees of latitude. Table 6.2 tabulates the number of data missions attempted during each OPAQUE deployment. Since a flight mission is logged every time the aircraft becomes airborne and the preliminary system calibration data are recorded, not every attempt will produce usable data. Similarly, even though the data flight is completed, weather conditions may have been so marginal that only portions of the measured data are interpretable and suitable for further use, as is implied by the listings in the data summary of Section 6.3. These partially complete poor weather flight sequences may in fact be among the most valuable collected since they represent the most likely conditions under which electro-optical system performance will require critical specifications.

Table 6.1. Project OPAQUE Flight Track & Ground Sites Location & Ground Elevations

Geographical Reference and Site Identification Code		Center of Flight Track		Ground Site		Approx Gnd Elev along track
		Latitude	Longitude	Latitude	Longitude	
Ground Sites						
Catania, Sicily	(CT)	-	-	37°24'N	14°55'E	-
Trapani, Sicily	(TR)	-	-	37°55'N	12°29'E	-
Bruz, France	(BR)	-	-	48°01'N	1°45'W	-
Birkhof, Germany	(BK)	-	-	48°13'N	9°11'E	-
Yeovilton, England	(YO)	-	-	51°01'N	2°37'W	-
Soesterberg, Netherlands	(SØ)	-	-	52°08'N	5°17'E	-
Meppen, Germany	(MP)	-	-	52°52'N	7°23'E	-
Flight Tracks						
Sigonella, Sicily	(SG)	37°24'N	15°20'E	-	-	Sea Level
Trapani, Sicily	(TR)	37°33'N	12°30'E	-	-	Sea Level
Bruz, France	(BR)	48°01'N	1°41'W	-	-	50 m
Birkhof, Germany	(BK)	48°15'N	9°05'E	-	-	762 m
Yeovil, England	(YO)	50°56'N	2°27'W	-	-	60 m
Soesterberg, Netherlands	(SØ)	51°56'N	5°35'E	-	-	6 m
Mildenhall, England	(ML)	52°24'N	1°41'E	-	-	Sea Level
Ahlhorn, Germany	(AL)	52°53'N	7°51'E	-	-	18 m
Meppen, Germany	(MP)	53°00'N	7°37'E	-	-	18 m
Rodby, Denmark	(RB)	54°41'N	11°08'E	-	-	Sea Level

Table 6.2. Geographical Distribution of Project OPAQUE Data Flights

Flight Track Ident	Attempted (and reported) Data Sequences				
	OPAQUE I Spring	OPAQUE II Fall	OPAQUE III Summer	OPAQUE IV Winter	OPAQUE V Summer
Sigonella, Sicily	0	0	0	2	0
Trapani, Sicily	0	0	0	3	4
Bruz France	0	5 (5)	3 (3)	0	0
Birkhof, Germany	0	0	0	8	5
Yeovil, England	5 (3)	0	0	5	3
Soesterberg, Netherlands	1 (1)	0	1 (0)	2	2
Mildenhall, England	0	0	0	2	0
Ahlhorn, Germany	0	0	2 (2)	0	0
Meppen, Germany	5 (2)	4 (3)	3 (3)	3	4
Rodby, Denmark	2 (2)	4 (4)	4 (4)	2	2
TOTAL	13 (8)	13 (12)	13 (12)	27	20

The location and physical layout of each of the host nation OPAQUE data sites are described in AFGL-TR-78-0011, Fenn (1978). The flight track locations with respect to these sites are illustrated in Figs. 6-1 through 6-8. Fig. 6-1 illustrates the track locations with respect to the overall European operating area, while the remainder of the figures illustrate each track area in slightly greater detail. As in Tables 6.1 and 6.2, the maps are presented in order of increasing degrees of latitude, and not necessarily in the order of their chronological use.

Fig. 6-1. Typical OPAQUE Flight Tracks

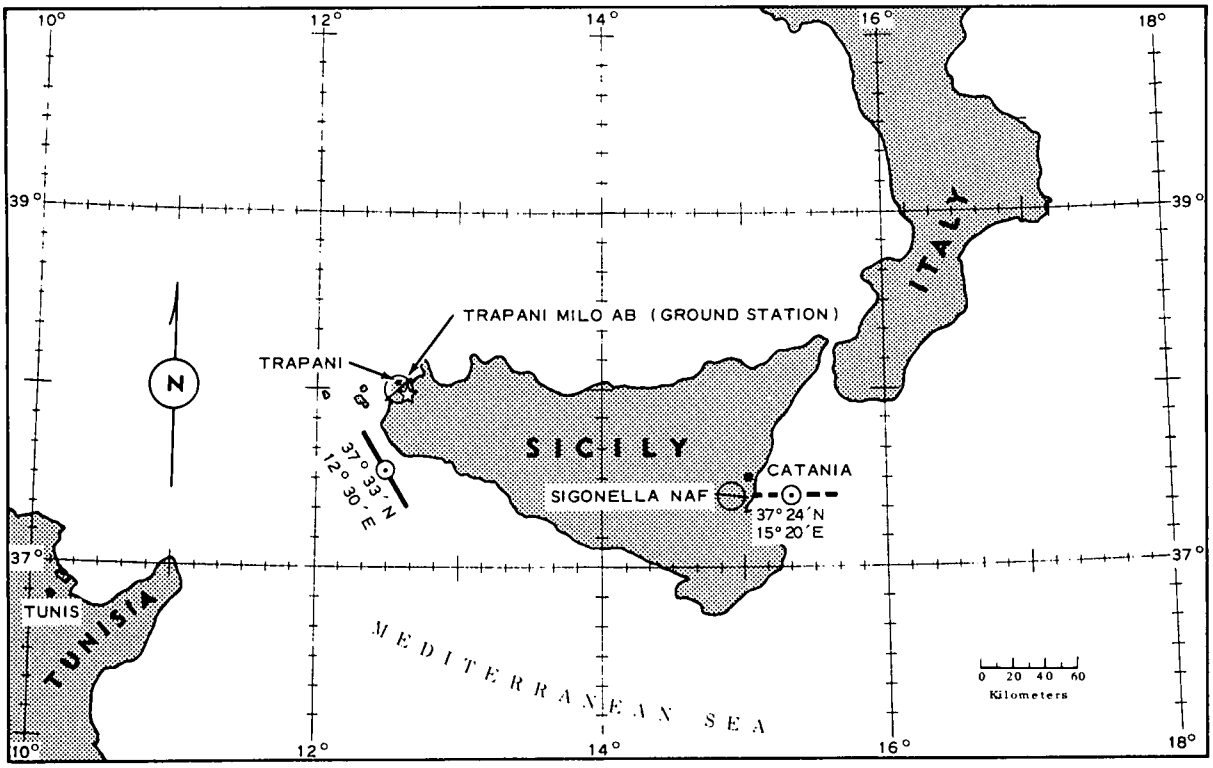

Fig. 6-2. Typical Trapani Track and Data Sites, Detail Map. Latitude and Longitude References are to Flight Track Center Point.

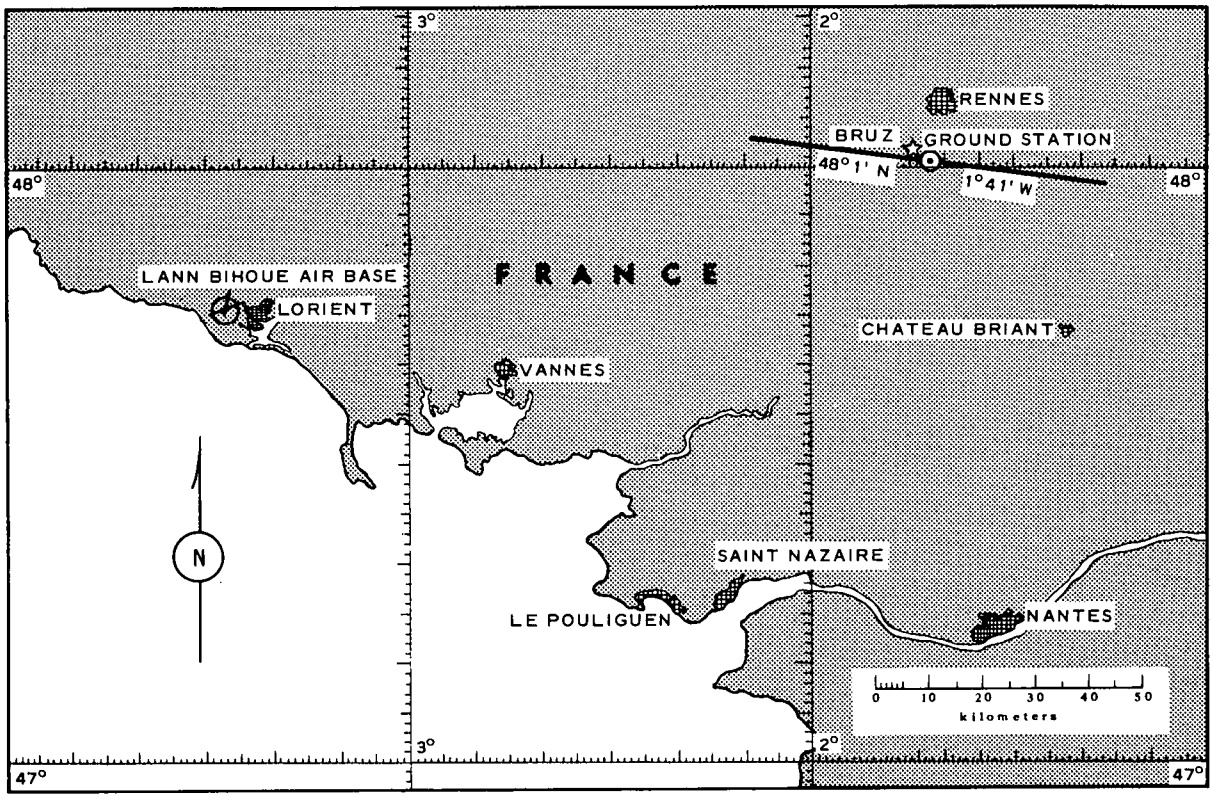

Fig. 6-3. Typical Bruz Track and Data Sites, Detail Maps. Latitude and Longitude References are to Flight Track Center Point.

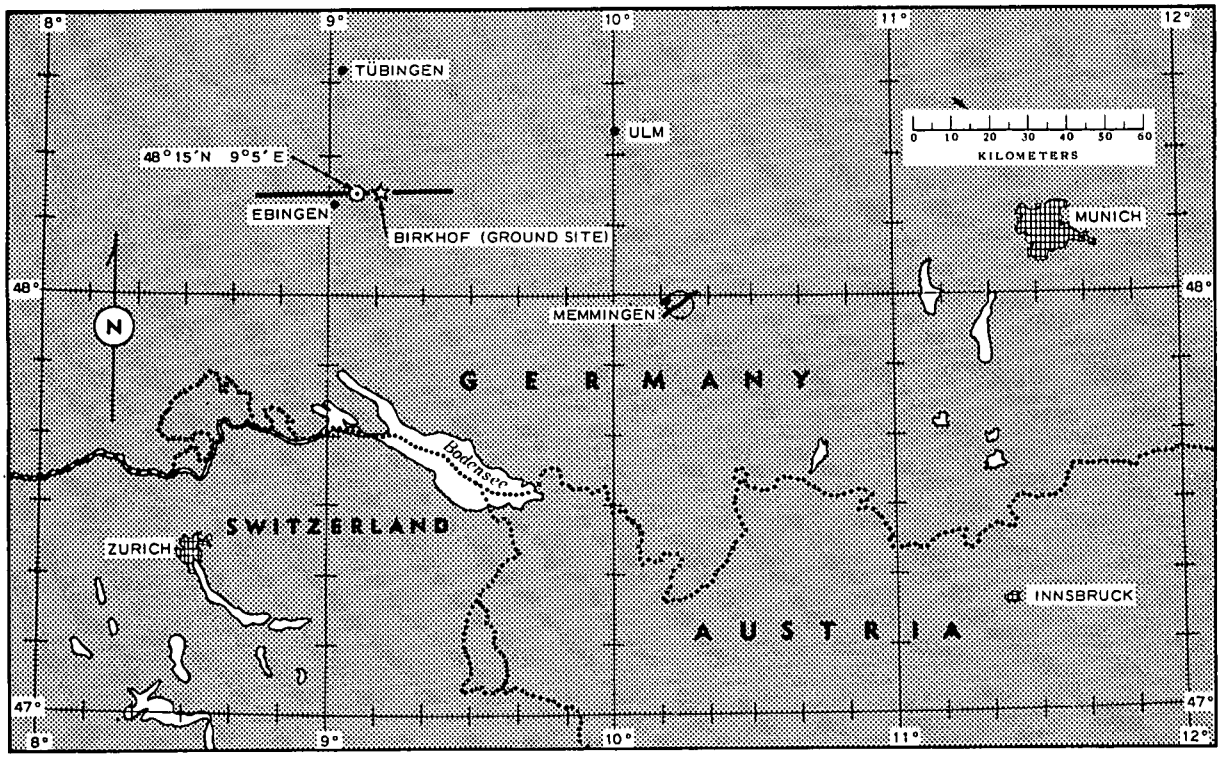

Fig. 6-4. Typical Birkhof Track and Data Sites, Detail Map. Latitude and Longitude References are to Flight Track Center Point.

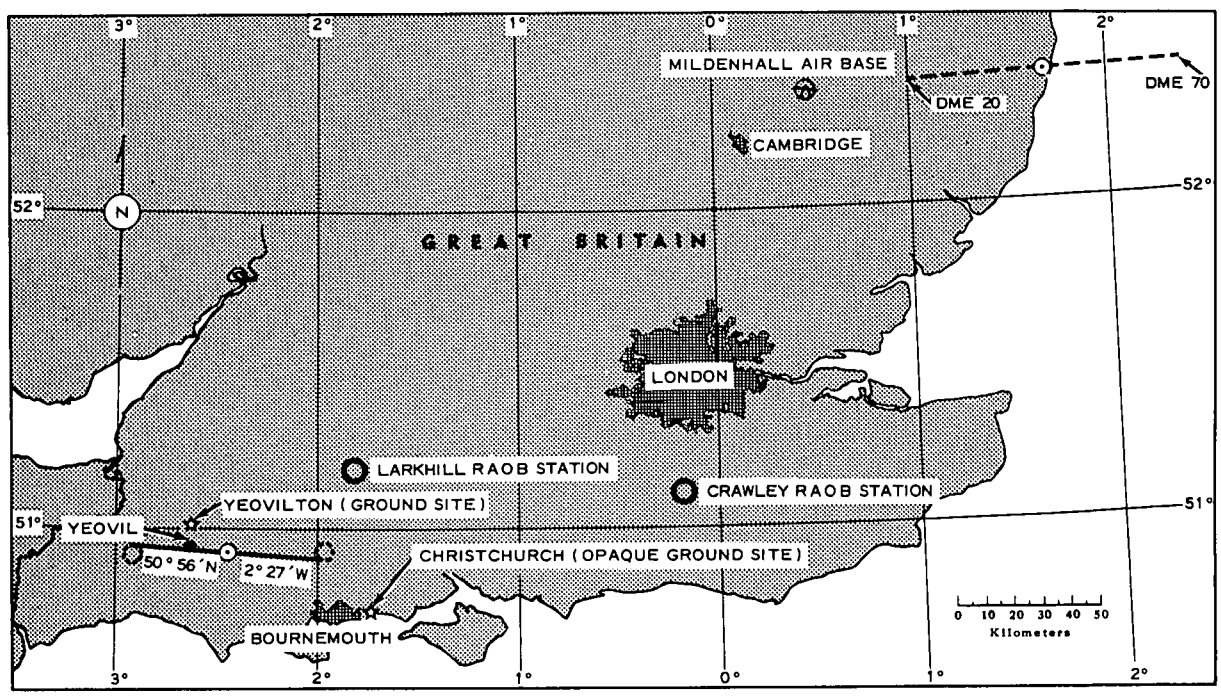

Fig. 6-5. Typical Yeovil Track and Data Sites, Detail Map. Latitude and Longitude References are to Flight Track Center Point.

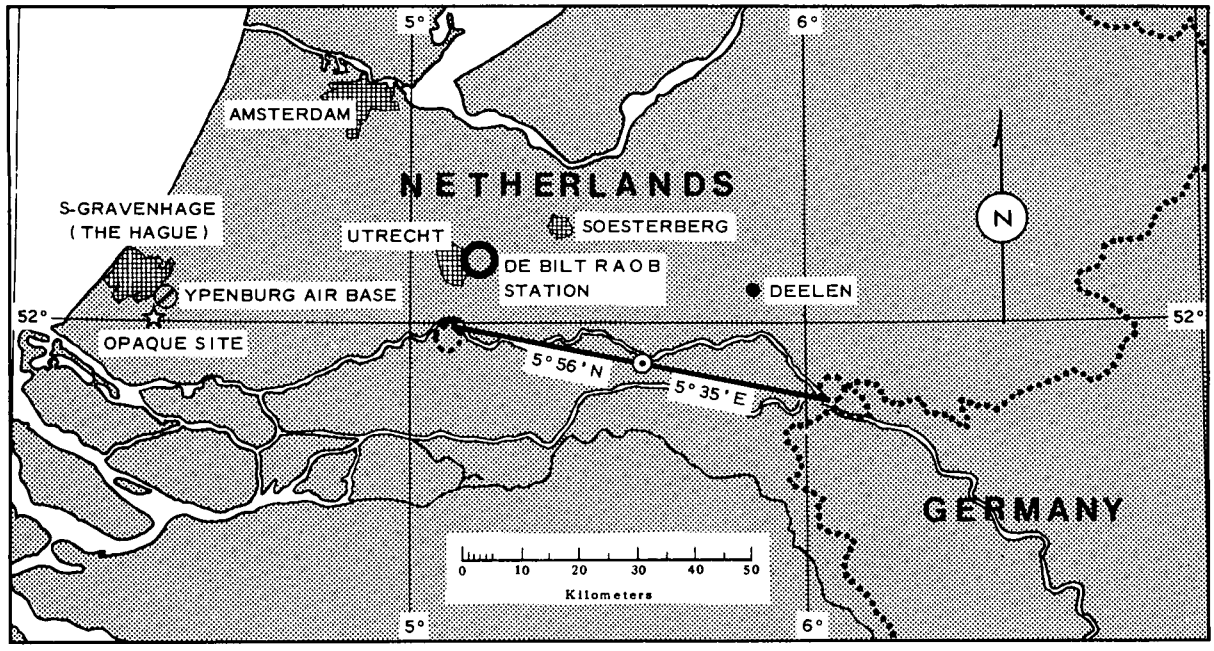

Fig. 6-6. Typical Soesterberg Track and Data Sites, Detail Map. Latitude and Longitude References are to Flight Track Center Point.

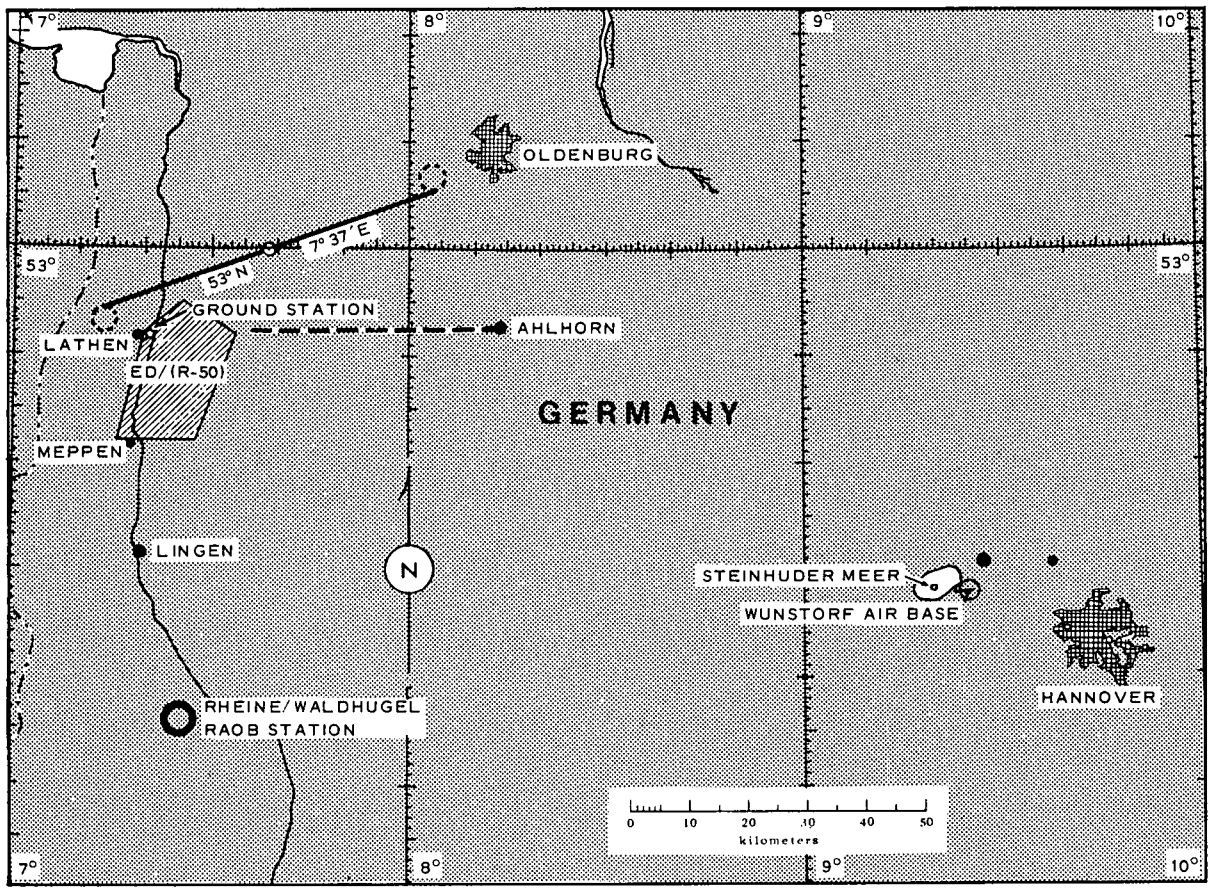

Fig. 6-7. Typical Meppen Track and Data Sites, Detail Map. Latitude and Longitude References are to Flight Track Center Point.

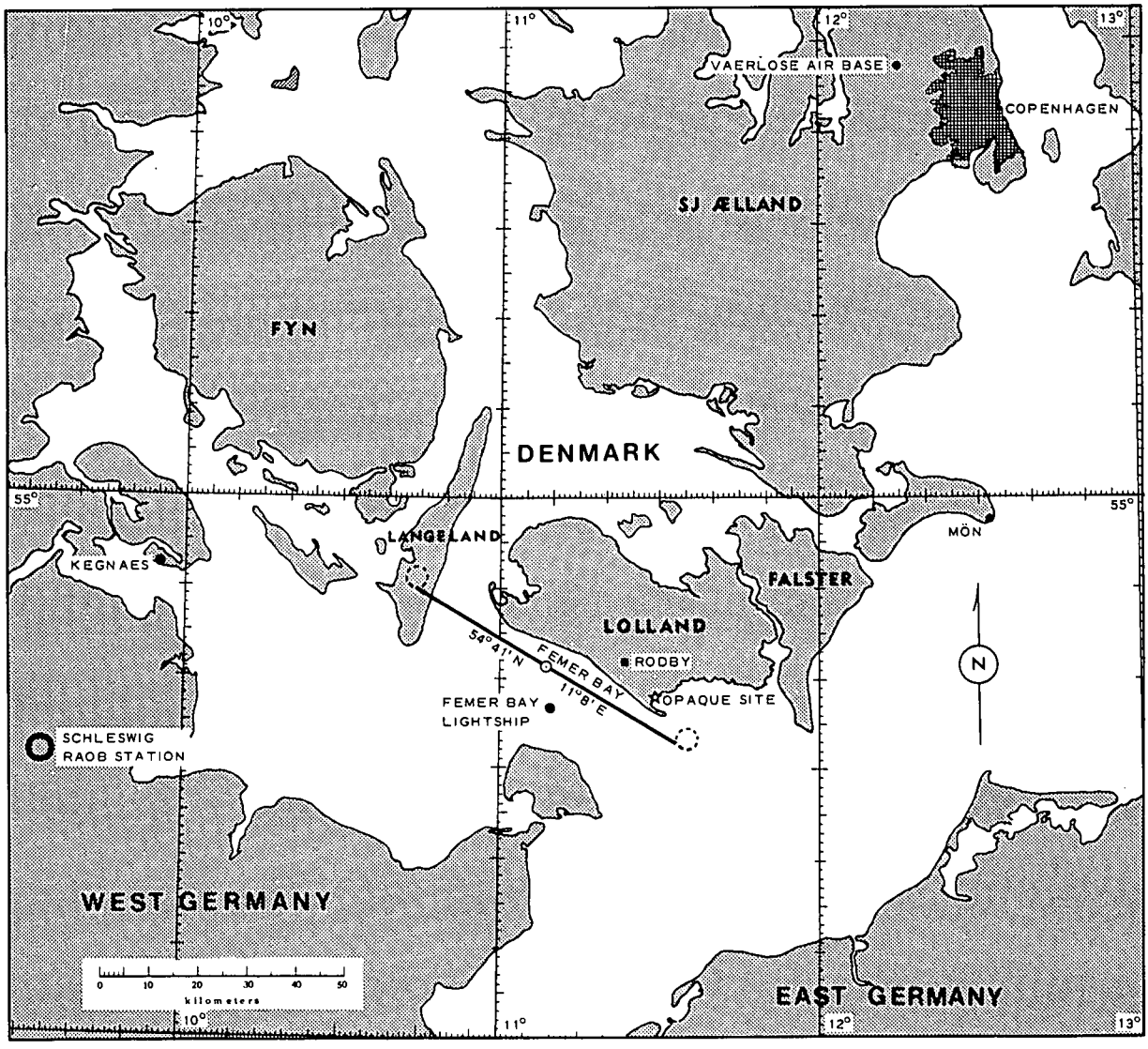

Fig. 6-8. Typical Rodby Track and Data Sites, Detail Map. Latitude and Longitude References are to Flight Track Center Point.

6.2. DESCRIPTION OF FIELD TRIPS

The five European deployments which were conducted by Geophysics Laboratory and Visibility Laboratory technical teams in conjunction with program OPAQUE are summarized in the following paragraphs. During each of these deployments the major goal was to achieve a selection of several flights over at least four of the operational OPAQUE ground sites. The degree to which this goal was achieved was for the most part dictated by weather and maintenance considerations, since flights were routinely scheduled on a daily basis.

Data from the first three deployments have been reported in the AFGL Technical Report series as noted in the Related Reports listing and Table 6.2 of this report. Data from the remaining two deployments are currently being processed for presentation during 1979.

OPAQUE I, SPRING, 1976, FLIGHT NOS. C-370 THROUGH C-382

The Spring deployment began with the Visibility Laboratory team departing San Diego on Wednesday, 31 March 1976. The team returned on Monday, 31 May 1976. During the 62 day interval between this team, in conjunction with the AFGL technical team and the aircraft flight crew, operated out of five different air bases in four different countries. As was to become the standard operating procedure, entry to the European theater was via Rhein-Main Air Base, near Frankfurt, Germany. Subsequent to final equipment checks and technical coordination at Rhein-Main, the operational excursions to the various OPAQUE sites was begun.

The operational sequence listed below is arranged in chronological order to simplify association of the flight locations with the flight numbering sequence and the temporal relationships between the site over-flights.

Order Visited	Staging Base Ident	Geographical Location	Site Map Ident
1.	Rhein-Main Air Base	near Frankfurt, Germany	Fig. 6-1
2.	Wunstorf Air Base	near Hannover, Germany	Fig. 6-7
3.	Soesterberg Air Base	near Utrecht, Netherlands	Fig. 6-6
4.	Mildenhall Air Base	near Cambridge, England	Fig. 6-5
5.	Vaerlose Air Base	near Copenhagen, Denmark	Fig. 6-8

During this first deployment there were two fundamental equipment differences from the configurations used in the preceding contract intervals. As noted in Section 3, all of the radiometer systems were fitted with new electronic circuitry resulting in a simplified more self-contained detector assembly, and the airborne integrating nephelometer was rebuilt into its folded path configuration.

The Visibility Laboratory ground station, which consisted of only the fly-away CRM system, was operational at two of the four primary sites. It was located at the American OPAQUE site on the Meppen Artillery Test Range while flights were out of Wunstorf A.B., and on Soesterberg A.B. while flights were conducted in the Netherlands. Since the British and Danish flight tracks were both quite remote from the staging air bases, it was not logistically practical during this first deployment to relocate the CRM system during missions in these two countries.

As noted in AFGL-TR-77-0078, Duntley, *et al.* (1977) which reported selected radiometric and meteorological data from eight of the flights during this springtime deployment, all of the data reflected daytime measurements with meteorological conditions ranging from clear to fully overcast with rain. Since many of the data sets previously obtained by the C-130 system have reflected primarily "clear day" conditions, these first OPAQUE sets which describe more cluttered meteorological situations are welcome additions to the program's optical documentation of realistic operational scenarios.

OPAQUE II, FALL, 1976, FLIGHT NOS. C-390 THROUGH C-402

The Fall deployment began with the Visibility Laboratory team departing San Diego on Wednesday, 13 October 1976. The team returned on Sunday, 12 December 1976. During the 60 day intervening period, the joint Air Force and Visibility Laboratory team repeated the basic operational pattern established during the preceding Spring deployment. However after initial checkout and coordination at Rhein-Main, the selection of operating sites was altered to include operations from three additional air bases in three different countries. This modified sequence is listed below, again in chronological order.

Order Visited	Staging Base Ident	Geographical Location	Site Map Ident
1.	Rhein-Main Air Base	near Frankfurt, Germany	Fig. 6-1
2.	Wunstorf Air Base	near Hannover, Germany	Fig. 6-7
3.	Vaerlose Air Base	near Copenhagen, Denmark	Fig. 6-8
4.	Lann Bihoue Air Base	near Lorient, France	Fig. 6-3

There were no significant instrumentation changes between the Spring and Fall deployments. However, the Visibility Laboratory fly-away ground station was repacked into a roll-around container to simplify the logistics of loading and off-loading the aircraft. This system still consisted of only the CRM radiometer. It was located at the Meppen OPAQUE site while flights were conducted out of Wunstorf Air Base and at the Bruz OPAQUE site while flights were conducted out of Lann Bihoue Air Base.

Selected radiometric and meteorological data from twelve of the flights conducted during this Fall deployment have been reported in AFGL-TR-77-0239, Duntley, *et al.* (1978a). Even more so than in the preceding deployments, efforts were made to conduct missions under a full spectrum of meteorological conditions, including those which were only marginal for visual flight conditions. As a result, at least four of the flights reported were conducted under cloud and overcast conditions that would have been unattempted during previous field deployments. With this non-clear day emphasis, the basic data priority has shifted to the collection of volume scattering coefficient profiles. The influences of increased profile importance, and "poor-weather" data collection, have combined to demand a change in the ground station configuration. The conditions encountered during the Fall deployment dictated the addition of a ground based integrating nephelometer to the ground system however difficult the resulting logistics might become. Steps to accomplish this end were implemented to acquire this additional system prior to the anticipated summer deployment.

OPAQUE III, SUMMER, 1977, FLIGHT NOS. C-410 THROUGH C-422

This, the first of two Summer deployments began with the Visibility Laboratory team departing San Diego on Tuesday, 28 June 1977. The team returned on Tuesday, 30 August 1977. During the 63 day intervening period, the joint Air Force and Visibility Laboratory team again operated the aircraft out of four different air bases in three different countries. The operational sequence for the OPAQUE III deployment however, was reversed from that of OPAQUE II, as is illustrated in the chronological listing below.

Order Visited	Staging Base Ident	Geographical Location	Site Map Ident
1.	Rhein-Main Air Base	near Frankfurt, Germany	Fig. 6-1
2.	Lann Bihoue Air Base	near Lorient, France	Fig. 6-3
3.	Vaerlose Air Base	near Copenhagen, Denmark	Fig. 6-8
4.	Wunstorf Air Base	near Hannover, Germany	Fig. 6-7

This reversed sequence was instituted to insure the opportunity to adequately document atmospheric conditions in conjunction with the French OPAQUE station at Bruz, since aircraft maintenance problems had somewhat distorted the operational schedule there at the termination of OPAQUE II.

The addition of the ground based integrating nephelometer system, which was discussed briefly in Section 3, to the Visibility Laboratory fly-away ground station was completed in time for its inclusion on the OPAQUE III deployment. Consequently, the continuation of scattering coefficient profile data between the aircraft's minimum flight altitude and the ground can be based upon interpolation between measured data points, rather than solely upon an assumed extrapolation technique. A basic design revision to the standardized radiometer MEMORY systems was tested in prototype during the OPAQUE III deployment. The stray light suppression accomplished by this modification significantly improved the quality of measurements made with the prototype system, and the decision was made to retrofit all radiometers with this redesigned MEMORY cutoff prior to OPAQUE IV.

The augmented fly-away ground station was operational at two of the three data sites visited during OPAQUE III. It was located at the Bruz OPAQUE site while the aircraft was operating out of Lann Bihoue Air Base in France and at the Meppen OPAQUE site while the aircraft was operating out of Wunstorf Air Base in Germany.

Selected radiometric and meteorological data from twelve of the flights conducted during this Summer deployment have been reported in AFGL-TR-78-0168, Duntley, *et al.* (1978b). The relaxation of the "acceptable weather" definition i.e. fly on any day under which VFR contact with the ground can be maintained up to at least 1000m AGL, as done during OPAQUE II, was a fortuitous decision, since this was a wet summer on all OPAQUE flight tracks. There were no "clear day" flights encountered during the OPAQUE III deployment, and there were at least three missions during which the aircraft penetrated intermittent rain squalls. Fortunately, there were no electronic or electrical malfunctions due to the rain even though the scanner and nephelometer systems were not originally designed as all-weather systems. These rainy day flights will provide the first set of data suitable for evaluation of the integrating nephelometer's performance under these previously avoided meteorological conditions.

OPAQUE IV, WINTER, 1978, FLIGHT NOS. C-430 THROUGH C-456

The Winter deployment began with the Visibility Laboratory team departing San Diego on Wednesday, 25 January 1978. The team returned on Monday, 10 April 1978. During this 72 day deployment, the longest of those up to this time, the joint Air Force and Visibility Laboratory team operated the aircraft out of four different bases in three different countries, not counting the initial staging into Rhein-Main Air Base. Two new bases, never before visited during the OPAQUE related missions, were added to the itinerary, one in Sicily and one in southern Germany. The chronological listing of the operational bases utilized during the OPAQUE IV deployment is shown below:

Order Visited	Staging Base Ident	Geographical Location	Site Map Ident
1.	Rhein-Main Air Base	near Frankfurt, Germany	Fig. 6-1
2.	Sigonella Naval Air Facility	near Catania, Sicily	Fig. 6-2
3.	Memmingen Air Base	S-W of Munich, Germany	Fig. 6-4
4.	Mildenhall Air Base	N-W of Cambridge, England	Fig. 6-5
5.	Wunstorf Air Base	near Hannover, Germany	Fig. 6-7

The only major instrumentation modification implemented for the OPAQUE IV deployment was with respect to the MEMORY cutoff system. This modification, discussed briefly in Section 3, was flown in prototype during OPAQUE III. The improved performance of dual irradiometer system upon which this modification had been retrofitted was so impressive that the decision to extend the modification to all systems was made immediately upon return to the Laboratory in September, 1977. The modification was accomplished on all of the airborne and ground based radiometer systems used by the Visibility Laboratory team during OPAQUE IV.

The fly-away ground station, which again included both the CRM and integrating nephelometer systems, was operational in the vicinity of all four of the primary OPAQUE flight tracks. While the aircraft operated out of Sigonella Naval Air Facility the ground station was located at Birgi Air Base near Trapani, Sicily. This base is the location for the Italian OPAQUE data site. When airborne operations moved to Memmingen Air Base, the ground station was relocated to Birkhof, Germany which is the location of the German OPAQUE data site. Only in the United Kingdom was the fly-away ground station not located on the official OPAQUE site. While the aircraft was operating out of Mildenhall Air Base the ground station was located at HMS Heron, Yeovilton Royal Naval Air Station, Yeovilton, England. This site, approximately 35 miles northwest from the British OPAQUE site at Christchurch, was chosen for its proximity to the actual flight track and for its suitability for air transport of the ground-based equipment to and from the site. When airborne operations returned to Germany out of Wunstorf Air Base, the ground fly-away ground station was relocated to the Meppen test range which was the site of the American supported OPAQUE data site.

In spite of the bad weather conditions that were anticipated for this Winter deployment, OPAQUE IV was the most productive trip to date. The weather was exceptionally permissive as is indicated by the completion of twenty five missions. The data from OPAQUE IV are being prepared for publication during 1979. The spectrum of weather conditions encountered was exceptionally broad, ranging from reasonably cloud free with moderate haze to low ceilings with rain and snow.

OPAQUE V, SUMMER, 1978, FLIGHT NOS. C-460 THROUGH C-479

This, the second Summer deployment, similar in season to OPAQUE III, began with the Visibility Laboratory team departing San Diego on Friday, 28 July 1978. The team returned on Saturday, 30 September 1978. During the 64 day intervening period, the joint Air Force and Visibility Laboratory team operated the aircraft out of six different air bases in four different countries. This represents the largest number of bases ever utilized during a single deployment. However, since all of these bases had been visited before, there were no operational difficulties and the exceptional cooperation of the host nation personnel made the exercise a remarkably smooth and efficient experience. The chronological listing of the operational bases utilized during this final OPAQUE deployment is shown below:

Order Visited	Staging Base Ident	Geographical Location	Site Map Ident
1.	Rhein-Main Air Base	near Frankfurt, Germany	Fig. 6-1
2.	Sigonella Naval Air Facility	near Catania, Sicily	Fig. 6-2
3.	Wunstorf Air Base	near Hannover, Germany	Fig. 6-7
4.	Memmingen Air Base	S-W of Munich, Germany	Fig. 6-4
5.	Mildenhall Air Base	N-W of Cambridge, England	Fig. 6-5
6.	Vaerlose Air Base	near Copenhagen, Denmark	Fig. 6-8

There were no instrumentation modifications imposed during the preparations for the OPAQUE V deployment, only normal maintenance and overhaul. The fly-away ground station was operational at or near four of the five primary OPAQUE flight tracks. As during the preceding OPAQUE IV deployment, it was in operation on the official OPAQUE data site at Trapani/Birgi Air Base, Sicily, and at both the Meppen and Birkhof sites in Germany. Similarly, the ground station was located at Yeovilton while the aircraft was operating out of Mildenhall, England.

The weather was much more cooperative during this second Summer deployment than it had been during the first, OPAQUE III. Even though there were few truly clear days, there were many marred only by minor cloud and haze conditions. Consequently, of the nineteen total missions, ten of them were classified as "full profile" missions, i.e. four straight and level altitudes in a total of four spectral bands. The remaining nine were assorted flights of lesser quality ranging all the way down to 5000 ft. ceilings with haze and light rain. The data from OPAQUE V are being prepared for publication during 1979.

6.3. DATA BANK SUMMARY

The field trips summarized in Section 6 of AFCRL-TR-75-0457, Duntley, *et al.* (1975b), plus the five described in Section 6.2 immediately preceding, provide a rather extensive data bank which can be used to derive atmospheric optical properties for both upward and downward paths of sight. An initial sorting of these flight data has been made to determine the number of flights which are sufficiently complete to warrant further processing. The resultant most probable classification for these sorted flights is illustrated in Table 6.3

During the pre OPAQUE deployments, e.g. HAVENVIEW II, SEMINOLE, etc., flights were selected for complete processing only. That is flights containing adequate data for the computation of directional path reflectance, $R_r^*(z,\theta,\phi)$, as outlined in both branches of Fig. 5-1, were processed and reported; but flights lacking data from at least three straight and level altitudes and three spectral bands were deleted and put into backlog.

Table 6.3. Available Data Bank

Deployment Title	Geographical Location	Season	Number** Flights	Flights Reported in AFGL-TR Format		Approximate Backlog	
				s-only	R*	s-only	R*
	European*						
OPAQUE V	IT,WG,UK,DK,NE	AUG-SEP	20	0	0	19	16
OPAQUE IV	IT,WG,UK,DK,NE	JAN-FEB-MAR	27	0	0	25	14
OPAQUE III	WG,FR	JUL-AUG	13	78-0168(12)	0	0	9
OPAQUE II	DK,WG,FR	OCT-NOV-DEC	13	77-0239(12)	0	0	10
OPAQUE I	WG,UK,NE,DK	APR-MAY	13	77-0078(8)	0	0	8
HAVENVIEW II	WG	MAY-JUN	18	0	76-0188(7)	11	8
HAVENVIEW I	WG,SP,MO	APR-MAY-JUN	25	0	72-0255(6)	15	14
	Continental U.S.						
SEEKVAL	Western Washington	JUL	11	0	75-0414(8)	3	3
SEMINOLE	Western Florida	JAN-FEB	11	0	0	11	9
GATEWAY	Southern Illinois	JAN	8	0	0	8	7
SENTRY	New Hampshire	APR	8	0	0	8	8
LOCAL I, II, III	Southern California	JAN-OCT	12	0	0	12	12
METRO	Southern Illinois	AUG	8	0	73-0422(5)	0	0
METRO	Southern Illinois	AUG	-	74-0298(3)	74-0298(3)	0	0
SNOWBIRD	Northern Michigan	MAR	8	0	0	8	5
ATOM	Central New Mexico	OCT-NOV	7	0	72-0461(6)	0	0

*WG - West Germany, UK - United Kingdom, FR - France, DK - Denmark, NE - Netherlands, IT - Italy (Sicily), SP - Spain, MO - Mocorro.

**For European Deployments: total attempted flights including weather aborts. For U.S. Deployments: total complete flights.

With the initiation of the OPAQUE program, this restrictive selection was abandoned. There was good reason to believe that the OPAQUE data base would eventually be addressed to operational problems characterized by generally low altitude regimes and poor weather meteorological conditions. Consequently, the actual flight planning on each deployment was altered to accept as adequate, weather conditions which previously would have been rejected as being too poor. This relaxation effects the nature of the data bank in that for the OPAQUE deployments, there are proportionally fewer flights meeting the $R_r^*(z,\theta,\phi)$ criteria outlined in the preceding paragraph. There are on the other hand, considerably more flights providing vertical profile data describing atmospheric volume scattering coefficients under a variety of moderate to heavy cloud conditions. Also there are for the first time, flights containing data suitable for the computation of $R_r^*(z,\theta,\phi)$ values under atmospheric conditions characterized by low ceilings, heavy haze, and intermittent rain and snow.

The processing of this extensive and diversified data bank will be approached in several phases in order to expedite the availability of selected parameters deemed particularly useful within the OPAQUE scenario. As one might infer from Table 6.3, the initial processing of the OPAQUE flight data concentrates on scattering coefficient profiles exclusively, i.e., only the procedures in the lower branch of Fig. 5-1 are utilized. Once all of the OPAQUE flights have been processed and reported to this level of completion, they will be recycled to pick up those flights where the data is adequate for $R_r^*(z,\theta,\phi)$ determinations. However, in this second pass, the requirements for utilization will be loosened to include any flight having at least two straight and level flight altitudes, with measurements in at least two optical filters. Thus, much of the low altitude, poor weather conditions that typified many of the OPAQUE flight missions can be used to derive limited but extremely valuable and unique sets of atmospheric optical properties.

7. DATA AVAILABILITY & EXAMPLES

The Air Force Geophysics Laboratory and the Visibility Laboratory have participated in several measurement programs related to studies of the European atmospheric optical-meteorological environment. Two of these preceded the current OPAQUE effort by several years. The data bases from each of these programs is quite similar in nature and content and thus is appropriate for supplementary inclusion in support of the OPAQUE concept. The first of these two related programs was conducted primarily in May 1972 under the program title HAVENVIEW. Six data flights were made slightly north of Memmingen, Germany about 65km southeast of the Birkhof OPAQUE track. Data from these flights were reported in AFCRL-72-0255, Duntley, *et al.* (1972a). The second related program was conducted in May 1973, under the program title HAVENVIEW II. Twenty-one flights were made along a track that overlayed, but was longer than the Meppen OPAQUE track illustrated in Fig. 6-7. Data from seven of these flights were reported in AFGL-TR-76-0188, Duntley, *et al.* (1976). Subsequent to these early European measurements, the NATO/OPAQUE program was developed and the measurements made during the interval covered by this report were all directed specifically toward OPAQUE applications.

Samples of the data collected and reported under the OPAQUE and the earlier HAVENVIEW II programs are included in the following paragraphs as illustrations of the presently available data base.

7.1. OPAQUE DATA BASE

Flight data from the first three OPAQUE deployments described in Section 6 have been reported in the corresponding scientific reports as listed in that same section. These reports have not included the directional path reflectance and path radiance data that can be computed in accordance with Fig. 5-1, but have been restricted to volume scattering coefficient profiles, irradiance profiles and a selection of appropriately contemporary meteorological properties. In the context of the overall OPAQUE data analysis program, computation of the more directional optical properties will be withheld pending the completion of scattering coefficient reports covering all five OPAQUE deployments. Subsequent to the issuance of the five scattering coefficient reports, emphasis will be shifted toward completing the more involved process of computing the desired directional properties.

The flight data summary tables which define the data flights included in each of the three previously published OPAQUE reports have been abstracted and reproduced herein as Tables 7.1, 7.2 and 7.3. The table entries are reasonably self-explanatory, but are commented on briefly in the original reports if one desires clarification.

Table 7.1. Flight Data Summary for OPAQUE I (AFGL-TR-77-0078)

Flight No.	Date (1976)	Total Time of Data Taking				Filter	Sun Zenith Angle (degrees)			Flight Altitude meters (AGL)	
		Start		End							
		GMT	LCT	GMT	LCT		Start	Transit	End	Min	Max
C-372	12 Apr	1141	1241	1343	1443	2,3	43.1	-	50.2	270	5760
		1347	1447	1538	1638	4,5	50.4	-	64.9	270	5760
C-373	1 May	1056	1156	1250	1350	2,3	38.5	35.7	36.8	570	5910
		1255	1355	1446	1546	4,5	37.0	-	48.1	570	5880
C-376	8 May	0900	1000	1047	1147	2,3	50.0	-	37.2	540	6060
		1053	1153	1240	1340	4,5	36.8	33.7	34.5	510	6120
C-377	10 May	0904	1004	1100	1200	2,3	48.9	-	35.6	360	6090
		1109	1209	1253	1353	4,5	35.1	33.2	34.6	360	6090
C-378	12 May	0944	1044	1025	1125	2,3	40.1	-	37.5	270	1800
		1032	1132	1118	1218	4,5	37.2	36.5	36.5	270	1590
C-379	17 May	0957	1057	1138	1238	2,3	38.0	35.3	35.7	300	6270
		1143	1243	1332	1432	4,5	35.8	-	44.3	270	6270
C-381	25 May	1058	1158	1241	1341	2,4	32.4	32.0	35.1	270	5490
		1246	1346	1416	1516	3,5	35.5	-	45.6	270	5460
C-382	26 May	0925	1025	1056	1156	2,4	39.4	-	32.3	330	5430

Samples of the meteorological and radiometric data appearing in each of these preceding OPAQUE reports are included in the following paragraphs. These sample plots are typical of the graphical displays used to document the character of each flight included in each report. Also included in the original reports, but not reproduced here are tabular listings of some of the data that is shown graphically.

Table 7.2. Flight Data Summary for OPAQUE II (AFGL-TR-77-0239)

Flight No.	Date (1976)	Total Time of Data Taking				Filter	Sun Zenith Angle (degrees)			Flight Altitude meters (AGL)	
		Start		End							
		GMT	LCT	GMT	LCT		Start	Transit	End	Min	Max
C-390	25 Oct	1230	1330	1425	1525	2,3	69.6	-	79.7	270	6090
		1429	1529	1615	1715	4,5	80.1	-	93.7	300	6090
C-391	26 Oct	1119	1219	1144	1244	2	67.4	-	67.9	270	5490
		1147	1247	1208	1308	3	68.0	-	68.8	270	5430
		1209	1309	1235	1335	4	68.9	-	70.2	300	5160
		1236	1336	1257	1357	5	70.3	-	71.6	840	5100
C-392	1 Nov	1115	1215	1208	1308	2,3	67.6	-	68.6	420	1410
		1212	1312	1253	1353	4,5	68.7	-	71.0	360	1170
C-393	2 Nov	1036	1136	1046	1146	2	68.3	-	68.1	300	1590
		1050	1150	1053	1153	3	68.0	-	68.0	270	1440
		1108	1208	1111	1211	4	67.9	-	67.9	360	1380
		1114	1214	1117	1217	5	67.9	-	67.9	330	1440
C-394	18 Nov	1147	1247	1221	1321	2,3	74.7	-	76.0	210	900
		1225	1325	1259	1359	4,5	76.2	-	78.3	300	900
C-395	19 Nov	1150	1250	1319	1419	2,3	75.0	-	79.9	300	4440
		1256	1356	1422	1522	4,5	78.2	-	85.8	300	4440
C-397	23 Nov	1201	1302	1257	1357	2,3	74.1	-	76.7	300	4320
		1238	1338	1259	1359	4	75.5	-	76.8	330	4320
		1259	1359	1317	1417	5	76.8	-	78.0	300	4320
C-398	2 Dec	1143	1243	1306	1406	2	70.1	70.0	71.8	420	4440
		1315	1415	1411	1511	4	72.2	-	76.3	450	4410
C-399	3 Dec	1013	1113	1250	1350	2,3	73.9	70.2	71.2	390	2610
		1116	1216	1230	1330	4,5	70.8	70.2	70.6	420	2580
C-400	4 Dec	1029	1129	1204	1304	2,3	73.0	70.3	70.3	480	5100
		1219	1319	1233	1333	4	70.5	-	70.8	480	5070
		1250	1350	1305	1405	5	71.3	-	72.0	480	5100
C-401	5 Dec	1040	1140	1227	1337	2,3	72.5	70.4	70.8	390	5190
		1233	1333	1428	1528	4,5	70.9	-	78.2	420	5190
C-402	6 Dec	1201	1301	1318	1418	2,3	70.6	-	72.9	390	3900
		1324	1424	1445	1545	4,5	73.2	-	79.9	420	3840

Table 7.3. Flight Data Summary for OPAQUE III (AFGL-TR-78-0168)

Flight No.	Date (1977)	Total Time of Data Taking				Filter	Sun Zenith Angle (degrees)			Flight Altitude meters (AGL)	
		Start		End							
		GMT	LCT	GMT	LCT		Start	Transit	End	Min	Max
C-410	4 Jul	1119	1219	1249	1349	2,3	27.2	25.2	26.3	150	3180
		1255	1355	1432	1532	4,5	26.6	-	37.8	120	3180
C-411	6 Jul	0902	1002	0959	1059	2,3	45.1	-	36.4	150	2875
		1003	1103	1113	1213	4,5	35.9	-	27.8	120	2850
C-412	7 Jul	0845	0945	1036	1136	2,3	48.0	-	31.7	180	5640
		1043	1143	1233	1333	4,5	31.0	25.4	25.8	150	5640
C-413	27 Jul	1441	1541	1455	1555	3	51.7	-	53.7	120	5670
		1458	1558	1517	1617	4	54.0	-	56.8	120	5580
		1525	1625	1540	1640	5	57.7	-	59.9	120	5700
		1543	1643	1603	1703	2	60.2	-	63.3	120	5340
C-414	28 Jul	0939	1039	1110	1210	2	40.7	-	34.3	120	3000
		0940	1040	1059	1159	3	40.5	-	34.6	60	3030
		0942	1042	1032	1132	4	40.4	-	36.0	930	3000
		0943	1043	1136	1236	5	40.2	-	33.9	30	3030
C-415	29 Jul	1027	1127	1123	1223	4,5	36.8	-	34.4	90	870
		1126	1226	1207	1307	2,3	34.4	34.3	34.9	60	870
C-416	1 Aug	1124	1224	1312	1412	2,3	36.7	36.7	42.4	120	4590
		1319	1419	1450	1550	4,5	43.0	-	53.9	180	4620
C-418	4 Aug	0847	0947	0905	1005	2	48.3	-	45.9	150	4530
		0910	1010	0930	1030	4	45.4	-	43.1	90	4590
		0930	1030	0949	1049	3	43.1	-	41.1	210	4620
		0953	1053	1008	1108	5	40.8	-	39.4	240	4560
C-419	4 AUG	1436	1536	1518	1618	2.3	50.1	-	56.0	120	750
		1524	1624	1608	1708	4,5	56.8	-	63.4	120	750
C-420	5 AUG	0840	0940	0957	1057	2,3	49.6	-	40.7	90	3060
		1002	1102	1119	1219	4,5	40.4	-	36.2	60	3060
C-421	10 Aug	1012	1112	1210	1310	2,3	41.4	39.2	40.4	120	5850
		1218	1318	1412	1512	4,5	40.7	-	51.3	120	5850
C-422	11 Aug	0953	1053	1040	1140	2,3	42.9	-	40.2	120	1560
		1044	1144	1120	1220	4,5	40.1	39.5	39.5	120	1560

METEOROLOGICAL DATA

Measurements of temperature, and relative humidity computed from measured temperature and dewpoint temperature are presented in graphical form as shown in Fig. 7-1 for each of the flights in the OPAQUE reports. The flight selected for illustration is Flight C-416 flown during OPAQUE III on 1 August 1977 over the Rodby, Denmark flight track. The weather conditions are typical of the OPAQUE flights being mostly scattered to broken clouds during the flight.

The temperatures were measured continuously by an AN/AMQ-17 aerograph system described briefly in AFCRL-70-0137, Duntley, *et al.* (1970). The dewpoint/frostpoint temperatures were measured using a Cambridge 137-C3 Aircraft Hygrometer System which is described briefly in AFCRL-72-0593, Duntley, *et al.* (1972c). The profile identification symbols used in Fig. 7-1 are related to the spectral filter sequence during which the data were measured; i.e., the temperature profile identified with the Filter 2 symbol was taken during the same time interval as the Filter 2 radiometric measurements; the temperatures coded as Filter 3 were taken simultaneously with the Filter 3 radiometric measurements, etc.

Radiosonde observations (RAOB) were available from European reporting sites in the vicinity of each of the flight tracks. The RAOB temperatures, and relative humidity computed from RAOB temperature and dewpoint depression measurements are shown superimposed upon the flight data illustrated in Fig. 7-1. The RAOB station was 103Km West of the center of the flight track for Flight C-416 and the observations were for 1200 GMT.

Additional meteorological information related to each OPAQUE flight is obtained from northern hemisphere surface charts for 0000 GMT and 1200 GMT and 500-millibar charts for 1200 GMT prepared by the National Oceanographic and Atmospheric Administration. A portion of the 1200 GMT surface charts for Flight C-416 has also been reproduced in Fig. 7-1.

Daily flight descriptions appear in the OPAQUE reports which include a discussion of the weather characteristics and a summary of the synoptic situation at the surface and 500-millibar levels during each of the flights. A tabular summary of the daily meteorological observations taken at weather stations nearest the flight track is normally included as are observations by an on-board meteorologist concerning the cloud and haze conditions, shadows, visibility of the solar disc, and slant path visibilities from various altitudes.

RADIOMETRIC DATA

In a manner similar to the presentation of the sample meteorological data, the radiometric data from Flight C-416 have also been abstracted from the parent report, and reproduced herein.

The flight data for each reported flight is preceded by a flight description summary sheet illustrated by Fig. 7-2. Following the flight description, the radiometric data are illustrated graphically as shown in Fig. 7-3.

FLIGHT NO. C-416

RODBY

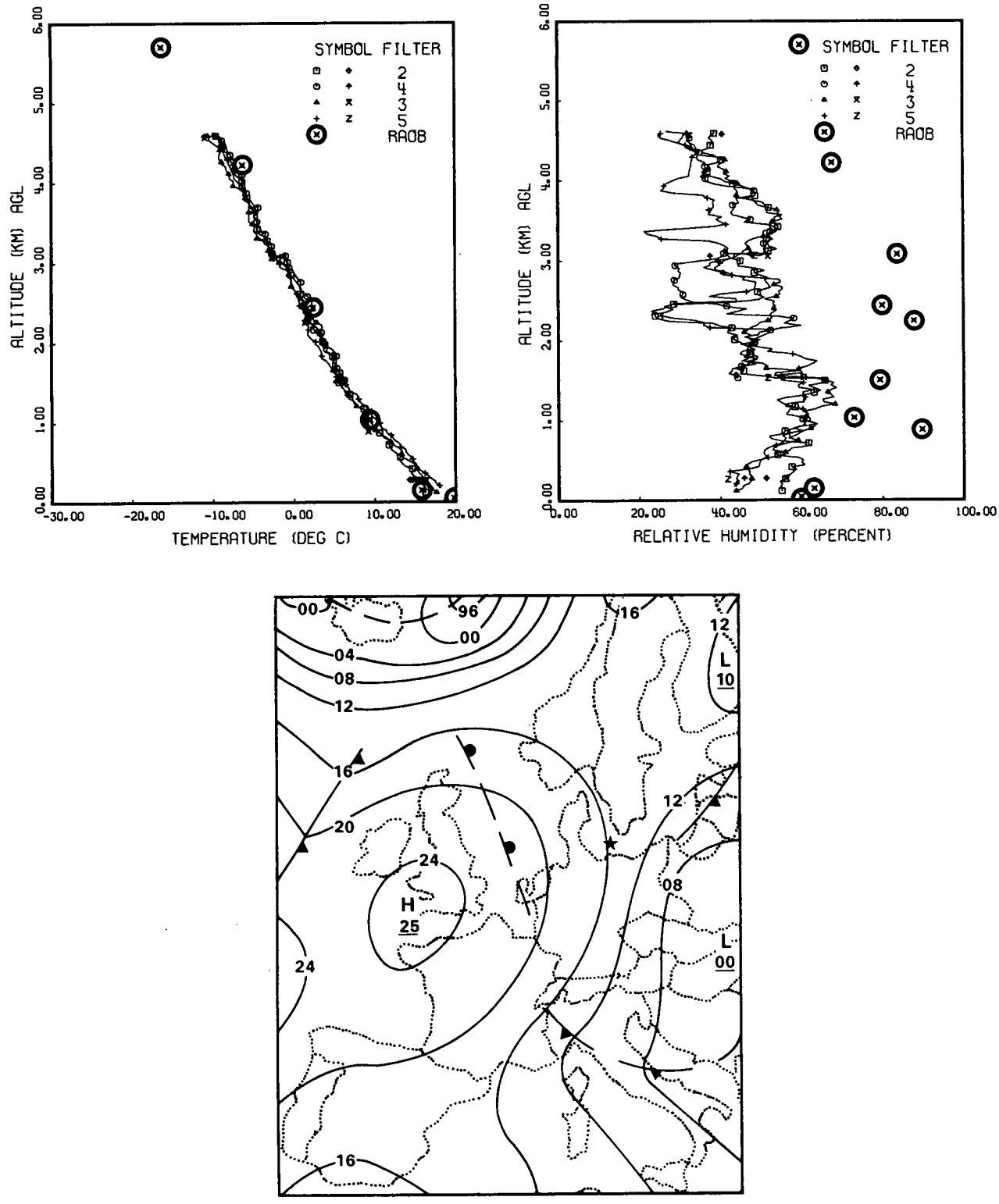

Fig. 7-1. Meteorological Data Graphs, Flight C-416, 1 August 1977 during OPAQUE III (AFGL-TR-78-0168).

FLIGHT C-416 - 1 AUGUST 1977 - DESCRIPTION OF FLIGHT & WEATHER CHARACTERISTICS

Filter Ident	Data Interval			Solar Zenith Angle			Maximum Flight Altitude (m)	Average Terrain Elevationn (m)
	Start (GMT)	End (GMT)	Elapsed (hrs)	Initial ST&LV (degrees)	Solar Transit (degrees)	Final V-PRO (degrees)		
2&3	1124	1312	1.8	36.7	36.7	42.4	4590	0
4&5	1319	1450	1.5	43.0	-	53.9	4620	0

Flight C-416 was an afternoon flight, after local apparent noon. There were partly cloudy skies throughout the flight with scattered low altitude cumulus and scattered cirrus above the highest flight altitude.

The approximate southeast to northwest Rodby track was located south of Lolland Island, Denmark. Typical terrain features along the nearby coast to the north of the track were flat cultivated farmlands interspersed with occasional woods and small towns. Directly beneath the track and to the south were the relatively shallow waters of Femer Bay.

The in-flight observer noted cumulus building up over the land and blowing off with bases 5110 meters (1700 feet) tops 1560 meters (5200 feet) and thin scattered to broken cirrus. There were multiple layers of light to moderate haze. The slant visibility varied from a low of 15 miles at 1500 meters (5000 feet) to a high of 30 miles at 3000 meters (10,000 feet).

Fehmarnbelt, 9 kilometers south of the track center point, reported 1/8 cumulus at 450 meters (1500 feet). 2/8 to 3/8 altostratus at 3600 meters (12,000 feet) and 3/8 to 6/8 cirrus at 6000 meters (20,000 feet). The layer of broken cirrus was thin and did not constitute a ceiling. Visibility was reported as 20.0 kilometers.

Kegnaes, 76 kilometers westnorthwest of the track center point, reported clear skies in early morning with 2/8 to 4/8 cirrus at 6000 meters (20,000 feet) afternoon. Visibility was recorded as 15.0 to 20.0 kilometers.

The radiosonde station at Schleswig was 103 kilometers west of the flight track center and located in an airflow that was parallel with the track.

The surface chart showed a dissipating cold front that extended through central Yugoslavia, north central Italy, then northwest into central Belgium and the North Sea. Ridging from the Atlantic High reached into Scandanavia with a closed 1025 millibar high in southwestern Britain. At 500 millibars there was a low system in southeastern Germany that extended over the flight track. In addition, there was a ridge from Spain to Britain. The flow was northeasterly and the air mass was unstable maritime polar.

Fig. 7-2. Flight Description Summary Sheet, Flight C-416.

FLIGHT NO. C-416

RODBY

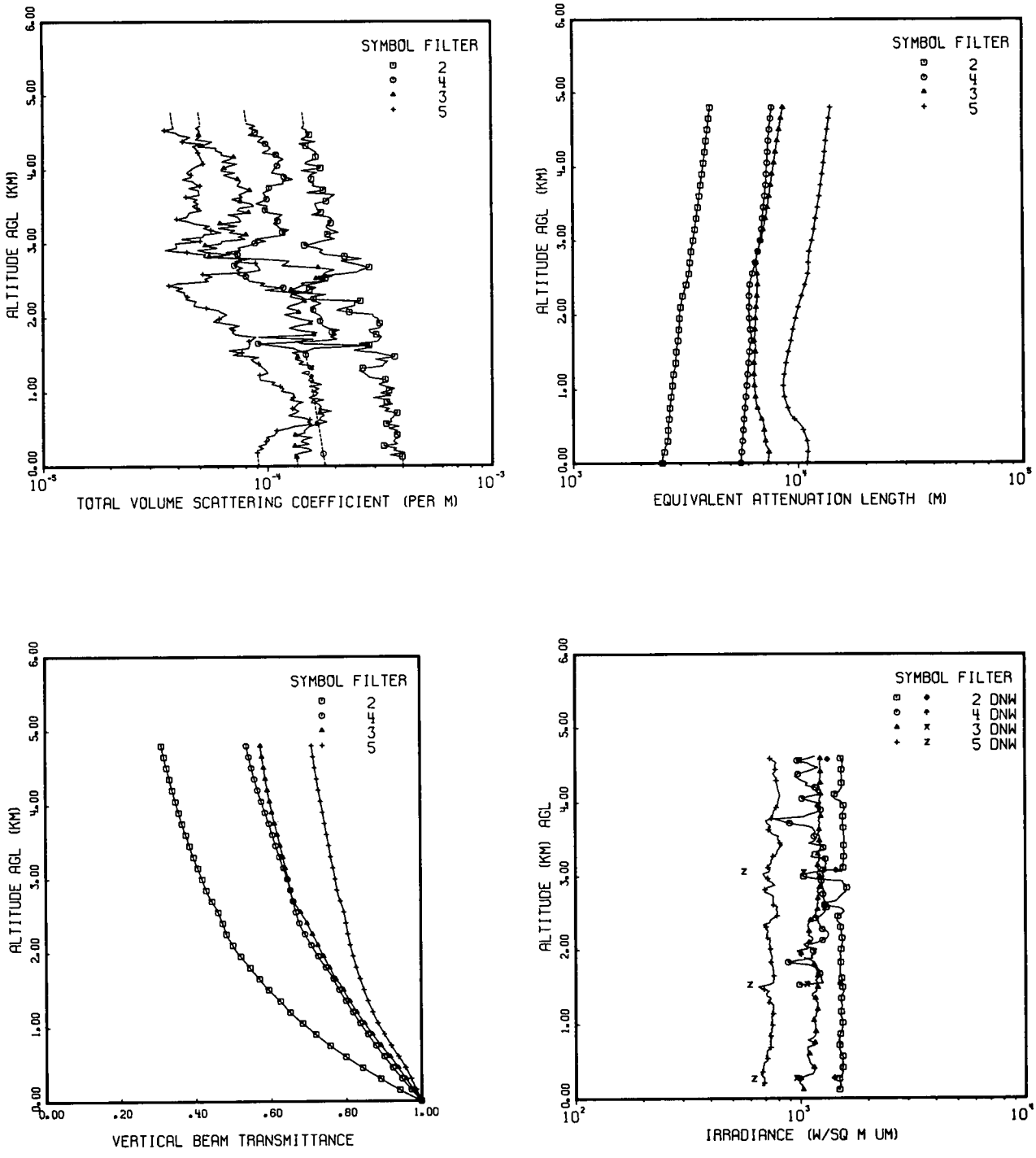

Fig. 7-3. Radiometric Data Graphs, Flight C-416, 1 August 1977 during OPAQUE III (AFGL-TR-78-0168).

The format explanations related to these data plots is repeated below for the convenience of those not familiar with the original report.

Total Volume Scattering Coefficient. The total volume scattering coefficient $s(z)$ in m^{-1} is graphed using a single average value for each 30-meter altitude interval. Identifying symbols for the spectral filters appear every fifth data point, or at 150-meter intervals. The extrapolated values are indicated by a dashed line.

Equivalent Attenuation Length. The equivalent attenuation length $\bar{L}(z)$ in meters, for the path between ground and altitude, is graphed for each 30-meter altitude interval. Spectral identifying symbols appear at 150-meter intervals or every fifth data point.

Vertical Beam Transmittance Between Ground and Altitude. The vertical beam transmittance $T_r(0,0°)$ or $T_r(z,180°)$ between ground and altitude is graphed for each 30-meter altitude interval. Spectral identifying symbols appear at 150-meter intervals or every fifth data point.

Downwelling Irradiance. The downwelling irradiance $H(z,d)$ is graphed as a function of altitude above ground level (AGL). These irradiances were measured by the dual irradiometer concurrently with the total volume scattering coefficient measurements. The downwelling irradiance during the ascent or descent is graphed using a single average value for each 30-meter altitude interval and the identifying symbol for the spectral filter appears every fifth data point; thus when data are continuous, the symbols appear at 150-meter intervals. The second symbol for each filter designates the average value measured during each three-minute straight and level flight element.

The tabular data which duplicates the information contained in these graphical representations, and is part of the display provided in each of the original OPAQUE data reports, is not reproduced as part of this sample. It is however readily available to all interested users.

7.2. HAVENVIEW II DATA BASE

Field data from earlier deployments which are similar in nature to the OPAQUE data, are referenced in two preceding reports, Duntley, *et al.* (1972a and 1976). These earlier data sets, while not taken in conjunction with the currently operating OPAQUE ground sites, were none the less supplemented with ground based measurements made by Visibility Laboratory personnel as well as several cooperating German research groups, e.g., Büchtemann and Höhn (1970), and thus are considered reasonable supplements to the overall OPAQUE effort.

The HAVENVIEW II data, Duntley, *et al.* (1976) was originally reported in the style currently contemplated for later use with the OPAQUE flight data. That is, the report contained computed values for the more directional optical properties, directional path reflectance, $R_r^*(z,\theta,\phi)$, path radiance, $N_r^*(z,\theta,\phi)$, etc., in addition to the scattering coefficient profiles. In order to acquaint potential data users with this more complete reporting style, the data for Flight C-289 have been abstracted from the parent report and are reproduced in the following paragraphs.

The flight data summary tables which define the data flights included in each of the two previously published HAVENVIEW reports have been abstracted and reproduced herein as Tables 7.4 and 7.5. The table entries are equivalent to those currently in use, however Table 7.4 does not list the applicable optical filters, which are described in the parent report. The early HAVENVIEW I optical filters were the same or similar to those currently used during program OPAQUE.

Table 7.4. Flight Data Summary for HAVENVIEW I Report (AFCRL-72-0255)

Flight Number	Date 1970	Total Time of Data-Taking				Sky Near Sun	Sun Zenith Angle			Maximum Flight
		Start		End			Start	Transit	End	
		GMT	LCT	GMT	LCT					
C-134	25 May	1508	(1608)	1641	(1741)	Cloud	50.6	-	61.7	2460
C-137	28 May	1418	(1518)	1543	(1643)	Clear	44.8	-	55.1	2490
C-138	29 May	0829	(0929)	1039	(1139)	Clear	42.6	-	29.7	4920
C-139	03 June	1247	(1347)	1511	(1611)	Cloud	31.3	-	44.8	4830
C-142	06 June	0825	(0925)	1045	(1145)	Clear	42.7	-	30.2	4950
C-143	06 June	1406	(1506)	1628	(1728)	Cloud	41.8	-	58.9	4980

Table 7.5. Flight Data Summary from HAVENVIEW II Report (AFGL-TR-76-0188)

Flight No.	Date (1973)	Total Time of Data-Taking				Filter	Sun Zenith Angle (degrees)				Maximum Flight Altitude (meters AGL)	Maximum Sensor or Object Altitude (meters AGL)
		Start		End			Start	Transit	End	Average		
		GMT	LCT	GMT	LCT							
C-273	16 May	758	858	833	944	4,5	52.1	-	48.4	50.3	840	1050
		844	944	922	1022	2,3	45.9	-	42.3	44.1	1020	1050
C-279	3 June	1108	1208	1120	1220	2	30.9	-	30.7	30.8	1116	1200
		1140	1240	1152	1252	3	30.8	-	31.1	30.9	1110	1200
C-280	4 June	1616	1716	1628	1728	4A	61.7	-	63.3	62.5	750	750
		1736	1836	1744	1844	4B	73.6	-	74.6	74.1	673	750
C-281	5 June	855	955	923	1023	4,5	41.9	-	39.3	40.6	863	900
C-282	5 June	1618	1718	1629	1729	4A	61.8	-	63.4	62.6	610	600
		1705	1805	1716	1816	4B	68.8	-	70.3	69.6	613	600
C-288	13 June	1150	1250	1158	1258	4	30.1	-	30.3	30.2	808	900
		1211	1311	1219	1319	5	30.9	-	31.3	31.3	810	900
		1234	1334	1243	1343	2	32.3	-	32.9	32.6	810	900
		1255	1355	1304	1404	3	34.0	-	34.7	34.4	800	900
C-289	14 June	1245	1345	1258	1358	2	33.1	-	34.1	33.6	1200	1200
		1314	1414	1325	1425	3	35.8	-	36.9	36.4	1200	1200
		1341	1441	1354	1454	4	38.9	-	40.4	39.6	1200	1200
		1405	1505	1419	1519	5	41.9	-	43.6	42.7	1211	1200

METEOROLOGICAL DATA

The presentation of meteorological data for HAVENVIEW II was similar to but not as complete as the presentation for the more recent OPAQUE data. A graph of airborne temperatures measured with the AMQ-17 was given for each flight, with RAOB temperatures from the closest station to the track superimposed on the graph. However, airborne measurements of dewpoint temperature were not available for the HAVENVIEW II vertical flight profiles, therefore there was no graph of computed relative humidity. Meteorological data for Flight C-289 are reproduced in Fig. 7-4.

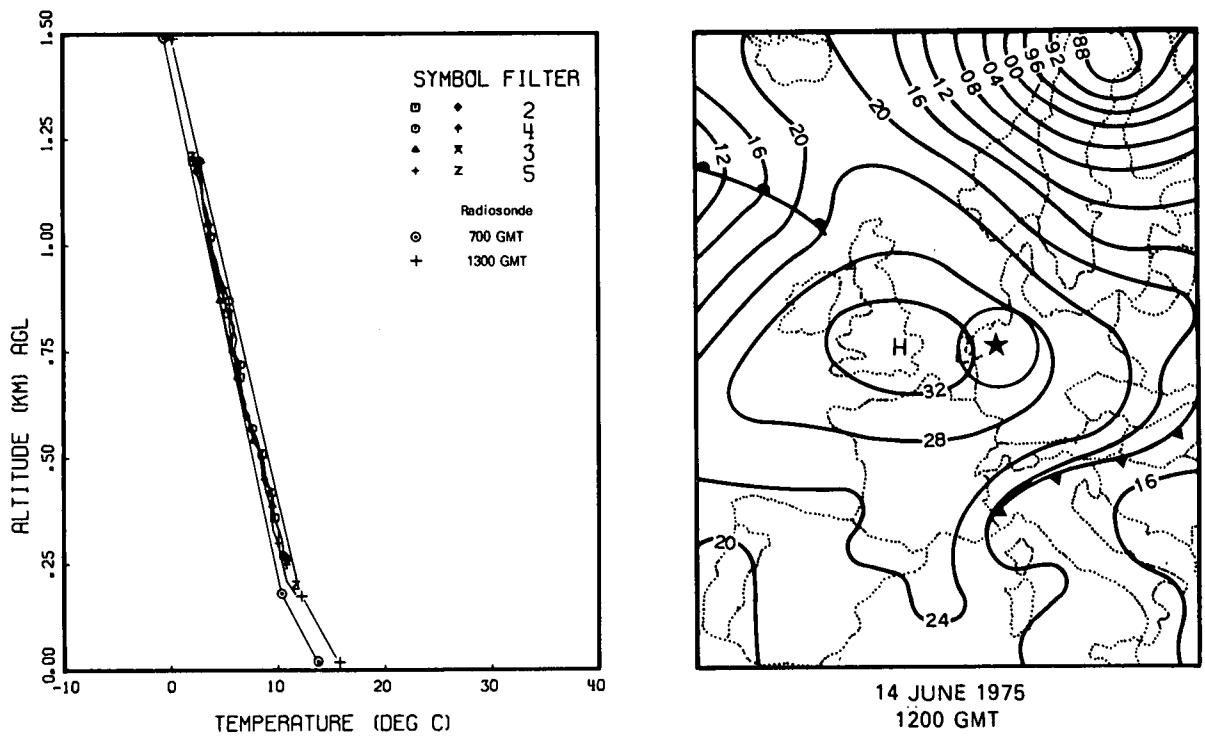

Fig. 7-4. Meteorological Data Graphs, Flight C-289, 14 June 1975, during HAVENVIEW II, (AFGL-TR-76-0188).

Flight C-289 was a low altitude flight under a broken layer of clouds, typical of those flights reported for HAVENVIEW II, in that all were made under relatively cloudy conditions. The flight description summary sheet for C-289, similar to those for each HAVENVIEW flight included in the parent report, is reproduced as Fig. 7-5. The comments included on this sheet were derived from northern hemisphere charts, on-board crew observations, etc., in a manner similar to that employed for the OPAQUE summaries.

RADIOMETRIC DATA

The radiometric data reported for the HAVENVIEW II flights was more extensive than that reported thus far for the OPAQUE missions. The inclusion of path radiance and directional path reflectance values for both upward and downward inclined paths of sight required significantly longer

FLIGHT C-289 - 14 June 1973 - DESCRIPTION OF FLIGHT & WEATHER CHARACTERISTICS

It was a sunlit afternoon with a broken layer of clouds. The flight was conducted over low lying flat terrain consisting mainly of cultivated farmlands interspersed with dark patches of dense woods. The data-taking commenced at 1245 GMT and continued until 1419 GMT. the sun zenith angle during sky radiance data-taking was 33.1 degrees at the beginning and 43.6 degrees at the end. The maximum flight altitude was 1211 meters. The average elevation of the terrain was 20 meters.

The ground station was not in operation on this date.

The radiosonde station at Meppen reported 0.9 cumulus at 1000 to 1499 meters and 0.1 cirrus at 1300 GMT.

FLIGHT LOG ENTRY

Time (GMT)	Elevation (meters AGL)	Aircrew Observations
		Special descents under the cloud deck, broken to overcast.
1235		Light haze, scattered to broken deck above.
1246	1050	Broken to overcast above, approximately 6 to 8 miles (10 to 13 kilometers) visibility.
1355	300	West end begins to go scattered.

Note: Flight elevations in approximate feet MSL have been converted to approximate meters AGL.

The surface charts show that a high centered south of Ireland moved eastward to near The Hague by 1800 GMT. A ridge was building over France and Germany. With increasing flow from the northwest at all levels, moisture was brought in from the North Sea and cloudiness increased throughout the day.

At 500 millibars there was a ridge of high from the Iberian Peninsula across France to Poland and eastern Russia. The flow over northwest Germany was strong northwesterly.

These data were taken from the 6-hourly chart analyzed by the National Meteorological Center and obtained from the National Climatic Center in Asheville. The 500-millibar charts are for 0000 GMT and 1200 GMT daily.

Fig. 7-5. Flight Description Summary Sheet, Flight C-289.

processing and editing times than for the simpler reporting format used for the OPAQUE flights. The computations for these more directional quantities required data not only from the integrating nephelometer, but also from the upper and lower hemisphere scanners. The derivation of the directional optical properties is accomplished using the procedures outlined in both upper and lower branches of Fig. 5-1, and the equations in Section 2.1 of the parent report, Duntley, *et al.* (1976).

In a manner similar to the presentation of the sample meteorological data, the radiometric data for Flight C-289 have also been abstracted from the parent report, and are reproduced herein as Figs. 7-6, 7-7, and 7-8.

The format explanations for total volume scattering coefficient, equivalent attenuation length, and vertical beam transmittance can be reviewed in Section 7.1.

The format explanations related to these data plots which are different from those contained in Section 7.1 are repeated below for the convenience of those not familiar with the original report.

Downwelling Irradiance. The downwelling irradiance $H(z,d)$ is graphed as a function of altitude above ground level (AGL). These irradiances are computed from the sky measurements and the sun irradiance at each of the flight profile level altitudes.

Path Radiance Between Ground and Altitude. The path radiance $N_r^*(z,\theta,\phi)$ is graphed for upward and downward-looking paths between ground and the altitude shown in Fig. 7-7. Each graph is for one path of sight for the four optical filters. The first graph is for the vertical upward path of sight, the second and third are for zenith angles 80 and 100 degrees, in the azimuth of the sun, and the fourth is for the vertical downward path of sight. These are data selected from the path radiance tables in Section 7.3 of Duntley, *et al.* (1976).

Directional Path Reflectance Between Ground and Altitude. The directional path reflectance $R_r^*(z,\theta,\phi)$ is also graphed for upward and downward-looking paths between ground and the altitude shown in Fig. 7-8. Each graph is for one path of sight and four optical filters. The first graph is for the vertical upward path of sight; the second and third are for zenith angles 80 and 100 degrees, in the azimuth of the sun, and the fourth is for the vertically downward path of sight. These selected paths of sight are the same as for the path radiance graphs. The data were selected from the many paths of sight tabulated in the directional path reflectance tables in Section 7.3 of Duntley, *et al.* (1976).

In the HAVENVIEW II report data on total volume scattering coefficient, irradiance, directional reflectance (sky or terrain), and equivalent attenuation length are also presented in tabular form. In addition, beam transmittance, path radiance and path reflectance are presented tabularly for seven paths of sight inclined at zenith angles 0°, 75°, 80°, 85°, 95°, 100°, and 180° at four azimuths with respect to the sun, 0°, 90°, 180°, and 270° for five path lengths between ground and altitude. This tabular data which duplicates and extends the information contained in the graphical representations is not reproduced as part of this sample. It is, as in the case of the OPAQUE tabular data, readily available to all interested users.

FLIGHT NO. C-289

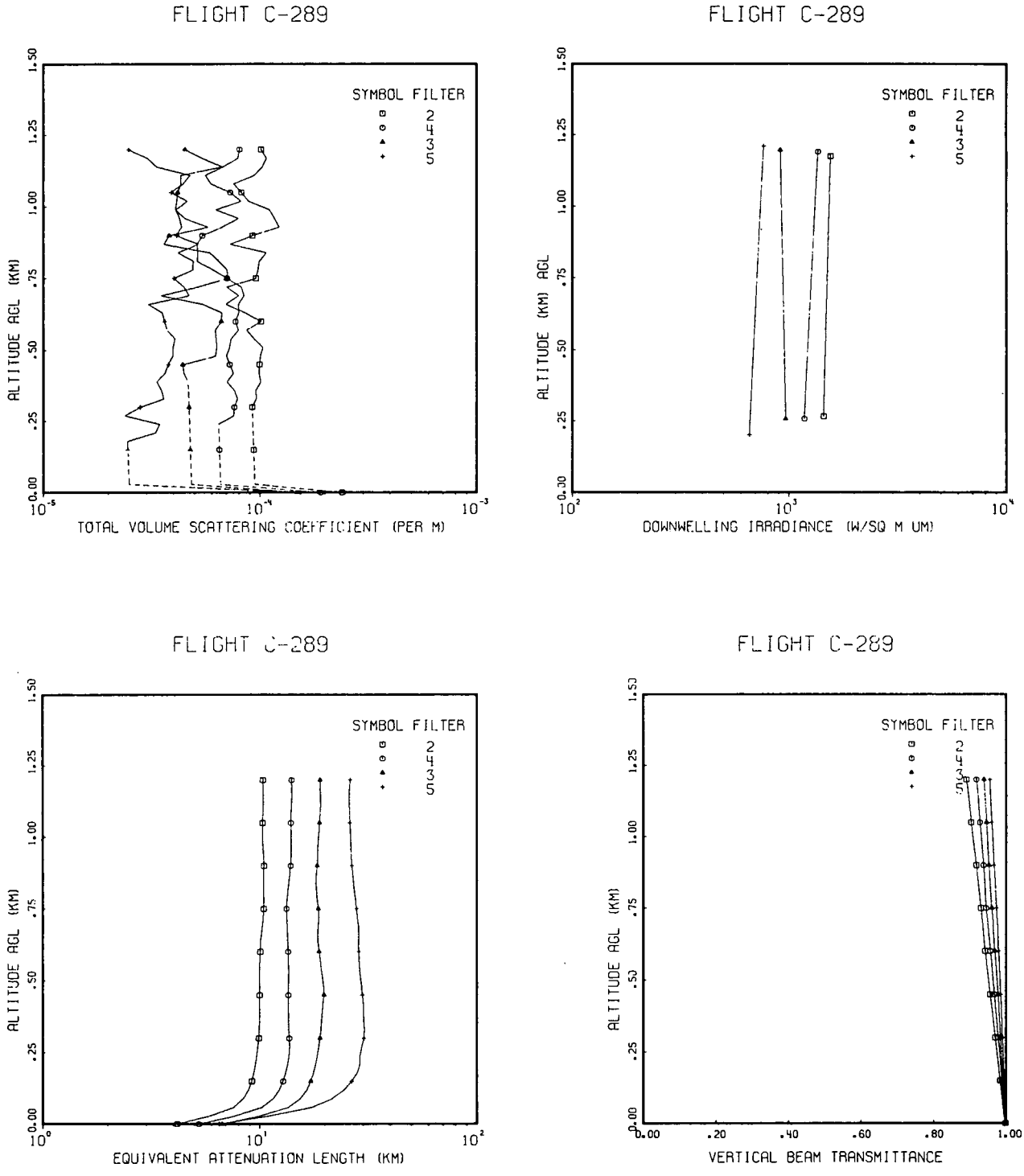

Fig. 7-6. Radiometric Data Graphs for Flight C-289, 14 June 1973, during HAVENVIEW II (AFGL-TR-76-0188).

FLIGHT NO. C-289

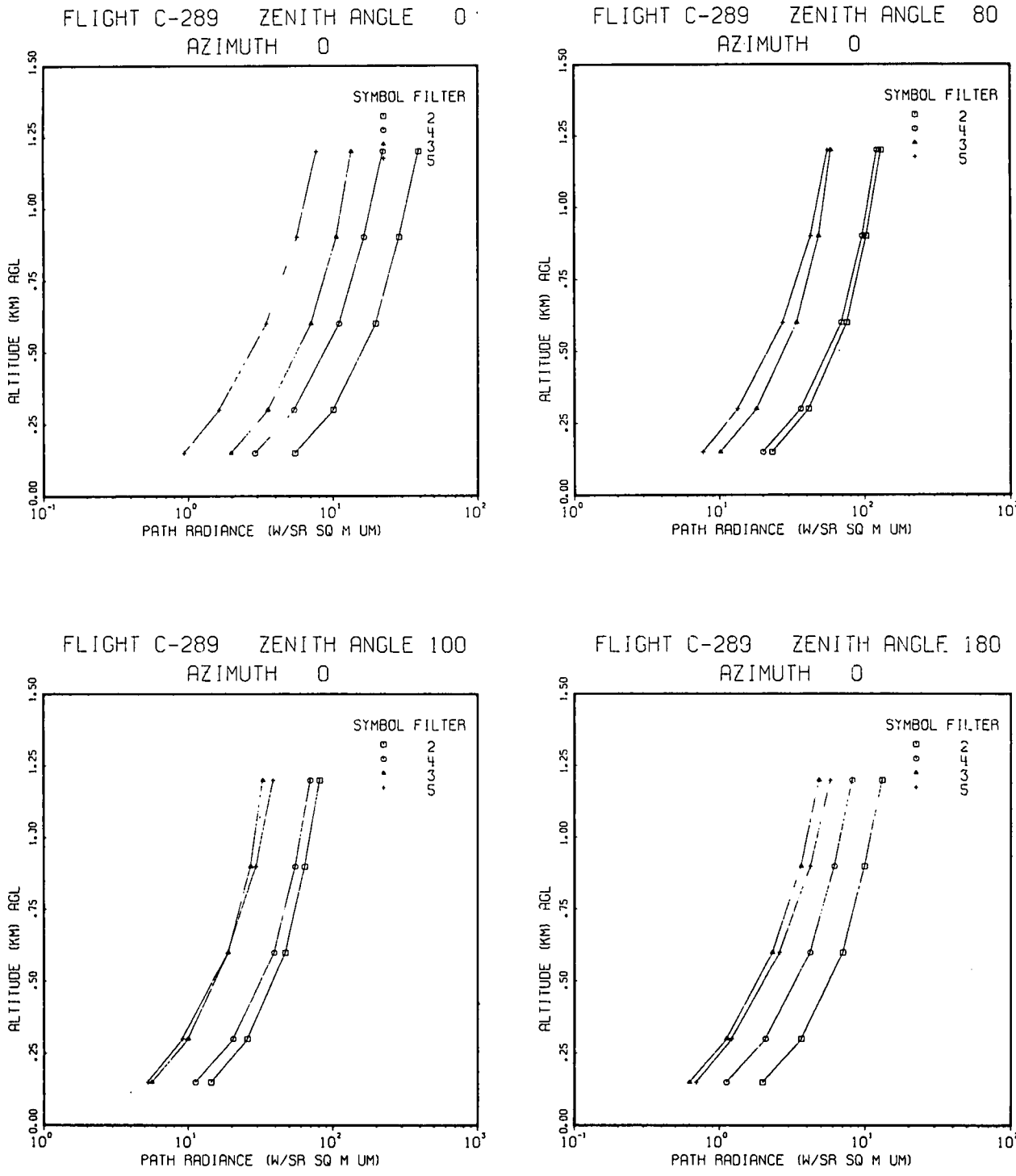

Fig. 7-7. Path Radiance Between Ground and the Altitude shown for Flight C-289, 14 June 1973, during HAVENVIEW II (AFGL-TR-76-0188).

FLIGHT NO. C-289

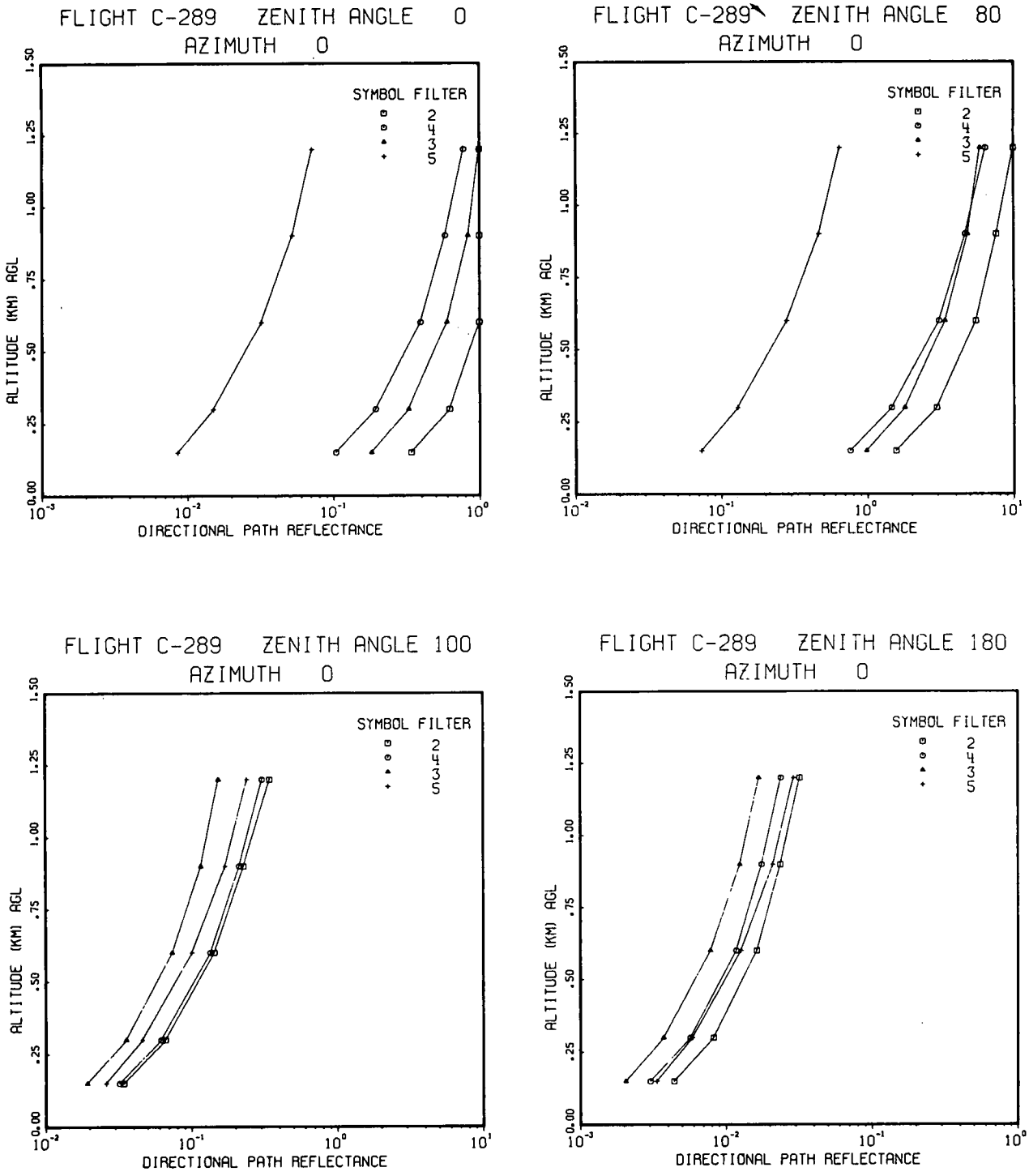

Fig. 7-8. Path Reflectance Between Ground and the Altitude shown for Flight C-289, 14 June 1973, during HAVENVIEW II (AFGL-TR-76-0188).

7.3. TYPICAL DATA COMPARISONS AND ANALYSIS

Portions of the data collected by the Geophysics and Visibility Laboratories during this contract interval have been reported previously as noted in the preceding sections. These data include flight data from the first three OPAQUE deployments, and a related supplement, flight data from two preceding HAVENVIEW deployments.

In order to present a quick overview of these data, portions of the original HAVENVIEW and OPAQUE data reports have been reproduced and presented herein with additional, but typical descriptive and analytic comment. For this summary presentation, the data have been grouped into composite sets covering all deployments to date. An individual comparison is made for each of several classes of data normally included in an OPAQUE data report. i.e. temperature, downwelling irradiance, and volume scattering coefficient profiles. A short summary of the cloud conditions encountered during these deployments is provided as a guide to the general weather environment.

METEOROLOGICAL DATA

The meteorological data reported for the OPAQUE deployments were more complete than for the two HAVENVIEW deployments. Climate maps and RAOB temperatures were not included in the HAVENVIEW I report, nor was there a detailed table of the description of cloud cover based upon the in-flight hemispherical pictures and observations by the on-board meteorologist. Airborne measurements of dewpoint-frostpoint temperature and hence computed relative humidities were unavailable for both HAVENVIEW deployments. The nearby weather station data tables were reported for HAVENVIEW I but not available for HAVENVIEW II. In-flight temperature measurements were reported for all flights, HAVENVIEW and OPAQUE.

Cloud Conditions. The upper hemisphere cloud conditions during the data-taking portion of the flights are summarized in Table 7.6. The flights are grouped into five categories as follows: I, clear during the entire flight; II, clear during a portion of the flight; III, scattered and/or broken clouds during the entire flight; IV, broken clouds varying with overcast during the flight; and V, overcast during the entire flight. The reported flights from the OPAQUE and HAVENVIEW deployments are grouped into these cloud categories in Table 7.6. The cloud descriptions upon which Table 7.6 is based are derived from the in-flight upper hemispherical pictures during the straight and level elements of the flight unless only vertical profile flight elements were flown. The picture descriptions in most cases are augmented by the descriptions reported by the meteorologist on-board the aircraft. Some of the flights have different cloud categories for various portions of the flight. In these cases the cloud category is noted for each filter.

The total number of flights under each cloud category is noted in the last row on Table 7.6. The bulk of the flights, 36 out of 45, are cloudy during the entire flight, that is, in cloud Categories III through V. This underscores the need for having adequate methods of obtaining path reflectance under cloudy day conditions.

Temperature. Temperature is generally a function of latitude and season with an expected diurnal and weather variability during any one season at a given latitude. The temperatures measured during

each flight during the radiometric data-taking for each filter have been averaged by altitude for the entire flight and graphed in one or more summary graphs for each deployment. These measured in-flight temperatures can be profitably compared to temperatures from the U.S. Standard Atmosphere Supplements (1966). The supplements provide temperatures for July and January for the two bracketing latitudes 45°N and 60°N as well as Spring, Fall temperature for 45°N.

Table 7.6. Reported European Data Flights Summarized by Cloud Category

Deployment	Season	Flights				
		I ○ Clear	II ○V◑ Part Clear Part Scattered	III ◑V◑ Scattered and/or Broken	IV ◑V⊕ Part Broken Part Overcast	V ⊕ Overcast
HAVENVIEW I	Spring '70	-	C-142	C-137 C-138		C-134 C-139 C-143
HAVENVIEW II	Spring '73	-	-	C-273 C-282 C-289	C-288(Filter 4)	C-279 C-280 C-281 C-282(Filters 2,3,5)
OPAQUE I	Spring '76	C-376 C-379	C-272 C-381 C-382	C-377(Filters 4,5)	C-377(Filters 2,3)	C-373 C-378
OPAQUE II	Fall '76	-	C-397 C-401(Filters 2,3)	C-390 C-391 C-395(Filters 4,5) C-398 C-400 C-401(Filters 4,5) C-402	C-395(Filters 2,3)	C-392 C-393 C-394 C-399
OPAQUE III	Summer '77	-	C-411(Filters 2,3) C-412	C-411(Filters 4,5) C-413(Filter 2) C-416 C-418(Filters 2,4) C-419 C-420(Filters 4,5) C-421	C-410 C-413(Filters 3,4,5) C-414 C-420(Filters 2,3)	C-415 C-418(Filters 3,5) C-422
Approx. No. of Flights		2	6+	13+	4+	15+

The temperatures for the Spring deployments are depicted in Fig. 7-9. The 45°N Spring/Fall temperature from the Supplements is depicted on each graph as well as two other curves to indicate expected latitudinal and/or seasonal differences. The HAVENVIEW I flights were at 48°N, very close in latitude to the latitude 45°N for the standard curves. The HAVENVIEW I temperatures cluster about the Spring/Fall curve and are bracketed by the July and January curves for 45°N. The HAVENVIEW II flights are all at low altitude so they are plotted on a different scale. The HAVENVIEW II flights were further North, at 53°, so HAVENVIEW II temperatures are generally equal or lower than the 45°N Spring/Fall as would be expected 8° further north. The OPAQUE I flights were for latitudes between 50°56'N and 53°N as indicated in the legend. The OPAQUE I temperatures are roughly equal to or lower than the 45°N Spring/Fall temperature curve, as expected.

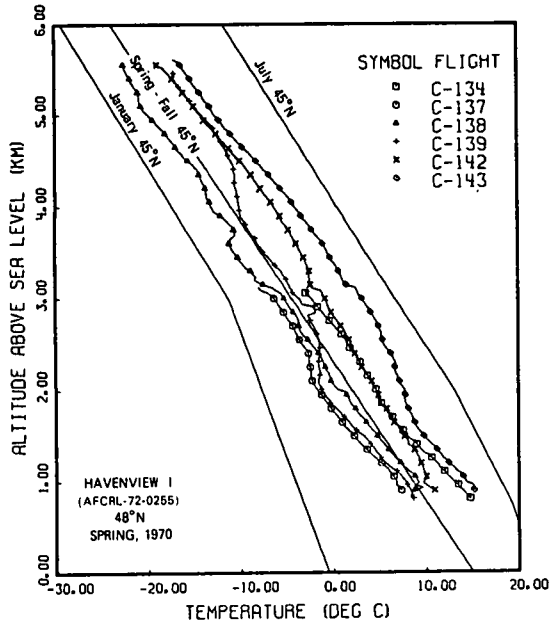

(a)

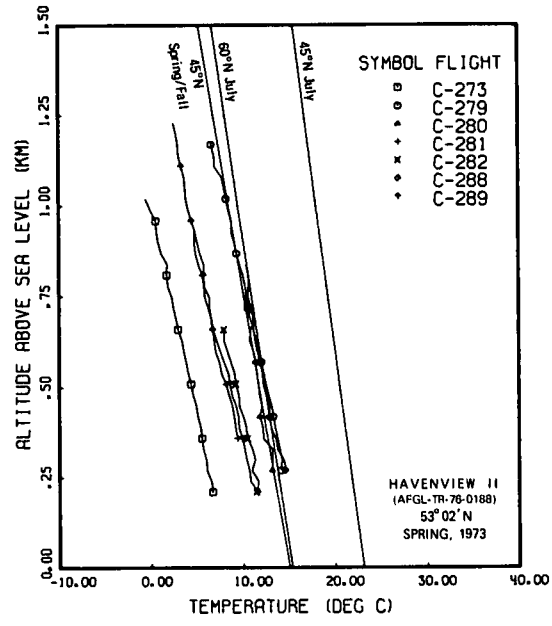

(b)

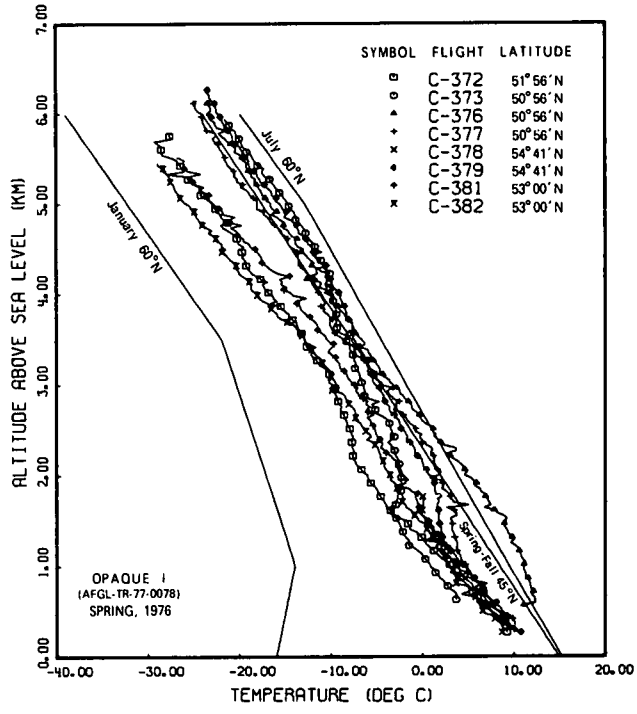

(c)

Fig. 7-9. Temperature Profiles from HAVENVIEW I, HAVENVIEW II and OPAQUE I Compared to Temperatures from U.S. Standard Atmosphere Supplements.

The temperatures for the Fall and Summer deployments, OPAQUE II and III, are depicted in Fig. 7-10. The 45°N Spring/Fall temperature curve is depicted again on the Fall deployment graphs of OPAQUE II. Comparison to this Spring/Fall curve serves to elucidate differences in temperature level and lapse rate from graph to graph and between individual flights. The OPAQUE II flights at 48°N (C-398 through C-402 at Bruz) are lower in temperature than the Spring flights at 48°N during HAVENVIEW I. The two flights during OPAQUE II with the highest temperatures were at 54°41'N at Rodby, C-390 and C-391. Both these flights also have strong temperature inversions at low altitude.

The OPAQUE III temperatures, in the lower half of Fig. 7-10, are compared to the standard curves for 45° and 60°N July. The temperatures at 48°N are slightly higher than the ones further north during this deployment. The temperatures for most of the flights in the 52°53'N to 54°41'N range of latitudes cluster about the 60°N July curve except for Flights C-413 at Rodby and C-414 at Ahlhorn which have lower temperatures than all the rest of the OPAQUE III flights.

RADIOMETRIC DATA

Total Volume Scattering Coefficient. The data reported for the total volume scattering coefficient were measured during the vertical profile flight elements and averaged for each 30 meter altitude increment. To more easily compare the scattering characteristics of the flights, the Filter 4 (pseudo-photopic*) total volume scattering coefficient profiles for each flight have been graphed in one or more summary graphs for each deployment. These graphs are presented in Figs. 7-11 and 7-12.

The total volume scattering coefficient graphs for the Spring deployments are depicted in Fig. 7-11. Note the changes in scale between the three graphs. HAVENVIEW I and II data are on a two log scale with limits of 1E-5 to 1E-3 whereas the OPAQUE I data are on a three log scale with limits of 1E-5 to 1E-2. Also the HAVENVIEW II data are on a different altitude scale since those flights were all at low altitude. These differences in scale make it inconvenient to make direct visual comparisons, however data trends are readily discernible.

The HAVENVIEW I data all indicate a heavy primary haze layer at low altitude and clear above 2 km. All the HAVENVIEW II flights were under a cloud layer at low altitude and the scattering data indicate less haze (clearer) than the HAVENVIEW II data at comparable altitudes. The OPAQUE I total volume scattering coefficient profiles are more complicated and show a wider range of values than either HAVENVIEW I or II. The OPAQUE I data show more than one haze layer, sometimes at high altitude. The OPAQUE I low altitude data (within the primary haze layer) range both hazier and clearer than the HAVENVIEW I data, but no flight is as clear at low altitude as some of the HAVENVIEW II flights. The high altitude data indicate mostly clear above 3 kilometers, with air clarity comparable to or greater than HAVENVIEW II at high altitude.

The total volume scattering coefficient graphs for the Fall and Summer deployments are depicted in Fig. 7-12. Again note the changes in scattering coefficient scale which complicate the visual comparisons. All the graphs in Figs. 7-11 and 7-12 were available in the data reports. For easier intercomparison between all the OPAQUE deployments I through V, all the data will soon be regraphed on a common scale even though that scale might not be optimum for each individual deployment or group of flights.

*The pseudo-photopic filter was designated as Filter 5 during HAVENVIEW I.

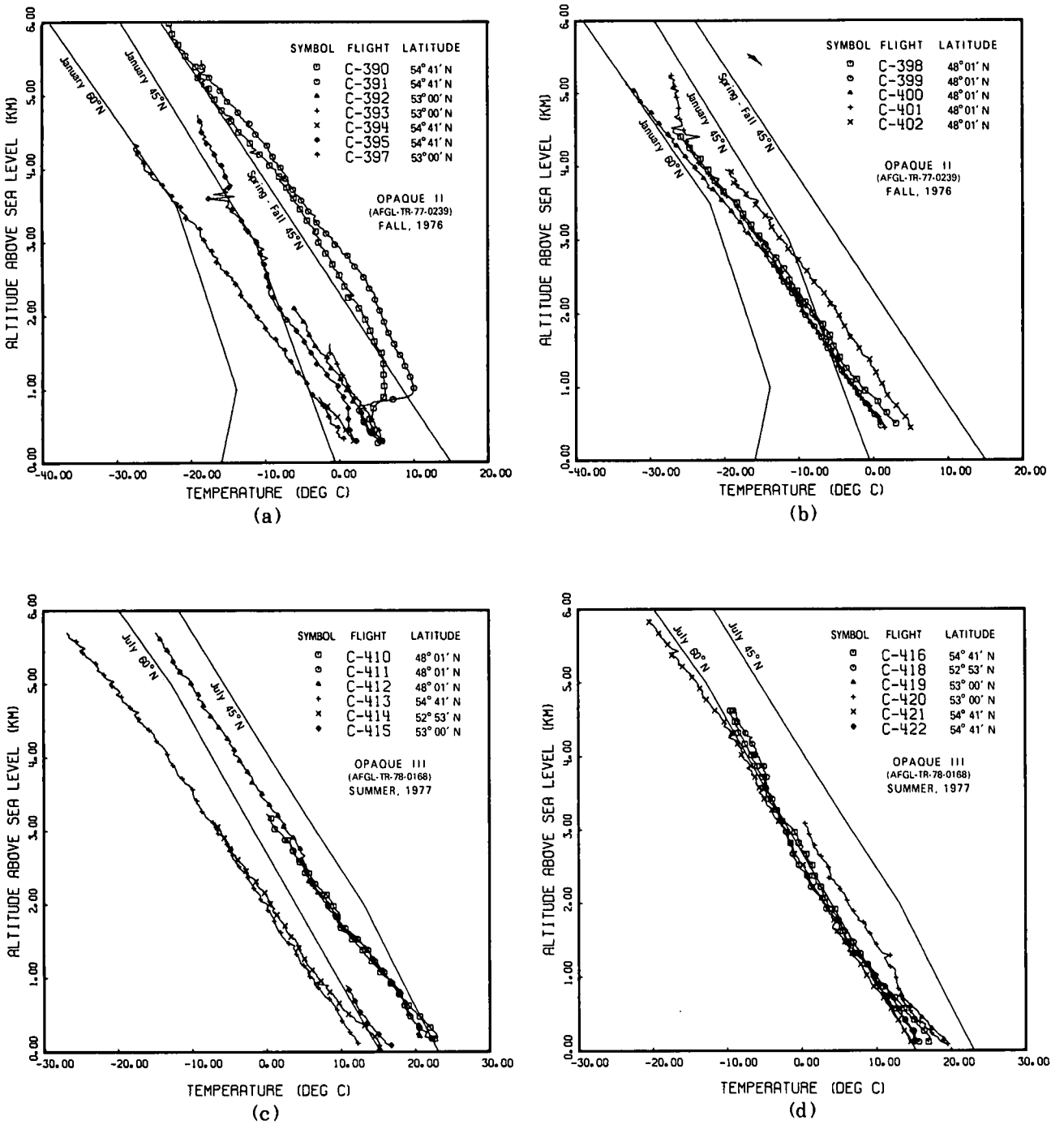

Fig. 7-10. Temperature Profiles from OPAQUE II and OPAQUE III Compared to Temperatures from U.S. Standard Atmosphere Supplements.

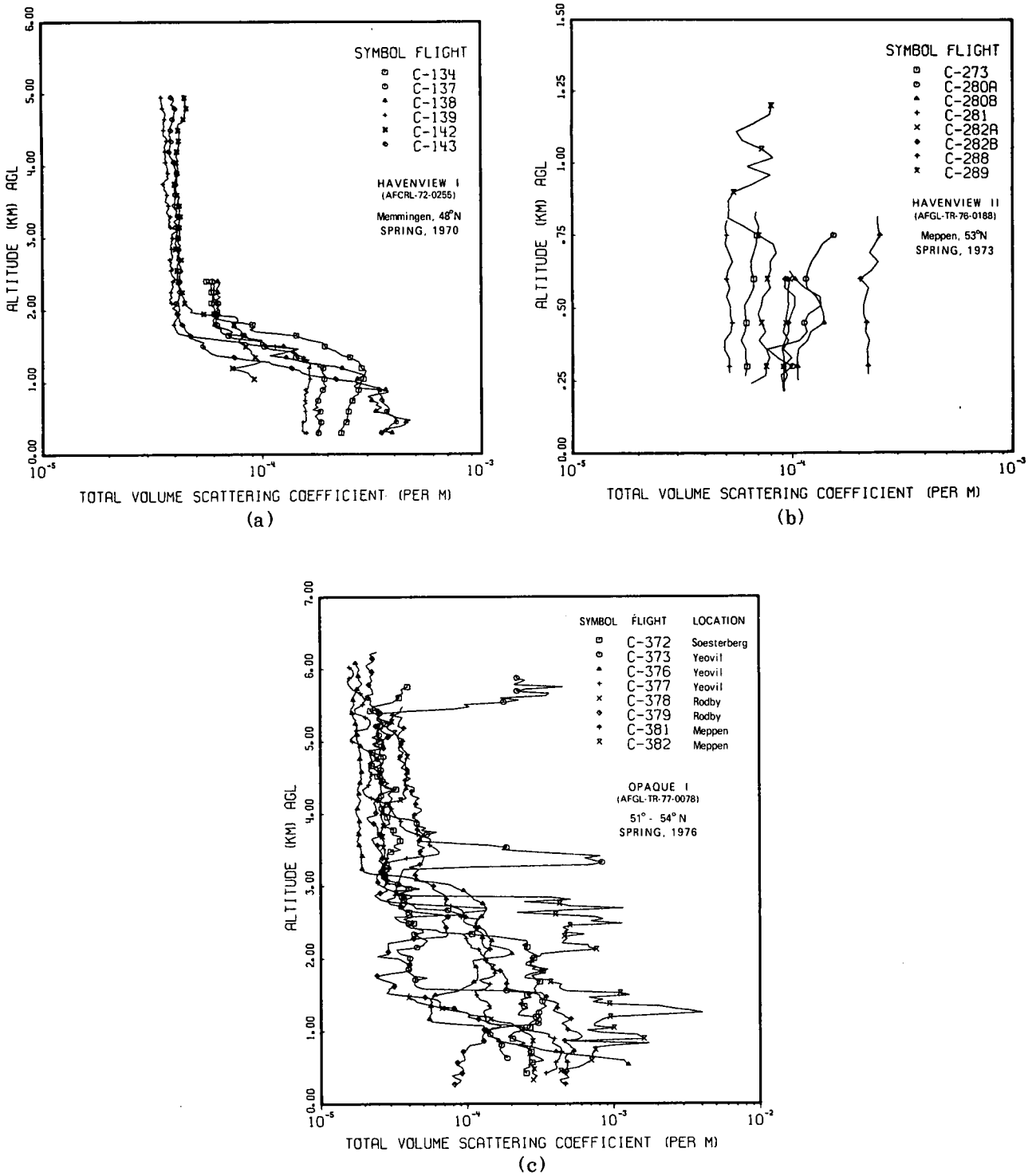

Fig. 7-11. Pseudo-Photopic Total Volume Scattering Coefficient Profiles for HAVENVIEW I, HAVENVIEW II and OPAQUE I.

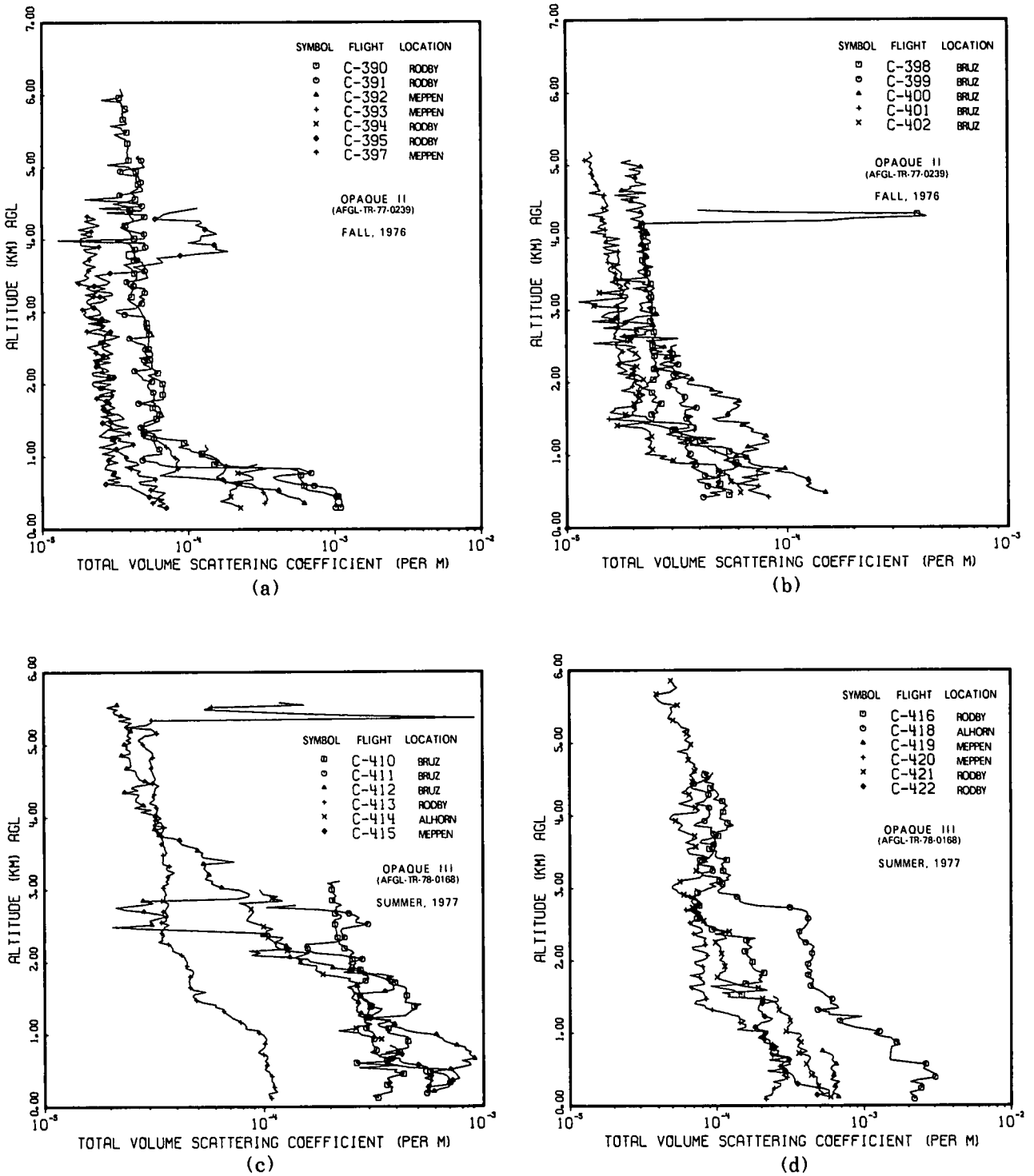

Fig. 7-12. Pseudo-Photopic Total Volume Scattering Coefficient Profiles for OPAQUE II and OPAQUE III.

The OPAQUE II Fall flights have profiles that are generally less complicated than the OPAQUE I profiles. The high altitude clear layer generally extends lower, including the 1.5 to 3 km altitudes in the high altitude regime. Also, except for a few high altitude haze or cloud layers, most of the profiles for OPAQUE II show only one low altitude primary haze layer.

The OPAQUE III Summer flights are generally both less clear at high altitude and hazier at low altitude than OPAQUE II with some of the haze layers extending up to 3 km as in OPAQUE I.

Irradiance. Downwelling irradiance was measured by the dual irradiometer during the vertical profile elements of each flight concurrently with the total volume scattering coefficient data. The orientation of the dual irradiometer was roughly +3½ degrees from horizontal during ascent and -3½ degrees during descent. The Filter 4 (pseudo-photopic) data were generally measured during an ascent.

Downwelling irradiance for the Filter 4 (pseudo-photopic) has been graphed in one or more summary graphs for each of the first three OPAQUE deployments in Figs. 7-13 and 7-14. The irradiances were averaged for each 30 meter altitude increment. The level of irradiance is a function of sun zenith angle and cloud cover, therefore the cloud cover for each flight is noted in the legend and the zenith angle range of the flights indicated for each graph. The variability of irradiance with altitude is primarily a function of amount and thickness of cloud cover and the variability of sun occultation by the clouds.

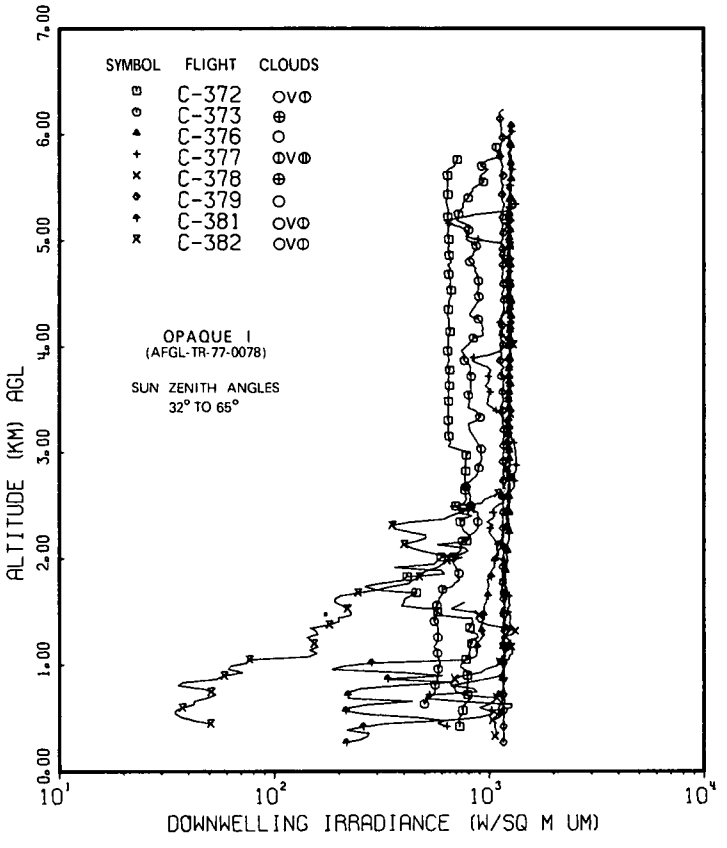

Fig. 7-13. Pseudo-Photopic Downwelling Irradiance Profiles for OPAQUE I.

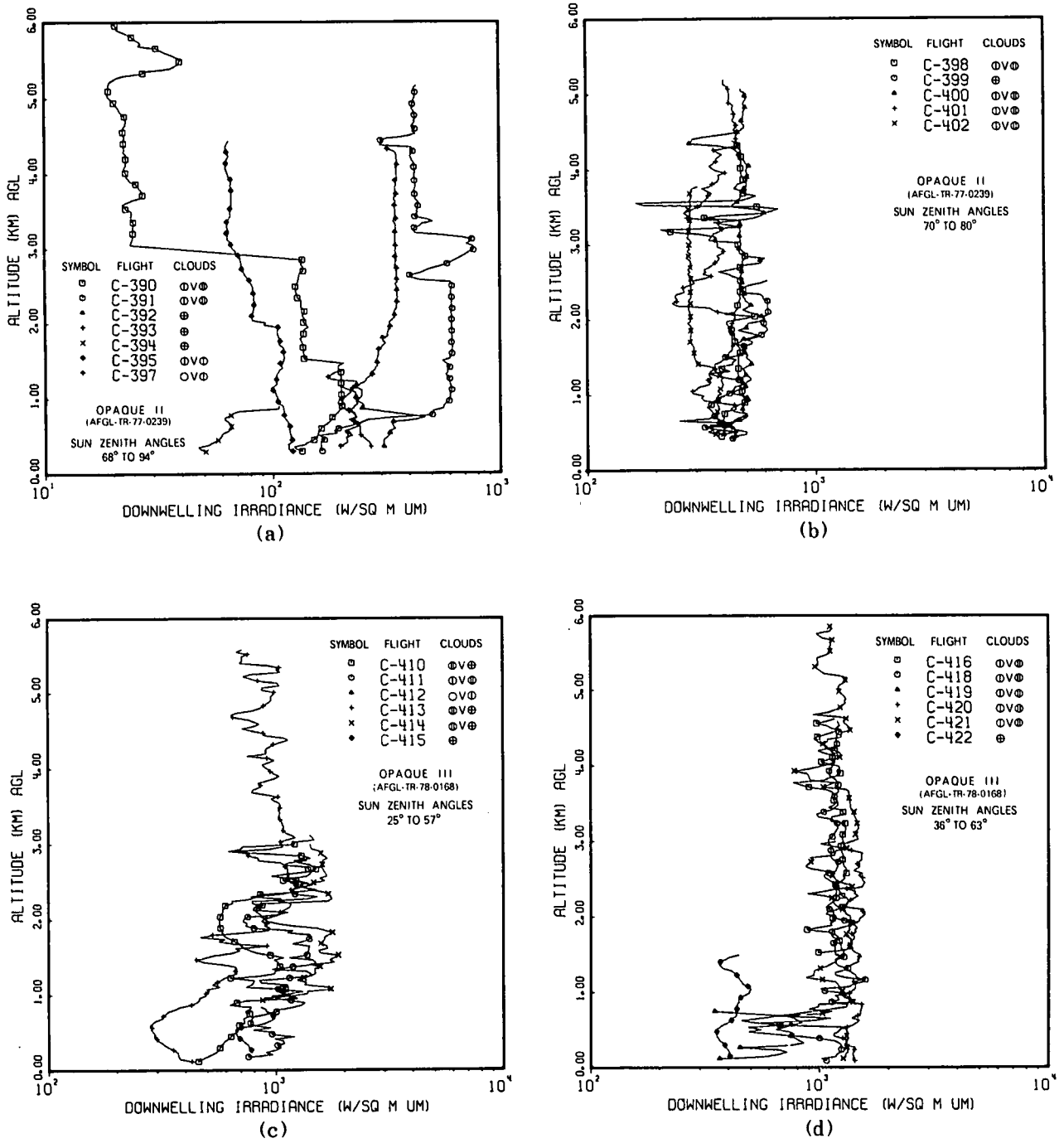

Fig. 7-14. Pseudo-Photopic Downwelling Irradiance Profiles for OPAQUE II and OPAQUE III.

The sun zenith angles during OPAQUE I (April-May or Spring) are roughly comparable to the sun angles during OPAQUE III (July-August or Summer) since both are near the Summer solstice in date. The generally high level of downwelling irradiance during these flights, near 1E3, regardless of cloud cover, is largely a function of the sun zenith angles, since the flights tended to be near noon. Flight C-382 is the exception, showing the effects of low altitude clouds and deteriorating weather.

The sun zenith angles during OPAQUE II (October-November-December, Fall) are larger since it was after the Fall equinox. Flights C-390 and C-395 were both late in the day at large sun zenith angles, θ_s=80°→94° for C-390 and θ_s=78→86° for C-395, all other OPAQUE II flights had finished by the time the sun reached 80°. The large shift in irradiance at 3 kilometers on Flight C-390 occurred because of the time lapse during the intervening straight and level flight element. The low altitude data were during a sun zenith angle of about 82 degrees whereas when the high altitude portion of the ascent began, the sun had dropped to an 88 degree zenith angle.

A more thorough analysis of these summarized data in conjunction with their counterpart data from OPAQUE IV and OPAQUE V is anticipated within the near future. At that time the complete four season documentation will be available for both climatological study, and an analysis of the variation between optical and meteorological properties as a function of the widely diverse weather conditions encountered during this extensive measurement program.

7.4. NUMERICAL EXAMPLES

Typical applications in which data generated during this contract interval might be utilized are illustrated in the following examples, which have been abstracted from Duntley, *et al.* (1976). For further explanation or definition of the terms and vocabulary used in the examples, one is referred to Appendix A and/or Appendix B.

The OPAQUE reports, Duntley, *et al.* (1977, 1978a and 1978b) contain only scattering coefficient and irradiance profiles. These data are appropriate for use in calculations illustrated by examples A and B.

The more complete set of optical atmospheric properties contained in the HAVENVIEW II report, Duntley, *et al.* (1976) are appropriate for use in all of the examples A through N.

It is apparent that full utilization of the OPAQUE data base must await the complete processing, referred to in previous sections, which will result in OPAQUE data bases equivalent to the HAVENVIEW II base. This continued processing effort is planned to begin during 1979.

EQUIVALENT ATTENUATION LENGTH AND BEAM TRANSMITTANCE EXAMPLES

The equivalent attenuation length table in Duntley, *et al.* (1976), can easily be used in Eq. (A.16) to obtain beam transmittance for intermediate object altitudes and zenith angles for the upward path of sight and for intermediate sensor altitudes and zenith angles for the downward path of sight. Thus, beam transmittance can be readily computed for more paths of sight than the seven zenith angles tabularly presented and for more path lengths than the five tabularly presented.

A. For an upward path of sight at 60-degree zenith angle, with an object altitude z_t at 1080 meters Eq. (A.16) would be written

$$T_{2160}(0, 60°) = \exp\left\{ [- 1080m/\bar{L}(1080)] \; sec\; 60° \right\} .$$

Using the equivalent attenuation length converted to meters for Flight C-289 Filter 4 from Section 7.3 in Duntley, *et al.* (1976), Eq. (A.16) becomes

$$T_{2160}(0, 60°) = \exp\left\{ [- 1080m/14000m] \; 2 \right\} = 0.857 .$$

B. For a downward path of sight at a zenith angle of 135 degrees from a sensor altitude of 750 meters, Eq. (A.16) would become

$$T_{1061}(750, 135°) = \exp\left\{ [- 750m/\bar{L}(750)] \; |sec 135°| \right\} .$$

Again using the values from Flight C-289 Filter 4, Eq. (A.16) becomes

$$T_{1061}(750, 135°) = \exp\left\{ [- 750m/13300m] \; 1.414 \right\} = 0.923 .$$

SKY REFLECTANCE, INHERENT CONTRAST AND INHERENT RADIANCE EXAMPLES

The effective sky reflectance tables in Duntley, *et al.* (1976) can be used with Eq. (A.8) to obtain inherent contrast of non-self-radiant objects against the sky background.

C. For an upward path of sight at 0 degree zenith angle, with an object at 1200 meters the maximum object altitude for Flight C-289, Eq. (A.8) would be written,

$$C_o(1200, 0°, 0°) = [{}_tR_o(1200, 0°, 0°)/{}_bR_o(1200, 0°, 0°)] - 1 .$$

Let us use an aircraft as an object. Lacking a direct measure of the reflectance of unpainted aluminum under the appropriate lighting conditions, we will assume a reflectance of 0.4 for this Filter 4 example. Note that the upwelling irradiance, $H(z_t, u)$, which is relatively diffuse, is used in determining the object reflectance for all upward paths of sight

regardless of the object surface orientation. Using the effective sky reflectance from Flight C-289 Filter 4, Eq. (A.8) becomes

$$C_o(1200, 0°, 0°) = [0.4/5.27] - 1 = -0.924 .$$

D. The inherent radiance of the aluminum would be found by using Eq. (7.1) from Duntley, *et al.* (1976), as follows,

$${}_tN_o(1200, 0°, 0°) = \frac{1}{\pi} {}_tR_o(1200, 0°, 0°)\ H(1200,u) .$$

Using the upwelling irradiance at 1200 meters $H(1200,u)$ for Flight C-289 from the Filter 4 table at the top of the page of reflectance, Section 7.3, Duntley, *et al.* (1976), and the aluminum reflectance assumed above, Eq. (7.1) becomes

$${}_tN_o(1200, 0°, 0°) = \frac{1}{\pi}\ 0.4\ (97.1\ w/m^2\mu m) = 12.4\ w/\Omega\, m^2\mu m .$$

TERRAIN REFLECTANCE, INHERENT CONTRAST AND INHERENT RADIANCE EXAMPLES

The terrain reflectance tables in Duntley, *et al.* (1976) can be used with Eq. (A.8) to obtain the inherent contrast of non-self-radiant objects against the terrain background.

E. For the downward path of sight let us assume a nadir path of sight at 180 degrees zenith angle. Eq. (A.8) would be written, thus

$$C_o(0, 180°, 0°) = [{}_tR_o(0, 180°, 0°)/{}_bR_o(0, 180°, 0°)] - 1 .$$

Let us compute the inherent contrast for Filter 4 of a hard packed yellowish dirt road for Flight C-289. For the surrounding fields, let us assume the reflectance equal to that of a lush meadow in autumn, 0.071 (Gordon and Church (1966) p. 796). The reflectance of dirt, hard-packed and yellowish from Gordon (1964) p. 559 is 0.243. Thus, Eq. (A.8) becomes

$$C_o(0, 180°, 0°) = [0.243/0.071] - 1 = 2.42 .$$

F. The inherent radiance of the road would be found by using Eq. (7.3) from Duntley, *et al.* (1976) which is

$$N_o(0,\theta,\phi) = \frac{1}{\pi} R_o(0,\theta,\phi)\ H(0,d)\ . \tag{7.1}$$

Thus the inherent radiance of the road for the nadir path of sight is

$${}_tN_o(0, 180°, 0°) = \frac{1}{\pi}\ {}_tR_o(0, 180°, 0°)\ H(0,d)\ .$$

Using the downwelling irradiance for Filter 4 for Flight C-289 from the irradiance table at the top of the reflectance page in Section 7.3 of Duntley, *et al.* (1976), with the dirt reflectance from above, Eq. (7.1) becomes

$${}_tN_o(0, 180°, 0°) = \frac{1}{\pi}\ 0.243\ [1180\ w/m^2\mu m] = 91.3\ w/\Omega\, m^2\mu m\ .$$

PATH RADIANCE AND APPARENT RADIANCE, UPWARD PATH EXAMPLE

The path radiance tables can be used with Eq. (7.2) Duntley, *et al.* (1976) to obtain the apparent radiance at ground level of an object or background at altitude,

$$N_r(0,\theta,\phi) = N_o(z_t,\theta,\phi)\ T_r(0,\theta) + N_r^*(0,\theta,\phi)\ . \tag{7.2}$$

G. For an upward path of sight at 0 degrees zenith angle, with the object at 1200 meters, Eq. (7.2) would be written

$$N_{1200}(0, 0°, 0°) = N_o(1200, 0°, 0°)\ T_{1200}(0, 0°) + N^*_{1200}(0, 0°, 0°)\ .$$

The appropriate transmittance and path radiance for the above equation are listed under 1200 meters, the object altitude in the tables for flight C-289 in Section 7.3 Duntley, *et al.* (1976). Using the aircraft as the object, the inherent radiance as computed earlier for Flight C-289 Filter 4 is 1.24E1. Then, using appropriate values from Flight C-289, Eq. (7.2) becomes

$$N_{1200}(0, 0°, 0°) = 12.4\ (0.918) + 22.2 = 33.6 w/\Omega\, m^2\mu m\ .$$

PATH RADIANCE AND APPARENT RADIANCE, DOWNWARD PATH EXAMPLE

The path radiance tables can be used with Eq. (7.4), Duntley, *et al.* (1976) to obtain the apparent radiance at altitude of an object or background at ground level,

$$N_r(z,\theta,\phi) = N_o(0,\theta,\phi)\ T_r(z,\theta) + N_r^*(z,\theta,\phi)\ . \tag{7.3}$$

H. For a downward path of sight at 180 degrees zenith angle, with the sensor at 1200 meters, Eq. (7.3) would be written

$$N_{1200}(1200, 180°, 0°) = N_o(0, 180°, 0°)\ T_{1200}(1200, 180°) + N^*_{1200}(1200, 180°, 0°)\ .$$

Using the previous example of a hard-packed yellow dirt road as an example with Filter 4 data from Flight C-289, Eq. (7.3) becomes

$$N_{1200}(1200, 180°, 0°) = 91.3\ (0.918) + 8.21 = 92.0\ w/\Omega\, m^2 \mu m\ .$$

PATH REFLECTANCE, CONTRAST TRANSMITTANCE AND APPARENT CONTRAST AGAINST NON-SKY BACKGROUND, UPWARD PATH EXAMPLE

The path reflectance tables in Duntley, *et al.* (1976) can be used with Eq. (A.3) to obtain the contrast transmittance at ground level of an object against a background other than the sky. For instance, the painted markings on an aircraft would be viewed against the aircraft as background (not the sky).

I. For an upward path of sight at 0 degrees zenith angle, with the object at 1200 meters, Eq. (A.3) would be written

$${}_b\tau_{1200}(0, 0°, 0°) = \left\{ 1 + [R^*_{1200}(0, 0°, 0°)/{}_bR_o(1200, 0°, 0°] \right\}^{-1}\ .$$

The reflectance of the unpainted aluminum surface has already been assumed to be 0.4 for Filter 4. The appropriate value of path reflectance is found at the object altitude 1200 meters in the Filter 4 tables for Flight C-289, and Eq. (A.3) becomes

$${}_b\tau_{1200}(0, 0°, 0°) = \left\{ 1 + [0.781/0.4] \right\}^{-1} = 0.339\ .$$

J. The final step would be to compute the apparent contrast. To obtain apparent contrast Eq. (A.1) can be transposed as follows

$$C_r(z,\theta,\phi) = C_o(z_t,\theta,\phi)\ {}_b\tau_r(z,\theta\phi)\ . \tag{7.4}$$

For an upward path of sight at 0 degrees zenith angle, with the object at 1200 meters, Eq. (7.4) would be written

$$C_{1200}(0,0°,0°) = C_o(1200,0°,0°)\ {}_b\tau_{1200}(0,0°,0°)\ .$$

If one assumes the diffuse reflectance of the black paint to be 0.04, its inherent contrast against the aircraft background is -0.90. Thus the apparent contrast at ground level of the black paint as seen against the aircraft background at 1200 meters is

$$C_{1200}(0,0°,0°) = -0.90(0.339) = -0.305\ .$$

PATH REFLECTANCE, CONTRAST TRANSMITTANCE AND APPARENT CONTRAST AGAINST SKY BACKGROUND, UPWARD PATH EXAMPLE

The path reflectance tables can be used with Eq. (A.3) to obtain the contrast transmittance at ground level of an object against a background of typical skies.

K. For illustrative purposes let us compute the contrast transmittance of any object viewed against the average zenith sky at 1200 meters from the sky reflectance table for C-289 in Section 7.3 of Duntley, *et al.* (1976). Eq. (A.3) becomes

$${}_b\tau_{1200}(0,0°,0°) = \left\{1 + [0.781/5.27]\right\}^{-1} = .871\ .$$

L. Now using the aircraft as the object, the inherent contrast for Filter 4 was computed earlier for Flight C-289 as -0.924, then

$$C_{1200}(0,0°,0°) = -0.924(0.871) = -0.805\ .$$

This is the apparent contrast of the aircraft at 1200 meters as viewed at ground level against the average zenith sky radiance.

Since the sky radiance during the seven HAVENVIEW II flights was quite variable, it is also reasonable to assume a range of effective sky reflectances for each given path of sight which would be consistent with the overall irradiance level and the path reflectance derived for each flight. Contrast transmittance with these various effective sky reflectances as background would be computed in a manner similar to the above example. This assumes that the sky radiance area is small enough in extent so as not to appreciably effect the path reflectance and takes cognizance of the sky radiance variability illustrated in Fig. 8-6 of Duntley, *et al.* (1976). The difficulty lies in determining reasonable effective sky reflectance values to utilize in each instance. The concept of effective sky reflectance is a new one, and as yet there is not a large body of data nor much experience in using the data now available. This is an area of inquiry which should be pursued further so that reasonable values of effective sky reflectance could be made available for clear and cloudy days for a range of values of sun zenith angle, space-to-altitude transmittance, and scalar albedo.

PATH REFLECTANCE, CONTRAST TRANSMITTANCE AND APPARENT CONTRAST, DOWNWARD PATH EXAMPLE

The path reflectance tables can also be used with Eq. (A.3) to obtain contrast transmittance at altitude of an object at ground level as seen against various backgrounds small enough in extent so as not to have an appreciable effect on the path reflectance.

M. For a downward path of sight at 180 degrees zenith angle, with the sensor at 1200 meters, Eq. (A.3) would be written thus

$$ {}_b\tau_{1200}(1200, 180°, 0°) = \left\{ 1 + [R^*_{1200}(1200, 180°, 0°)/{}_bR_o(0, 180°, 0°)] \right\}^{-1} . $$

Using our previous example of the lush meadow as a background and a path reflectance value from Flight C-289 for Filter 4 Eq. (A.3) becomes

$$ {}_b\tau_{1200}(1200, 180°, 0°) = \left\{ 1 + [0.0239/0.071] \right\}^{-1} = 0.748 . $$

N. Again, a concluding step would be to compute the apparent contrast at 1200 meters of the object, in this case the yellow dirt road. Rewriting Eq. (7.4) for the downward path case, it becomes

$$ C_{1200}(1200, 180°, 0°) = C_o(0, 180°, 0°)\ {}_b\tau_{1200}(1200, 180°, 0°) . $$

The inherent contrast of the road against the meadow background was computed earlier as 2.42. Thus the apparent contrast of the road at 1200-meter altitude is

$$C_{1200}(1200, 180°, 0°) = 2.42(0.748) = 1.81 ,$$

which is a relatively high apparent contrast.

7.5. GRAPHICAL AIDS TO ANALYSIS

The OPAQUE airborne data base resulting from the flights described in Section 6 contains a variety of measured optical and meteorological properties, which lend themselves to studies aimed at identifying anticipated optical/meteorological linking relationships. In an initial effort to expedite these studies, several display formats have been developed for automatic computer generation. These displays are generated by program DIOGPLOT, and are produced automatically for each flight that is processed, unless specifically deleted. This automatic feature was initially proposed in the OPAQUE II report, AFGL-TR-77-0239, Duntley, *et al.* (1978a), and partially demonstrated in the OPAQUE III report, AFGL-TR-78-0168, Duntley, *et al.* (1978b). In these two earlier reports the examples presented were plots illustrating photopic scattering coefficient and relative humidity versus altitude as in Fig. 7-15c. The full selection of automatic displays is represented in Fig. 7-15 and 7-16 which reproduce the displays generated for Flight C-418 made in the vicinity of Ahlhorn, Germany during the OPAQUE III deployment.

The information contained in plots 7-15a&b are the basic measured data for the flight, and the presentations in 7-15c&d plus those in 7-16a,b,c&d, represent derived relationships of general interest. Several general comments related to these illustrative samples are contained in the following brief paragraphs.

Plots 7-15a&b are typical of those found in each of the previously referenced data reports and are fully described therein. Plot 7-15c which represents the common plot of one profile from each of the 7-15a&b plots has also been presented in the prior publications. The remaining five, however, represent alternative but related data illustrated here for the first time.

Fig. 7-15d plots the ratio of the total to Rayleigh volume scattering coefficient as a function of altitude. The Rayleigh volume scattering coefficient ${}_{R}s(z)$ is

$${}_{R}s(z) = {}_{R}s(0)\ P(z)/[\ T(z)3.516x10^{3}\ ] \qquad (7.5)$$

where $P(z)$ is pressure in dynes cm^{-2}, $T(z)$ is temperature in degrees kelvin. The number $3.516x10^{3}$ is the density at standard sea level pressure and 15°C Celsius temperature times the universal gas constant. It has units of dynes $cm^{-2}°k^{-1}$. The ${}_{R}s(0)$ is computed for each optical passband based upon monochromatic values for 15° Celsius and sea level pressure.

The ratio $s(z)/_R s(z)$ is of interest because it would be constant if the total volume scattering coefficient were to decrease at the same rate as the density. This ratio multiplied by the ground level Rayleigh scattering coefficient $_R s(0)$ is sometimes referred to as the equivalent ground level scattering coefficient.

Fig. 7-16a represents the absolute humidity AH (or density of water vapor, ρ_w) vs. altitude. It is computed from the equation

$$AH = \rho_w = \frac{P_s(t_d)\ M_w}{83.1432(t + 273.15°)} \tag{7.6}$$

where P_s is the saturated vapor pressure at dewpoint or frostpoint temperature, M_w is the mass per mole of water which equals 18.01534 g/mol, and t and t_d are temperature and dewpoint temperature.

Fig. 7-16b represents the Mie volume scattering coefficient as a function of altitude. It is computed from the equation

$$_M s(z) = s(z) - {}_R s(z)\ . \tag{7.7}$$

Fig. 7-16c represents a cross plot of the relative humidity and the $s(z)/_R s(z)$ ratio at the same altitude, and Fig. 7-16d represents a cross plot of the absolute humidity and the Mie volume scattering coefficient at the same altitude. Fig. 7-16c&d are intended to help determine the quantitative relationship between the parameters and to illustrate the degree of correlation.

Whereas each of the graphic presentations shown in Figs. 7-15 and 7-16 have data representing each of four different spectral bands, specific applications related to photopic studies are simplified by automatically deleting all but the Filter 4 (i.e. photopic) data. Neither this option nor curve fitting procedures suitable for the data in Figs. 7-16c&d are illustrated in this sample though both are helpful to the analyst.

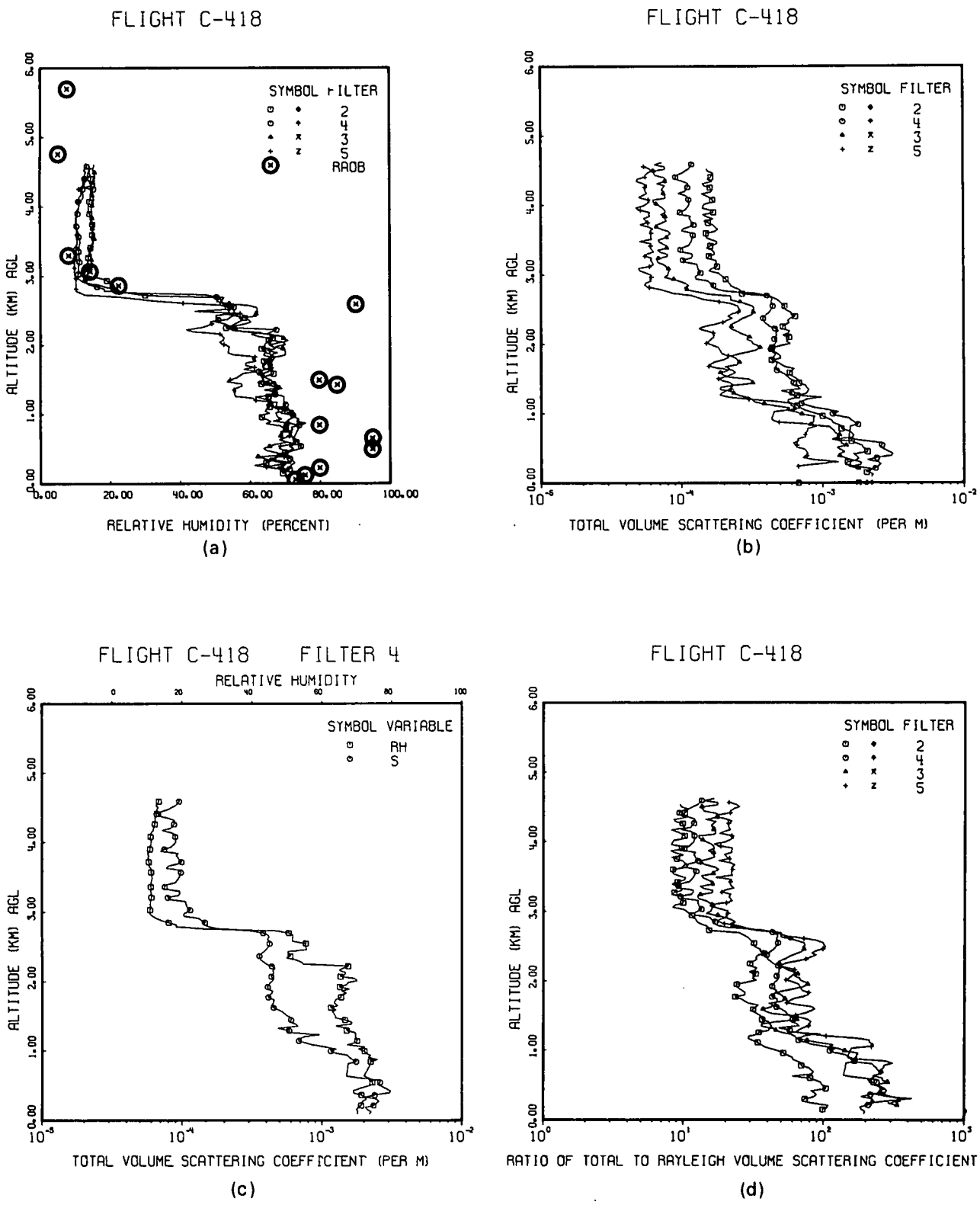

Fig. 7-15. Graphical Data for Flight C-418, OPAQUE III.

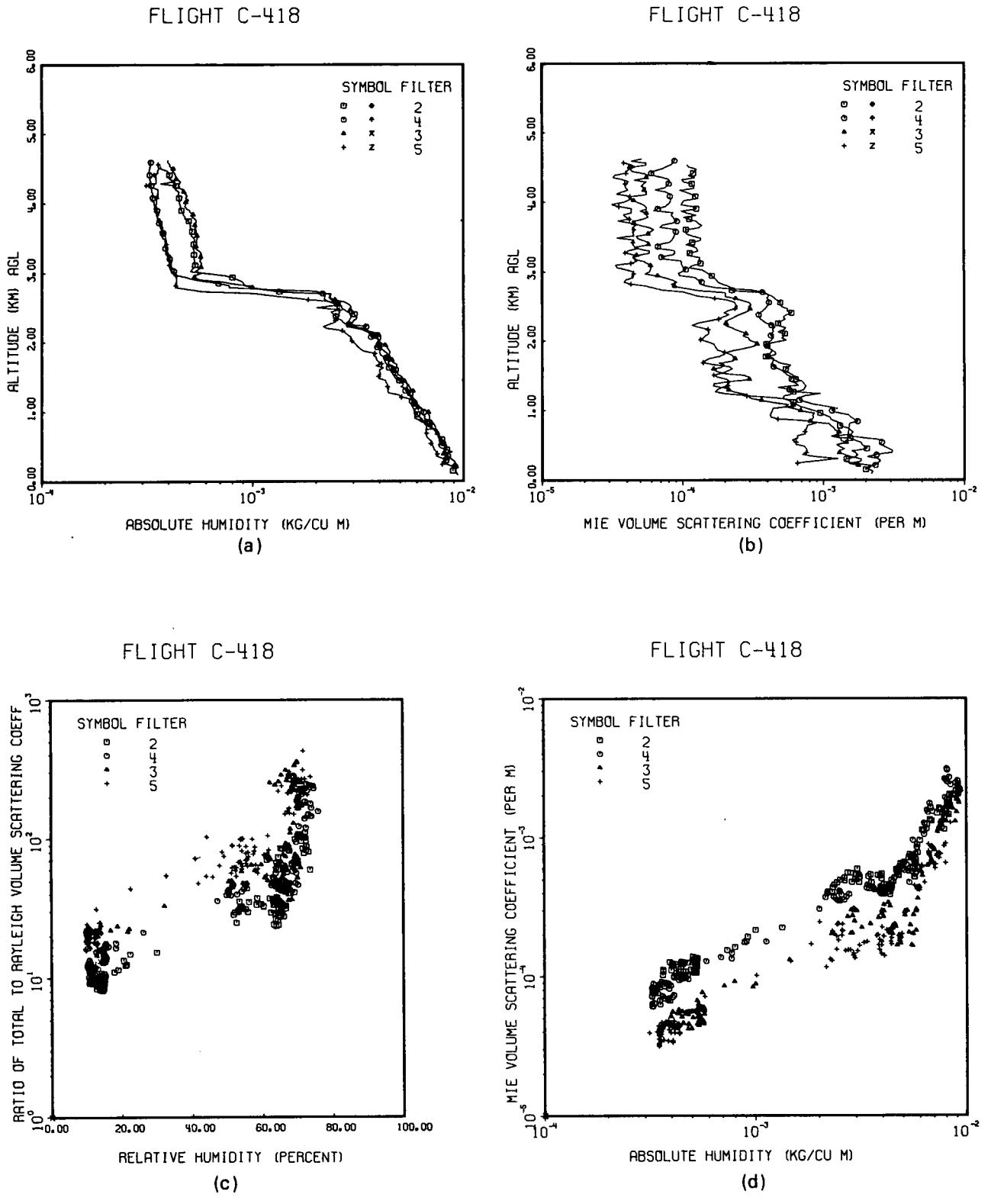

Fig. 7-16. Graphical Data for Flight C-418, OPAQUE III.

8. RECOMMENDATIONS

As an outgrowth of the experience and expertise gained during the analysis and evaluation of the data gathered during this contract interval, several potentially powerful techniques have been developed, and numerous improvements to procedural and computational efficiencies have been accomplished. Some further comment related to these techniques and how they might influence the goals of the technical program is summarized in the following paragraphs.

Non Rayleigh Model Atmospheres. Additional computations of atmospheric optical properties using the Gordon (1969) model atmosphere equations with the Barteneva (1960) proportional directional scattering functions should be encouraged. The utilization of these derived properties as referenced in Section 2, as well as in a broad range of related parametric studies would be of exceptional value to the analyst in general, and specifically in his efforts to establish the boundary conditions anticipated for real world data bases. The computer program for evaluating the model atmosphere equations is relatively fast and inexpensive and thus lends itself to modification for direct interactive communication between the analyst and the computer.

Cloudy Day Techniques. Throughout the five OPAQUE deployments discussed in this report, there was a continuing trend to accumulate flight data under increasingly poor weather conditions. Since the cloudy and overcast conditions which typified many of the OPAQUE data flights, constitute a large portion of the real world's normal weather pattern, the optical atmospheric properties associated with these conditions are as critically needed as are the properties associated with clear days. The need for these cloudy day optical properties is particularly pressing in the context of the European OPAQUE program. Thus, it is recommended that efforts related to improving the computational and analytic procedures appropriate for cloudy day data, as discussed briefly in Section 2, be expanded, and directed specifically toward the OPAQUE data set.

Climatological Relationships. A continuing goal of the measurement program sponsored by the Geophysics Laboratory and conducted by the Visibility Laboratory has been the accumulation of a large body of data appropriate for direct application to the interpretation of the relationship between the optical properties of the atmosphere and the meteorological specification of that atmosphere. Now that the OPAQUE program has made a major contribution toward establishing this extensive data bank as a usable tool, a major program of data analysis and research to explore and define the linking relationships between the optical and meteorological properties documented within the data base is the next logical step.

As an extension of the studies suggested above it seems reasonable to approach the problem of defining the specific geographical area over which each particular set of optical/meteorological properties might remain constant, or stable enough for useful extrapolation. Since the major airborne data system described in Section 3 is no longer available for the support of an additional data study of this type, the development of a small, optically equivalent and nearly real time system would offer an attractive experimental option. One conceptual configuration for a system of this type has been devised by the Visibility Laboratory, and development of the prototype hardware seems feasible at a relatively moderate cost.

Sky and Terrain Radiance Compendium. Since many user applications require the availability of the basic radiance measurements acquired during the C-130 data collection program, as evidenced by numerous recent requests, a special effort should be made to provide these data in a convenient manner. One attractive option would be to generate a compendium of sky and terrain measurements wherein each data set was represented by a pair of iso-radiance plots as illustrated in Fig. 5-3. These plots could be keyed to an extensive tape library which contained the original tabular data, which in turn could be recalled by terminal for hard-copy presentation.

9. ACKNOWLEDGEMENTS

To be conducted successfully, a research program such as the one reported herein requires the active support of many organizations and individuals. To all of those who so willingly contributed their skills, talents, and inspiration, the authors gratefully acknowledge their debt.

Dr. Robert W. Fenn, Chief, Atmospheric Optics Branch, AFGL
Scientific Counsel and Technical Monitor
Major Ted S. Cress, USAF, Project Organization and
Coordination
Mr. Raymond S. Silva, Operational Services Division, Field
Requirements Section AFGL for continuing logistical
support and advice
4950th Test Wing (DOC & MAOP) Wright-Patterson Air Force
Base, for all aircrew and aircraft maintenance
assignments.

Visibility Laboratory, Technical Field Team:
Mr. Nils R. Persson, Jr.
Mr. George F. Simas
Mr. Steven J. Bettinger
Mr. Robert L. Stapleford

Visibility Laboratory, Data Processing and Analysis Team
Mr. Nils R. Persson, Jr.
Ms. Janet E. Shields
Ms. Catharine F. Edgerton
Mr. Steven J. Bettinger

Visibility Laboratory, Editorial and Reproduction Team
Mr. John C. Brown
Mr. James Rodriguez
Ms. Alicia G. Hill

10. REFERENCES

Barteneva, O. D. (1960), "Scattering Functions of Light in the Atmospheric Boundary Layer," Bull. Acad. Sci. U.S.S.R., Geophysics Series, 1237-1244.

Beutell, R. G. and A. W. Brewer (1949), "Instruments for the Measurement of the Visual Range," J. Sci. Instr. **26**, 357-359.

Boileau, A. R. (1964), "Visibility, VI. Atmospheric Properties," Applied Optics **3**, 570-581.

Boileau, A. R., and J. I. Gordon (1966), "Atmospheric Properties and Reflectances of Ocean Waters and Other Surfaces for a Low Sun," Applied Optics, **5**, 803-813.

Brown, D. R. E. (1952), *Natural Illumination Charts,* Report 374-1, Project Ns-714-100, Department of the Navy, Bureau of Ships, Washington, D. C.

Büchtemann, W., and D. H. Höhn (1970), "Spectral Radiance of the Sky and Terrestrial Irradiance in the Wavelength Range from 0.38 to 0.84 μm," Astronomisches Institut der Universität Tübingen (Translation).

Duntley, S. Q., A. R. Boileau, and R. W. Preisendorfer (1957), "Image Transmission by the Troposphere I," J. Opt. Soc. Am. **47**, 499-506.

Duntley, S. Q. (1964), "Visibility, I. Introduction and II Summary," Applied Optics **3**, 550-556.

Duntley, S. Q. (1969), "Directional Reflectance of Atmospheric Paths of Sight," Duntley Rep. No. 69-1.

Duntley, S. Q., R. W. Johnson, J. I. Gordon, and A. R. Boileau (1970), "Airborne Measurements of Optical Atmospheric Properties at Night," University of California, San Diego, Scripps Institution of Oceanography, Visibility Laboratory, SIO Ref. 70-7, AFCRL-70-0137.

Duntley, S. Q., R. W. Johnson, and J. I. Gordon (1972a), "Airborne Measurements of Optical Atmospheric Properties in Southern Germany," University of California, San Diego, Scripps Institution of Oceanography, Visibility Laboratory, SIO Ref. 72-64, AFCRL-72-0255.

Duntley, S. Q., R. W. Johnson, and J. I. Gordon (1972b), "Airborne and Ground-Based Measurements of Optical Atmospheric Properties in Central New Mexico," University of California, San Diego, Scripps Institution of Oceanography, Visibility Laboratory, SIO Ref. 72-71, AFCRL-72-0461.

Duntley, S. Q., R. W. Johnson, and J. I. Gordon (1972c), "Airborne Measurements of Optical Atmospheric Properties, Summary and Review," University of California, San Diego, Scripps Institution of Oceanography, Visibility Laboratory, SIO Ref. 72-82, AFCRL-72-0593.

Duntley, S. Q., R. W. Johnson, and J. I. Gordon (1973), "Airborne Measurements of Optical Atmospheric Properties in Southern Illinois," University of California, San Diego, Scripps Institution of Oceanography, Visibility Laboratory, SIO Ref. 73-24, AFCRL-TR-73-0422.

Duntley, S. Q., R. W. Johnson, and J. I. Gordon (1975a), "Airborne Measurements of Optical Atmospheric Properties in Western Washington," University of California, San Diego, Scripps Institution of Oceanography, Visibility Laboratory, SIO Ref. 75-24, AFCRL-TR-75-0414.

Duntley, S. Q., R. W. Johnson, and J. I. Gordon (1975b), "Airborne Measurements of Optical Atmospheric Properties, Summary and Review II," University of California, San Diego, Scripps Institution of Oceanography, Visibility Laboratory, SIO Ref. 75-26, AFCRL-TR-75-0457.

Duntley, S. Q., R. W. Johnson, and J. I. Gordon (1976), "Airborne Measurements of Optical Atmospheric Properties in Northern Germany," University of California, San Diego, Scripps Institution of Oceanography, Visibility Laboratory, SIO Ref. 76-17, AFGL-TR-76-0188.

Duntley, S. Q., R. W. Johnson, and J. I. Gordon (1977), "Airborne Measurements of Atmospheric Volume Scattering Coefficients in Northern Europe, Spring 1976," University of California, San Diego, Scripps Institution of Oceanography, Visibility Laboratory, SIO Ref. 77-8, AFGL-TR-77-0078.

Duntley, S. Q., R. W. Johnson, and J. I. Gordon (1978a), "Airborne Measurements of Atmospheric Volume Scattering Coefficients in Northern Europe, Fall 1976," University of California, San Diego, Scripps Institution of Oceanography, Visibility Laboratory, SIO Ref. 78-3, AFGL-TR-77-0239.

Duntley, S. Q., R. W. Johnson, and J. I. Gordon (1978b), "Airborne Measurements of Atmospheric Volume Scattering Coefficients in Northern Europe, Summer 1977," University of California, San Diego, Scripps Institution of Oceanography, Visibility Laboratory, SIO Ref. 78-28, AFGL-TR-78-0168.

Fenn, R. W. (1978), "OPAQUE - A Measurement Program on Optical Atmospheric Properties in Europe, Vol. I, The NATO OPAQUE Program," AFGL-TR-78-0011, Special Reports No. 211.

Goldberg, L. (1954), "The Absorption Spectrum of the Atmosphere," Chap. 5 in *The Earth as a Planet,* G. P. Kuiper, Ed., University of Chicago Press, Chicago.

Gordon, J. I., J. L. Harris, and S. Q. Duntley (1963), "Earth-to-Space Contrast Transmittance Measurements from Ground Stations," University of California, San Diego, Scripps Institution of Oceanography, Visibility Laboratory, SIO Ref. 63-2.

Gordon, J. I. (1964), "Visibility, III. Optical Properties of Objects and Backgrounds," Applied Optics **3**, 556-562.

Gordon, J. I., and P. V. Church (1966), "Sky Luminances and the Directional Luminous Reflectances of Objects and Backgrounds for a Moderately High Sun," Applied Optics **5**, 793-801.

Gordon, J. I. (1969), "Model for a Clear Atmosphere," J. Opt. Soc. Am. **59**, 14-18.

Gordon, J. I., J. L. Harris, Sr., and S. Q. Duntley (1973), "Measuring Earth-to-Space Contrast Transmittance from Ground Stations," Appl. Opt. **12**, 1317-1324.

Johnson, F. S. (1954), "The Solar Constant," Journal of Meteorology **11**, 431-439.

Kasten, F. (1965), "A New Table and Approximation Formula for the Relative Optical Airmass," Arch. Met. Geophys. Bioklim. **B14**, 206-233.

Kushpil', V. I., and L. F. Petrova (1971), "Determination of the Atmospheric Transmittance from Sky Brightness Distribution," Optical Technology **38**, No. 4, 191-193.

Tousey, R., and E. O. Hulburt (1947), "Brightness and Polarization of the Daylight Sky at Various Altitudes Above Sea Level," J. Opt. Soc. Am. **37**, 78-92.

Tyler, J. E., and R. W. Preisendorfer (1962), "Light," Chap. 8 in *The Sea,* M. N. Hill, Ed., Interscience Publishers, Inc., N.Y., Vol. 1, pp. 397-451.

U.S. Standard Atmosphere (1962), U.S. Government Printing Office, Washington, D.C. 20402.

U.S. Standard Atmosphere Supplements (1966), U.S. Government Printing Office, Washington, D.C. 20402.

APPENDIX A

GLOSSARY AND NOTATION

The notation used in reports and journal articles produced by the Visibility Laboratory staff follows, in general, the rules set forth in pages 499 and 500, Duntley *et al.* (1957). These rules are:

Each optical property is indicated by a basic (parent) symbol.

A presubscript may be used with the parent symbol as an identifier, e.g., b indicates background while t denotes an object.

A postsubscript may be used to indicate the length of a path of sight, e.g., r denotes an *apparent* property as measured at the end of a path of sight of length r, while o denotes an *inherent* property based on the hypothetical concept of a photometer located at zero distance from an object.

A postsuperscript $^{\bullet}$ or postsubscript $_{\bullet}$, is employed as a mnemonic symbol signifying that the radiometric quantity has been generated by the scattering of ambient light reaching the path from all directions.

The parenthetical attachments to the parent symbol denote altitude and direction. The letter z indicates altitude in general; z_t is used to specify the altitude of an object. The direction of a path of sight is specified by the zenith angle θ and the azimuth ϕ. In the case of irradiances, the downwelling irradiance is designated by d, the upwelling by u.

$A(z)$	Albedo at altitude z, defined by the equation $A(z) \equiv H(z,u)/H(z,d)$.
${}_sA(z)$	Scalar albedo at altitude z, defined by the equation ${}_sA(z) \equiv h(z,u)/h(z,d)$.
AGL	Above ground level.

$C_0(z_t,\theta,\phi)$ Inherent universal contrast determined for a path of sight of zero length at altitude of the object z_t in the direction of zenith angle θ and azimuth ϕ. This property is defined by the equation

$$C_0(z_t,\theta,\phi) \equiv \frac{{}_tN_0(z_t,\theta,\phi) - {}_bN_0(z_t,\theta,\phi)}{{}_bN_0(z_t,\theta,\phi)} .$$

$C_r(z,\theta,\phi)$ Apparent universal contrast as determined at altitude z from the end of path of sight of length r in the direction of the zenith angle θ and azimuth ϕ. This property is defined by the equation

$$C_r(z,\theta,\phi) \equiv \frac{{}_tN_r(z,\theta,\phi) - {}_bN_0(z_t,\theta,\phi)}{{}_bN_o(z_t,\theta,\phi)} .$$

g Acceleration of gravity.

$H(z)$ Scale height at altitude z, the height of a homogeneous atmosphere having the density of the layer at altitude z.

$H(z,d)$ Irradiance produced by downwelling flux as determined on a horizontal flat plate at altitude z. In this report d is used in place of the minus sign in the notation $H(z,-)$ which appears in Duntley (1969). This property may be defined by the equation

$$H(z,d) \equiv \int_{2\pi} N(z,\theta',\phi')\cos\theta' \, d\Omega$$

$H(z,u)$ Irradiance produced by the upwelling flux as determined on a horizontal flat plane at altitude z. Here u is substituted for the plus sign formerly used in the notation $H(z,+)$.

$h(z)$ Scalar irradiance. This may be defined as the radiant flux arriving at a point, from all directions about that point, at altitude z (Tyler and Preisendorfer, 1962):

$$h(z) \equiv h(z,d) + h(z,u) .$$

$h(z,d)$ Scalar irradiance produced by downwelling flux. This may be defined as the radiant flux from the upper hemisphere arriving at a point at altitude z.

${}_kh(z,d)$ Scalar irradiance defined as the radiant flux from the upper hemisphere sky (flux from the sun is not included) arriving at a point at altitude z.

${}_sh(z)$ Scalar irradiance defined as the radiant flux from the sun arriving at a point at altitude z.

$h(z,u)$ Scalar irradiance produced by upwelling flux. This may be defined as the radiant flux from the lower hemisphere arriving at a point at altitude z.

$L(z)$ Attenuation length at altitude z. This property is the reciprocal of the attenuation coefficient, that is,

$$L(z) \equiv \alpha(z)^{-1}.$$

$\bar{L}(z)$ Equivalent attenuation length is defined as

$$\bar{L}(z) \equiv \frac{-z}{\ln T_z(0,0)}.$$

$m_\infty(z,\theta)/m_\infty(z,0)$ Relative optical airmass.

$N(z,\theta,\phi)$ Radiance as determined from altitude z in the direction specified by zenith angle θ and azimuth ϕ.

${}_bN_0(z_t,\theta,\phi)$ Inherent background radiance as determined at altitude of the photometer z_t at zenith angle θ and ϕ.

${}_bN_r(z,\theta,\phi)$ Apparent background radiance as determined at altitude z from the end of a path of sight of length r at zenith angle θ and azimuth ϕ. This property may be defined by the equation

$${}_bN_r(z,\theta,\phi) \equiv {}_bN_0(z_t,\theta,\phi)\,T_r(z,\theta) + N_r^*(z,\theta,\phi)\ .$$

${}_sN_\infty(0,\theta_s,0°)$ Apparent radiance of the center of the solar disk as determined at ground-level altitude from the end of path of sight of length ∞ from out of the atmosphere to ground at zenith angle of the sun θ_s.

${}_tN_0(z_t,\theta,\phi)$ Inherent radiance of an object as determined at altitude of the photometer z_t at zenith angle θ and azimuth ϕ.

${}_tN_r(z,\theta,\phi)$ Apparent radiance of an object as determined at altitude z. from the end of a path of sight of length r at zenith angle θ and azimuth ϕ. This property may be defined by the equation

$${}_tN_r(z,\theta,\phi) \equiv {}_tN_0(z_t,\theta,\phi)\,T_r(z,\theta) + N_r^*(z,\theta,\phi)\ .$$

$N_q(z,\theta,\phi)$ Equilibrium radiance at altitude z with the direction of the path of sight specified by zenith angle θ and azimuth ϕ. This property is a point function of position and direction.

$\bar{N}_q(z,\theta,\phi)$ Effective equilibrium radiance for a path of sight from out of the atmosphere to altitude z in the direction specified by zenith angle θ and azimuth ϕ. This property may be defined by the equation

$$\bar{N}_q(z,\theta,\phi) \equiv N_\infty^*(z,\theta,\phi)/[1 - T_\infty(z,\theta)]\ .$$

This property may also be denoted as a function of angle from light source (sun or moon) β, i.e., $\bar{N}_q(z,\beta)$.

$N_*(z,\theta,\phi)$ Path function at altitude z with the direction of the path of sight specified by zenith angle θ and azimuth ϕ. This property is defined by the equation

$$N_*(z,\theta,\phi) \equiv \int_{4\pi} \sigma(z,\beta') N(z,\theta',\phi') d\Omega \ .$$

This property also is a point function of position and direction.

$N_r^*(z,\theta,\phi)$ Path radiance as determined at altitude z at the end of a path of sight of length r in the direction specified by zenith angle θ and azimuth ϕ.

$N_\infty^*(0,\gamma_s,180°)$ Sky radiance at a scattering angle of 90° from the sun. Also the path radiance for the path of sight of length ∞ from out of the atmosphere to ground-level altitude at a zenith angle equal to the solar elevation angle γ_s.

$n(z)$ Index of refraction at altitude z.

$P(z)$ Pressure at altitude z.

${}_sP(t)$ Saturated vapor pressure at ambient temperature.

${}_sP({}_dt)$ Saturated vapor pressure at dewpoint or frostpoint temperature.

psia Pressure, absolute, pounds per square inch.

psid Pressure, differential, pounds per square inch.

${}_bR_0(z_t,\theta,\phi)$ Inherent background reflectance as determined at the altitude of an object z_t and viewed at zenith angle θ and ϕ.

$R_q(z,\theta,\phi)$ Equilibrium reflectance is defined as $R_q(z,\theta,\phi) = N_q(z,\theta,\phi)\ \pi/H(z,d)$.

$R_r^*(z,\theta,\phi)$ Directional path reflectance as determined at altitude z at the end of a path of sight of length r in the direction specified by zenith angle θ and azimuth ϕ.

RH Relative humidity in percent $RH = [{}_sP({}_dt)/{}_sP(t)]100$

$R/M(0)$ Universal gas constant.

$\overline{S_\lambda T_\lambda}$ Standardized relative spectral response of filter/cathode combination where S_λ is spectral sensitivity of the multiplier phototube cathode and T_λ is spectral transmittance of optical filter.

$s(z)$ Total volume scattering coefficient as determined at altitude z. This property may be defined by the equation

$$s(z) \equiv \int_{4\pi} \sigma(z,\beta)\, d\Omega$$

In the absence of atmosperic absorption, the total volume scattering coefficent is numerically equal to the attenuation coefficient.

$_{M}s(z)$ Total volume scattering coefficient for Mie scattering at altitude z.

$_{R}s(z)$ Total volume scattering coefficient for Rayleigh scattering at altitude z.

t Ambient temperature °C.

$_{d}t$ Dewpoint or frostpoint temperature, °C.

$T(z)$ Temperature in degrees Kelvin at altitude z.

$T_r(z,\theta)$ Beam Transmittance as determined at altitude z for a path of sight of length r at zenith angle θ. This property is independent of azimuth in atmospheres having horizontal uniformity. It is always the same for the designated path of sight or its reciprocal.

VV Visibility as estimated by the meteorologists $VV = 3/s(z)$.

W_λ Spectral emittance (power/unit of area) of electromagnetic flux from a plane surface.

$_{c}W_\lambda$ Spectral emittance of calibration source.

W'_λ Spectral emittance of anticipated field scene.

$\bar{y}$ Symbol for visual efficiency function.

ZSV Zero scale value. The zero point on the linear scale when the radiometric or photometric quantity x is equal to a reference radiometric or photometric quantity x_0 as shown in the equation

$$\log[x_0/x] = 0 .$$

z Altitude, usually used as above ground level.

z_t Altitude of an object.

$\alpha(z)$ Volume attenuation coefficient as determined at altitude z. In the absence of atmospheric absorption, the attenuation coefficient is numerically equal to the volume scattering coefficient.

β — Symbol for scattering angle of flux from a light source. It is equal to the angle between the line from the source to the observer and the path of sight.

β' — Symbol for scattering angle of flux from a discrete part of the sky. It is equal to the angle between the direction specified by θ' and ϕ' and the path of sight.

γ_s — Elevation angle of the sun. The solar elevation angle is the complement of the sun zenith angle, $\gamma_s = 90° - \theta_s$.

Δ — Symbol to indicate incremental quantity and used with r and z to indicate small, discrete increments in path length r and altitude z.

δ_λ — Response area is defined as $\delta_\lambda = \sum(\overline{S_\lambda T_\lambda})\Delta\lambda$.

ϵ_λ — Spectral emissivity of tungsten filament.

ζ — Symbol for radius of the earth.

θ — Symbol for zenith angle. This symbol is usually used as one of two coordinates to specify the direction of a path of sight.

θ' — Symbol for zenith angle usually used as one of two coordinates to specify the direction of a discrete portion of the sky.

λ — Symbol for wavelength.

$\bar{\lambda}$ — Mean wavelength is defined as

$$\bar{\lambda} \equiv \sum \lambda(\overline{S_\lambda T_\lambda})\Delta\lambda/\delta_\lambda \ .$$

$\rho(z)$ — Density at altitude z.

σ — Symbol for volume scattering function. Parenthetical symbols may be added; for example, β may be used to designate the scattering angle from a source. In Gordon (1969) the parenthetical symbols are z and β for altitude and scattering angle.

$\sigma(z,\beta)/s(z)$ — Proportional directional volume scattering function. This may be defined by the equation

$$\int_{4\pi} [\sigma(z,\beta)/s(z)] \equiv 1.$$

${}_b\tau_r(z,\theta,\phi)$ — Contrast transmittance as determined at altitude z at the end of a path of sight of length r and specified by zenith angle θ and azimuth ϕ. This property is *not* independent of azimuth and is *not* the same for the designated path of sight and its reciprocal.

ϕ Symbol for azimuth. The azimuth is the angle in the horizontal plane of the observer between a fixed point and the path of sight. The fixed point may be, for example, true north, the bearing of the sun, or the bearing of the moon. This symbol is usually used as one of two coordinates to specify the direction of a path of sight.

ϕ' This symbol for azimuth is usually used as one of two coordinates to specify the direction of a discrete portion of the sky.

Ψ Angular solar radius at true earth-to-sun distance.

$\overline{\Psi}$ Angular solar radius at mean solar distance.

Ω Symbol for solid angle.

For a hemisphere: $\Omega = 2\pi$ steradians;
For a sphere: $\Omega = 4\pi$ steradians.

APPENDIX B

DISCUSSION OF TERMINOLOGY

CONTRAST TRANSMITTANCE IN THE TROPOSPHERE

Contrast transmittance ${}_b\tau_r(z,\theta,\phi)$ is defined as the ratio of the apparent contrast $C_r(z,\theta,\phi)$ to the inherent contrast $C_o(z_t,\theta,\phi)$;

$$ {}_b\tau_r(z,\theta,\phi) = C_r(z,\theta,\phi)/C_o(z_t,\theta,\phi) \ . \tag{A.1} $$

The parenthetical modifiers indicate the altitude z of the sensor and the zenith angle θ and azimuth ϕ of the path of sight. In this report, ϕ will always be in terms of azimuth from light source (sun or moon). The path length r in the direction of the path of sight is between the altitude of the object z_t and the sensor altitude z. For the inherent contrast the path length is zero. The presubscript b on the contrast transmittance ${}_b\tau_r(z,\theta,\phi)$ indicates background. The contrast transmittance is a function of the inherent background radiance ${}_bN_o(z_t,\theta,\phi)$, the atmospheric beam transmittance $T_r(z,\theta)$ and the path radiance $N_r^*(z,\theta,\phi)$ of the path of sight as shown in Eq. (A.2) [Duntley (1964) Eq. (2.4)]:

$$ {}_b\tau_r(z,\theta,\phi) = [1 + N_r^*(z,\theta,\phi)/{}_bN_o(z_t,\theta,\phi)\ T_r(z,\theta)]^{-1} \ . \tag{A.2} $$

As noted in the glossary, beam transmittance is considered as being independent of azimuth, and thus its notation is typically simplified from the general form by omitting the azimuth designator ϕ.

DIRECTIONAL PATH REFLECTANCE

The concept of directional path reflectance [Duntley (1969) p. 3] is utilized in an alternate form of Eq. (A.2),

$$ {}_b\tau_r(z,\theta,\phi) = [1 + R_r^*(z,\theta,\phi)/{}_bR_o(z_t,\theta,\phi)]^{-1} \ , \tag{A.3} $$

where ${}_bR_o(z_t,\theta,\phi)$ is the directional background reflectance. By definition, the directional path reflectance for downward-looking paths of sight is

$$R_r^*(z,\theta,\phi) = \pi N_r^*(z,\theta,\phi)/[H(z_t,d)\ T_r(z,\theta)]\ , \tag{A.4}$$

where $H(z_t,d)$ is the downwelling irradiance. For upward-looking paths of sight the upwelling irradiance $H(z_t,u)$ is used instead of the downwelling irradiance in Eq. (A.4).

We chose to present the atmospheric data for upward- and downward-inclined paths of sight in the form of directional path reflectance since, in this form, it can be easily utilized with the directional reflectance of a variety of backgrounds smaller in extent but different from the heterogeneous background which contributed to the path radiance and upwelling and downwelling irradiance. The directional path reflectance is also the most convenient form of presenting the atmospheric data for easy use to obtain contrast transmittance.

BACKGROUND REFLECTANCE

The inherent background reflectance for downward-looking paths of sight is defined as

$${}_bR_o(z_t,\theta,\phi) = \pi\, {}_bN_o(z_t,\theta,\phi)/H(z_t,d)\ , \tag{A.5}$$

where $H(z_t,d)$ is the downwelling irradiance at the object altitude [Gordon (1964) p. 558 or Boileau and Gordon (1966) p. 805]. Note that the downwelling irradiance is used in the definition of reflectance for downward paths of sight regardless of the background surface orientation. The inherent background reflectance may be obtained from either (1) a measurement by a ground-based telephotometer† or (2) measurements by an airborne telephotometer. In Duntley, *et al.* (1976), airborne telephotometer data from the lowest altitude of flight not extrapolated to ground level were used to obtain the terrain reflectances reported for each flight.

The effective inherent background reflectance for an upward-looking path of sight is similarly

$${}_bR_o(z_t,\theta,\phi) = \pi\, {}_bN_o(z_t,\theta,\phi)/H(z_t,u)\ . \tag{A.6}$$

INHERENT CONTRAST

The inherent contrast of an object $C_o(z_t,\theta,\phi)$ against a background is defined as the ratio of the inherent object to background radiance minus 1:

$$C_o(z_t,\theta,\phi) \equiv {}_tN_o(z_t,\theta,\phi)/{}_bN_o(z_t,\theta,\phi) - 1\ . \tag{A.7}$$

† Although the measurements are radiometric as opposed to photometric, the instrument used to perform these measurements is referred to herein as a "telephotometer" in lieu of the more precise term "teleradiometer." This is in keeping with the practice established in previous publications.

Inherent contrast can also be computed from the directional reflectance of the object and background,

$$C_o(z_t,\theta,\phi) = {}_tR_o(z_t,\theta,\phi)/{}_bR_o(z_t,\theta,\phi) - 1 \ . \tag{A.8}$$

DOWNWELLING AND UPWELLING IRRADIANCE

The downwelling irradiance used to compute the directional path reflectance $R_r^*(z,\theta,\phi)$ and the apparent terrain reflectance is computed from data at the lowest altitude of flight by the equation

$$H(z,d) = {}_sh(z)\cos\theta_s + \int_{2\pi} N(z,\theta',\phi')\cos\theta' d\Omega \ , \tag{A.9}$$

where ${}_sh(z)$ is the sun scalar irradiance at altitude z, θ_s is the sun zenith angle, and $N(z,\theta',\phi')$ is the sky radiance at direction θ', ϕ'. When the sky is fully overcast, the first term is essentially zero.

The upwelling irradiance $H(z,u)$ is computed by deleting the first term in Eq. (A.9) and replacing the sky radiances with apparent terrain radiances from the lower hemisphere scanner. The θ' would then be the nadir angle so that $\cos\theta'$ is positive. The albedo $A(z)$ is the ratio of the upwelling to downwelling irradiance $H(z,u)/H(z,d)$.

A second type of irradiance is the scalar or nondirectional irradiance:

$$h(z,d) = {}_sh(z) + \int_{2\pi} N(z,\theta',\phi')\, d\Omega \ . \tag{A.10}$$

The scalar irradiance is not weighted by the cosine. The upwelling irradiance from zenith angles between 90 and 180 degrees is designated by $h(z,u)$ and computed by using Eq. (A.10) without the first term. The total scalar irradiance is the sum of the upwelling and downwelling scalar irradiances, $h(z)=h(z,u)+h(z,d)$. The scalar albedo is defined as the ratio of upwelling to downwelling scalar irradiance, $h(z,u)/h(z,d)$. For a full discussion of scalar irradiances and scalar albedo uses refer to Gordon (1969).

TOTAL VOLUME SCATTERING COEFFICIENT

A direct measure of air clarity is the atmospheric attenuation coefficient $\alpha(z)$. The parenthetical modifier indicates the altitude z. The attenuation coefficient is the sum of the total volume scattering coefficient and the absorption coefficient. If there is no absorption, the attenuation coefficient is numerically equal to the total volume scattering coefficient $s(z)$.

The total volume scattering coefficient may be defined by the equation

$$s(z) \equiv \int_{4\pi} \sigma(z,\beta)\, d\Omega \ ,$$

where $\sigma(z,\beta)$ is the volume scattering function at altitude z and scattering angle β. The integrating nephelometer used to make the total volume scattering coefficient measurements performs the integral in Eq. (A.11) optically. It utilized a parallel light beam and a cosine-law collector viewing the scattered flux. The instrument is similar in principle to one of four instruments for measuring total volume scattering coefficient described by Beuttell and Brewer (1949).

BEAM TRANSMITTANCE FROM TOTAL SCATTERING COEFFICIENTS

The beam transmittance $T_r(z,\theta)$ is obtained directly from the total scattering coefficient $s(z)$ by means of Eq. (A.12). (Refer also to Boileau (1964) p. 570.) When there is no significant atmospheric absorption in the passbands of the measurements, e.g., from smoke, dust, or smog, the attenuation coefficient $\alpha(z)$ is equivalent to the total volume scattering coefficient $s(z)$. Therefore,

$$T_r(z,\theta) = \exp\left[-\sum_{i=1}^{n}\alpha(z_i)\,\Delta r\right] = \exp\left[-\sum_{i=1}^{n}s(z_i)\,\Delta r\right], \tag{A.12}$$

where Δr is the incremental path length. The summations are made using the trapezoidal rule. The measured total volume scattering coefficient data are extrapolated to ground level when no ground-based measurements are available. The extrapolation assumes that the scattering particles are the same at all altitudes, but decrease or increase according to the density at each altitude $\rho(z)$:

$$s(0) = \frac{s(z)\rho(0)}{\rho(z)}\,. \tag{A.13}$$

Similarly, upward extrapolations are made to the highest reported altitude above ground level when the highest flight altitude is less. Extrapolation in this case is based on the scattering coefficient measured at highest flight altitude. The densities used for the extrapolations are from the U.S. Standard Atmosphere (1962). The density at each altitude is obtained by truncated Chebyshev expansion using the coefficients for the atmosphere between 0 and 80 kilometers [U.S. Standard Atmosphere Supplements (1966), p. 69].

All altitudes reported are between ground level and 6 kilometers maximum. For all paths of sight at zenith angles less than 85 degrees or greater than 95 degrees, Δr equals $\Delta z\ sec\theta$ for these altitudes. The Δr is always nonnegative since Δz is defined as $z_1 - z_2$ (the subscripts increase with the flux direction). See Fig. B-1. The $|\Delta z|$ used is 30 meters (98.4 feet). For zenith angles greater than 95 degrees, the beam transmittance can also be expressed as a function of the vertical beam transmittance $T_r(z, 180°)$ as follows:

$$T_r(z,\theta) = T_r(z, 180°)^{|sec\theta|}\,. \tag{A.14}$$

For upward paths of sight for zenith angles less than 85 degrees, the beam transmittance can similarly be expressed as a function of the vertical upward transmittance $T_r(z, 0°)$.

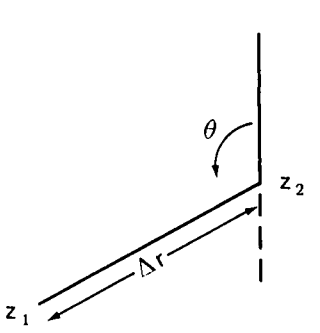

Fig. B-1. Path Length Geometry for Steeply Inclined Paths of Sight.

ATTENUATION LENGTH

The attenuation length $L(z)$ is defined as the reciprocal of the atmospheric attenuation coefficient $\alpha(z)$. Therefore, when there is no significant absorption, it is also equivalent to the reciprocal of the atmospheric total volume scattering coefficient:

$$L \equiv \frac{1}{\alpha(z)} = \frac{1}{s(z)} \, . \tag{A.15}$$

The equivalent attenuation length $\bar{L}(z)$ is a pseudo-attenuation length which, when combined with its altitude z, can be used directly in the equation [Boileau (1964), Eq. (6.1)]

$$T_r(z,\theta) = \exp[-z/\bar{L}(z)]|\sec\theta| \, , \tag{A.16}$$

where $\theta > 95°$ and path length r is between ground level and altitude z. Combining Eq. (A.16) and Eq. (A.12) and appropriately rearranging, the following expression may be obtained for effective attenuation length.

$$\bar{L}(z_n) = \frac{z_n}{\sum_{i=1}^{n} s(z_i)\,\Delta z} \, . \tag{A.17}$$

For $\theta < 85°$, the $\bar{L}(z)$ values should be interpreted as applying to the object altitude with the sensor at ground level.

EARTH CURVATURE AND REFRACTION

For the paths of sight at zenith angles from 90 to 95 degrees, the Δr for $|\Delta z| = 30$ meters (98.4 feet) is significantly longer at ground level than at 6 kilometers due to the curvature of the earth. Also for upward-looking paths of sight from 85 to 90 degrees, the Δr for $\Delta z = 30$ meters (98.4 feet) is significantly shorter at 6 kilometers than at ground level due to the curvature of the earth. Thus, for

paths of sight between 85 and 95 degrees in zenith angle, Eq. (A.14) and (A.16) should not be used. Instead, Eq. (A.12) should be used with the appropriate Δr values.

The incremental path length Δr_i is computed from

$$\Delta r_i = \left\{ 1 - \left[\frac{n(z)}{n(z_i)} \frac{(\zeta + z)}{(\zeta + z_i)} \sin\theta \right]^2 \right\}^{-1/2} \Delta z \ . \tag{A.18}$$

This is the classical equation for computing incremental path length at paths of sight affected by earth curvature and refraction. The $n(z)$ is the refractive index, z is the sensor or observer altitude, ζ is the radius of the earth. The derivation of Eq. (A.18) is given in detail in Duntley, *et al.* (1976).

The square of the refractive index ratio based on an alternate form by Kasten (1965) rewritten in terms of the refractive index at ground level z = 0 is as follows:

$$\left[\frac{n(z)}{n(z_i)} \right]^2 = 1 + 2[n(0)-1] \left[\frac{\rho(z)}{\rho(0)} - \frac{\rho(z_i)}{\rho(0)} \right] . \tag{A.19}$$

The density values for computing the refraction effect were, as before, based on the U.S. Standard Atmosphere (1962). The refractive index used for ground level was 1.000276, appropriate to a wavelength of 700 nanometers at 15 degrees centigrade. The maximum error in using the Δr based on 700 nanometers for wavelengths of 478 to 770 nanometers is 0.2 percent.

PATH RADIANCE

Path radiance $N_r^*(z,\theta,\phi)$ for the path of sight θ is the integration or summation of the path function $N_*(z,\theta,\phi)$ weighted by the beam transmittance $T_{ri}(z,\theta)$. Path length r_i is from the incremental path Δr to the sensor at z:

$$N_r^*(z,\theta,\phi) = \sum_{i=1}^{m} N_*(z_i,\theta,\phi)\ T_{ri}(z,\theta)\ \Delta r \ . \tag{A.20}$$

Refer to Duntley, *et al.* (1957), Eq. (17) on p. 502.

PATH FUNCTION

Image-forming light is lost by scattering and absorption in each elementary segment of the path of sight, and contrast-reducing path radiance is generated by the scattering of the ambient light which reaches the segment from all directions. The quantitative description of this scattered component of path-segment radiance involves a quantity called the "path function," $N_*(z,\theta,\phi)$. The "path function" depends upon the directional distribution of the lighting on the segment due to its surroundings. It can be operationally defined in terms of the (limiting) ratio of the path radiance associated with a short path to the path length by the relation [Duntley, *et al.* (1957) p. 501]

$$N_*(z,\theta,\phi) = \lim(\Delta r \to 0)\ N_{\Delta r}^*(z,\theta,\phi)/\Delta r \ . \tag{A.21}$$

In experimental practice, the path length Δr should be sufficiently short so that no change in the ratio can be detected if Δr is made shorter.

In lieu of a direct measurement of path function, it may be derived from related quantities. Path function, attenuation length, and equilibrium radiance are related by [Duntley, *et al.* (1957), Eq. (11)]

$$N_q(z,\theta,\phi) = N_*(z,\theta,\phi)\ L(z)\ . \tag{A.22}$$

By substituting Eq. (A.15) into Eq. (A.22) and rearranging, path function is expressed as a function of the total volume scattering coefficient and the equilibrium radiance:

$$N_*(z_i,\theta,\phi) = N_q(z_i,\theta,\phi)\ s(z_i)\ . \tag{A.23}$$

EQUILIBRIUM RADIANCE

For each segment of every path of sight in any lighted atmosphere there is an equilibrium radiance that will be transmitted unchanged because the loss (attenuation of image-forming light) is exactly counter balanced by the gain due to the scattering of sunlight and sky light toward the sensor. The equilibrium radiance is a point function of position and direction which may vary from point to point throughout the path of sight.

The equilibrium radiance [Duntley, *et al.* (1957), p. 502, and Gordon (1969), p. 15] is first computed from the measurements made at each of the altitudes of level flight and then interpolated and extrapolated to obtain values at each 30-meter (98.4 foot) interval z_i. Equilibrium radiance is interpolated rather than path function since the equilibrium radiance for the fully sunlit case is relatively invariant with altitude, whereas path function is sensitive to changes in aerosol scattering as well as the lighting distribution. To compute the equilibrium radiance the following equation is used (refer to Gordon (1969), Eq. (16*) on p. 16):

$$N_q(z,\theta,\phi) = {}_sh(z)\ \frac{\sigma(z,\beta)}{s(z)} + \int_{4\pi} N(z,\theta',\phi')\ \frac{\sigma(z,\beta')}{s(z)}\ d\Omega\ , \tag{A.24}$$

where ${}_sh(z)$ is the scalar irradiance of the sun (or full moon), β is the angle between the sun and the path of sight, and $N(z,\theta',\phi')$ is the apparent radiance of the sky or ground for direction θ' and ϕ'. When the sky is fully overcast, the first term in Eq. (A.24) is essentially zero. The ratio $\sigma(z,\beta')/s(z)$ is the proportional directional volume scattering function at angle β' and altitude z. The β' is the angle between the path of sight at θ, ϕ, and the radiance θ', ϕ'. It is found by

$$\cos\beta' = \sin\theta\ \sin\phi\ \sin\theta'\ \sin\phi' + \sin\theta\ \cos\phi\ \sin\theta'\ \cos\phi' + \cos\theta\ \cos\theta'\ . \tag{A.25}$$

---

* Equation 16 applies equally well to real and model atmospheres.

It is the scalar irradiance which designates the flux that enters into the computations of equilibrium radiance and path function when the directional radiances are not known or used. It is the directionality of that flux combined with the directionality of the proportional directional volume scattering function which produces the unique equilibrium radiance associated with each path of sight.

PROPORTIONAL VOLUME SCATTERING FUNCTION

The proportional volume scattering function $\sigma(z,\beta)$ for scattering angles 0° to 180° is derived from a catalog of values of photopic proportional volume scattering functions published by Barteneva (1960) and the measured values of volume scattering function $\sigma(z, 30°)$ and $\sigma(z, 150°)$. The procedure for obtaining the proportional volume scattering function to be used in Eq. (A.24) is described in detail in Duntley, *et al.* (1976) Eqs. (2.27) through (2.31).

SUN IRRADIANCE

Although the scanner radiance measurements include a measure of the apparent sun radiance, the sun is not always fully in the field of view. Therefore, the sun irradiance used in the computations of the irradiance and the equilibrium radiance is based upon the sun irradiance out of the atmosphere ${}_sh(\infty)$ for the appropriate broadband filter and the beam transmittance from out of the atmosphere to altitude z, $T_\infty(z,\theta_s)$:

$$ {}_sh(z) = {}_sh(\infty)\ T_\infty(z,\theta_s)\ . \tag{A.26}$$

The sun irradiance values for mean solar distance ${}_sh(\overline{\infty})$ are computed from spectral sun irradiance from Johnson (1954). The sun irradiance at true solar distance ${}_sh(\infty)$ is equal to the irradiance at mean distance times the square of the ratio of the angular solar radius Ψ at true solar distance to the radius $\overline{\Psi}$ at mean distance:

$$ {}_sh(\infty) = {}_sh(\overline{\infty}) \left(\frac{\Psi}{\overline{\Psi}} \right)^2 . \tag{A.27}$$

The angular solar radius at mean solar distance is 16.016 minutes of arc. The radii at true distance are obtained from the ephemeris for the appropriate date.

BEAM TRANSMITTANCE FROM SKY RADIANCE RATIOS

When the sky at the highest flight altitude is clear, the transmittance from out of the atmosphere to the highest flight altitude due to scattering is computed from the ratio of sky radiances at equivalent scattering angles from the sun. This method stems from the suggested nomographic method of Kushpil' and Petrova (1971) for obtaining beam transmittance from sky radiance ratios at equivalent scattering angles from the sun. Kushpil' and Petrova do not give equations for the sky radiance ratio as a function of beam transmittance, but such an equation is derived in the following paragraph.

A sky radiance is a path radiance from out of the atmosphere to the altitude of measurement $N^*_\infty(z,\theta,\phi)$. On clear days with no absorption, we have found the sky radiance to be a function of an effective equilibrium radiance $\bar{N}_q$ and the beam transmittance [Gordon, *et al.* (1963), Gordon (1969), and Gordon, *et al.* (1973)]:

$$N^*_\infty(z,\theta,\phi) = \bar{N}_q(z,\theta,\phi)\,[1 - T_\infty(z,\theta)]\ . \tag{A.28}$$

Thus, the ratio of two sky radiances, at angles θ and θ', would be

$$\frac{N^*_\infty(z,\theta,\phi)}{N^*_\infty(z,\theta',\phi')} = \frac{\bar{N}_q(z,\theta,\phi)\,[1 - T_\infty(z,\theta)]}{\bar{N}_q(z,\theta',\phi')\,[1 - T_\infty(z,\theta')]}\ . \tag{A.29}$$

When the scattering angle from the sun is equivalent for the two paths of sight, the equilibrium radiances are equivalent. Thus, Eq. (A.29) simplifies to

$$\frac{N^*_\infty(z,\theta,\phi)}{N^*_\infty(z,\theta',\phi')} = \frac{[1 - T_\infty(z,\theta)]}{[1 - T_\infty(z,\theta')]}\ . \tag{A.30}$$

Equation A.30 can be expressed as a function of the vertical transmittance $T_\infty(z,0°)$ and the relative optical airmass $m_\infty(z,\theta)/m_\infty(z,0°)$:

$$\frac{N^*_\infty(z,\theta,\phi)}{N^*_\infty(z,\theta',\phi')} = \frac{\left[1 - T_\infty(z,0°)^{m_\infty(z,\theta)/m_\infty(z,0°)}\right]}{\left[1 - T_\infty(z,0°)^{m_\infty(z,\theta')/m_\infty(z,0°)}\right]}\ . \tag{A.31}$$

Equation A.31 cannot be directly solved for the vertical transmittance, but by using iterative means, which is a simple task with a computer, a vertical transmittance is obtained which provides a solution to Eq. (A.31) within a tolerance of 0.1 percent.

An error analysis of the transmittance obtained by Eq. (A.31) indicates that the precision error difference of the two radiances is generally multiplied by a factor of between 1 and 2 for many zenith angle combinations. Thus, a series of measurements is used, and the transmittances are averaged to enhance the reliability of the resultant transmittance due to scattering. A validation of the sky radiance ratio method of obtaining beam transmittance was presented in Duntley, *et al.* (1972c), Section 2.1.

Atmospheric absorption acts to reduce the incoming sun irradiance but has no effect on the sky radiance relative distribution. Thus, the transmittance based on sky radiance ratios is due to scattering only, and the transmittance losses due to absorption must be added as a separate factor. Tousey and Hulburt (1947) calculated a photopic transmittance of 0.977 due to absorption by ozone at the top of the atmosphere. the photopic transmittance from out of the atmosphere to the highest flight altitude is the product of the transmittance due to scattering and the transmittance due to absorption.

When the sky at the highest altitude is not completely free of clouds, the beam transmittance from space to altitude may be specified on the basis of ground-based contrast reduction meter measurements or other measurements such as downwelling irradiance measured simultaneously with sky radiance, which yield an estimate of space-to-altitude transmittance.

The transmittance for the lower flight altitudes is the product of the transmittance from out of atmosphere to the highest altitude $T_\infty(z_m, 0°)$ and the transmittance between the two flight altitudes $T_r(z, 0°)$:

$$T_\infty(z, 0°) = T_\infty(z_m, 0°)\ T_r(z, 0°)\ . \tag{A.32}$$

The conversion from vertical transmittance to transmittance at the zenith angle of the sun is made using the relative airmass $m_\infty(z, \theta_s)/m_\infty(z, 0°)$:

$$T_\infty(z, \theta_s) = T_\infty(z, 0°)^{m_\infty(z, \theta_s)/m_\infty(z, 0°)}\ . \tag{A.33}$$

The relative airmass equals $sec\theta$ for $\theta_s = 70°$ to an accuracy of 1 percent. Also, the relative airmass at altitudes up to 6 kilometers equals the relative airmass at sea level, $m_\infty(6, \theta_s)/m_\infty(6, 0°) = m_\infty(0, \theta_s)/m_\infty(0, 0°)$, to an accuracy of 1 percent for $\theta_s = 86°$. Sea level relative airmass values from Kasten (1965) are used for θ_s 70 → 86°.

The sun zenith angle θ_s changes during the flight interval. In order to reduce this source of variability in the resultant data, an average sun zenith angle for each filter or the total flight is used in Eq. (A.33) as well as in computing the irradiance in Eq. (A.9) and the scattering angle β in Eq. (A.24).

SKY AND TERRAIN RADIANCE

The arrays of sky and terrain radiance measurements have missing values due to the sampling schedule and include values which are questionable due to: possible inclusion of the sun in the field of view; portions of the airplane such as tail or propellers extending into path of sight; values above or below the calibrated range of the sensor; and irregularities in the angular pattern. In order to obtain a basic data array of optimum quality, these well-defined but improper values must be removed and the blank values replaced. To do this, the upper and lower hemisphere data arrays are handled separately, and in the following manner.

Since the terrain radiances have a relatively narrow range, questionable values are simply replaced by interpolations between adjacent valid data points. The same procedure is used for sky radiances under overcast or partial cloud.

For clear skies, in order to evaluate and replace the questionable sky radiance measurements, the effective equilibrium radiance as a function of angle from sun β is established on the basis of the sky radiance measurements $N^*_\infty(z, \theta, \phi)$ of known validity. The effective equilibrium radiance $\bar{N}_q$ is computed by rearranging Eq. (A.28) as follows:

$$\bar{N}_q(z, \theta) = N^*_\infty(z, \theta, \phi)/[1 - T_\infty(z, \theta)]\ . \tag{A.34}$$

An average effective equilibrium radiance for each 5 degrees of β is then calculated and the proportional standard deviation from that average function established. The value of the average effective equilibrium radiance at $\beta = 0°$ is determined using Barteneva's method of assuming log $\bar{N}_q(\beta)$ linear with $\cos\beta$ for small values of β. The questionable sky radiance measurements are then replaced using the average equilibrium radiance function and Eq. (A.28).